Student thesis series INES nr 584

High tide flooding in near future projections for popular travel destinations

David Adrian Ebert

2023
Department of
Physical Geography and Ecosystem Science
Lund University
Sölvegatan 12
S-223 62 Lund
Sweden

David Adrian Ebert (2023).
High tide flooding in near future projections for popular travel destinations
Master degree thesis, 30 credits in *Physical Geography and Ecosystem Science*
Department of Physical Geography and Ecosystem Science, Lund University

Level: Master of Science (MSc)
Course duration: *February* 2022 until *June* 2022

Disclaimer

High tide flooding in near future projections for popular travel destinations

---

David Adrian Ebert

Master thesis, 30 credits in *Physical Geography and Ecosystem Science*

Supervisor
Lina Eklund, Associate Senior Lecturer and Researcher
Department of Physical Geography and Ecosystem Science, Lund University

Exam committee:
Anna Maria Jönsson, Professor
Department of Physical Geography and Ecosystem Science, Lund University

Kristina Blennow, Visiting Professor
Department of Physical Geography and Ecosystem Science, Lund University

Acknowledgements

It was the work of Thomspon et al. (2021) that first drew my attention to this area of research and its importance.

I would also like to thank the creator of UTide, Dan Codiga, for taking the time to answer my questions regarding his leading tidal analysis software. I would like to thank the team at the Global Extreme Sea Level Analysis (GESLA) project for consolidating the data needed to conduct this thesis, and for the helpful emails regarding the platform.

Finally, I would like to thank my supervisor Lina Eklund, and the examination committee Anna Maria Jönsson and Kristina Blennow for the valuable feedback and enthusiasm for the project.

Abstract

High tide flooding (HTF) is becoming more common in coastal regions of the United States, although this phenomenon remains largely undocumented in published literature from other parts of the world. No matter the emissions scenario over the next decades, sea level rise (SLR) is projected to continue worldwide until at least the end of the 21st century, continually pushing the frequency and severity of HTF.

Despite the expectation of continued SLR long-term and the resulting implications on future HTF, there is a lack of continuous near future, high granularity projections of HTF useful to decision-makers, urban planners, residents and travelers to cities with high coastal flooding risks. Accordingly, this thesis presents a novel HTF projection framework and early warning system specialized to model localized HTF frequency into the near future (over the next ~19-year nodal cycle), designed with the specific and unique ability to identify years and months/seasons of the greatest predicted HTF frequencies. The capabilities of the HTF projection framework presented in this thesis were shown by conducting monthly granularity predictions of minor and moderate HTF and presenting seasonal event patterns among the world's top ten popular travel destinations projected to be at the most risk from potential SLR. The data input was drawn exclusively from higher frequency tide gauge records. Novel features of the projection framework included the characterization of intra-annual sea level change (SLC) due to earlier melting periods of sea and land ice, less multi-year ice, delayed freeze-up in the winter, and cascading effects on thermohaline circulation. Another novel method implemented took into account the correlation of astronomical tides with intra-annual sea level variability. Additionally, the methods implemented considered the combined effects of seasonal SLC and modulations by precessions in the Moon's orbital path around the Earth affecting the heights of the highest astronomical tides, while a representation of seasonal extremes in mean sea levels in a second projection of SLC was also included to quantify the upper bounds of projected HTF frequencies. Deterministic seasonal predictions of surge, wave setup, and swash were also implemented.

Large increases in the frequency of HTF were projected during the 2020's in Bangkok and Manila. The following decade, New York City and Jacksonville were projected to suffer increasing HTF frequencies as well. Furthermore, HTF events were projected to be concentrated during particular month(s) or season(s). In Bangkok, 89% of HTF days were projected to occur between October and February. In Manila, HTF frequency was projected to be nearly four times higher between June and August than during any other month. HTF in Jacksonville was projected to be clustered between October and December, while HTF in New York City was projected to be most common in October and December. In addition, surprising differences in intra-annual SLC trends were found mainly in Europe, while effects of lunar precession on high tide levels and thus HTF frequency were found to be widespread; especially noticeable in Bangkok, Cardiff, and Manila. Results were discussed in the context of published existing and planned coastal flooding defense adaptation and mitigation strategies and infrastructure. Results gave insight into years and months of the greatest HTF frequencies in major metropolises over the near future: HTF days in Bangkok were projected to exceed eighty every year between 2025 and 2028, and again in 2036, before reaching one hundred in 2037. December through February were projected to be the most affected months with the majority of days in December experiencing at least minor HTF. Bangkok was found to be the most vulnerable city to HTF in the near future due to unprecedented increases in

HTF frequency combined with unfinished flood barriers, drainage capacity already being consistently overwhelmed by HTF, as well as exponential urban growth and unenforced planning laws. Manila was also projected to suffer unprecedented increases in HTF frequencies during the 2020's, peaking in 2027 and 2028. Summer months were projected to bring the highest frequency in HTF, with up to 10 HTF days per month. Recent local initiatives such as the Manila Bay Sustainable Development Masterplan and the North Manila Bay Flood Protection Strategy were found to be positioned to relocate those living in flooding-prone areas while improving the city's resilience to HTF. In light of the results found here, this dissertation also includes a discussion of further potential in diversifying methods related to the prediction of seasonal surge, wave setup, and swash in the face of existing climatic shifts and changes in thermohaline circulation.

Keywords: *Physical Geography and Ecosystem analysis, High tide flooding, Projections, Adaptation and mitigation strategies, Lunar precession, Nodal cycle, Cycle of lunar perigee*

Table of Contents

Introduction

In the summer of 2021, Thompson et al. predicted a sudden inflection point in mass and unprecedented high-tide flooding (HTF) events in multiple coastal regions of the United States during the mid 2030's, while also describing the impact of the nodal cycle (a rhythmic fluctuation in the Moon's orbital path around the Earth) on the frequency of these events (Haigh et al. 2011, Thompson et al. 2021).

HTF, or so-called "nuisance flooding', results in lasting conditions that impede daily life by flooding roads, driveways and basements, while straining stormwater and wastewater systems. While the impacts of HTF may seem minor, they can create severe problems even outside of hurricane or storm seasons, periodically rendering coastal infrastructure designed to operate within past sea level ranges inoperable. Businesses are interrupted, property values decline while insurance premiums increase, and social and economic activity is stifled (Hino et al. 2019; Collini, 2021).

HTF frequency and severity is very affected by sea level rise; even relatively small shifts in mean sea level can translate to a much greater inland reach of high tides, increasing the severity of individual storm surges and the likelihood of exceeding critical flooding thresholds (Miller et al. 2013; Taherkhani et al. 2020; Andreatta & Kirksey 2022). Global mean sea levels (GMSL) are projected to rise a further 20 – 50 cm and at increasing rates throughout the century, even when following the most stringent emission reduction plans (IPCC, 2019: Summary for Policymakers). This is substantial in terms of impacting HTF frequency, as a sea level increase of less than 10 cm is enough to double HTF frequencies at certain locations (Vitousek et al. 2017; Taherkhani et al. 2020). In addition, regional departures from projections in GMSL of up to 30% due to varying regional thermal expansion, ocean dynamics, land and sea ice loss, and importantly subsidence of land, will cause further increased risk of HTF in certain regions (Oppenheimer et al., 2019). However, it is the combined effect of SLR and fluctuations in the Moon's orbit around the Earth affecting the gravitational force on the oceans that will cause more sudden increases in HTF events and severity (Thompson et al. 2021). There are two precessions in the orbital path of the Moon that specifically affect astronomical high tide heights in a cyclical manner. One is the ~18.61-year nodal cycle (illustrated in Figure 6), and the other is the ~8.85-year cycle of lunar perigee (illustrated in Figures 4 and 5), which affects tides on a ~4.425-year cycle (Haigh et al. 2011). Both have periodical shifts between suppressing and amplifying high tides following a sinusoidal signal. The timing of the amplifying and suppressing parts of these cycles, and indeed their modulating strength on the highest tides vary according to the location on the face of the Earth (Haigh et al. 2011; Ray and Merrifield 2019). Thompson et al.'s (2021) study projects that multiple coastal regions of the U.S. will be hit by such a sudden rise in HTF in the mid 2030's, due to the tide-amplifying phase of the nodal cycle.

Several studies employing global coastal ocean models with characterizations of parameters such as storm surge, wave setup, and bathymetry show that vulnerability to coastal flooding will increase throughout the century as sea levels rise, citing large factors of increase (Tebaldi et al. 2012; Caldwell et al. 2015; Kirezci et al. 2020; Muis et al. 2020). However, past studies focus on

projecting reductions in the return periods of extreme sea level events, and the simulation of extreme sea levels during future decades until the end of the 21st century (Vousdoukas et al. 2016; Idier et al. 2017; Vitousek et al. 2017; Wahl et al. 2017; Kirezci et al. 2020; Muis et al. 2020; Szewczyk et al. 2020; Vousdoukas et al. 2020), which does not communicate expected changes in HTF frequencies critical to effectively planning for projected SLR impacts, or seasonal clustering of HTF events (Thompson et al. 2021). Also, projections over time frames necessary to near-future planning are typically left out, with projections being overwhelmingly focused on the middle and end of the century (Taherkhani et al. 2020). In addition, these studies are based on mean sea level (MSL) rise projections of either decadal or annual granularity, which are typically based on emissions scenarios or extrapolations of long-term (40 – 50 year) trends in local sea levels. Consequently, there is no characterization of intra-annual cycles in climate modulated mean, non-tidal sea level variability. Also, as rates in GMSL rise have been shown to be accelerating (Oppenheimer et al. 2019), the latest trends in sea level change (SLC) are likely to be different from the extrapolations of 40–50-year trends. While some climate models do have the ability to account for seasonal sea level anomalies in certain regions, the model biases in important factors such as sea surface temperature, and timing of the months with the appropriate sea surface temperatures remain widespread (Wang et al. 2022). Furthermore, although the highest resolution models do characterize certain components relevant to sea level at horizontal grid resolutions of up to 25 km (Held et al. 2019; Andrews et al. 2020; Semmler et al. 2020), Strandberg and Lind (2021) have shown that higher horizontal grid resolution does not necessarily improve model agreement with observations. Deriving seasonal and monthly climatic influences on MSL from local tide gauges provides more information to make locally-informed decisions (Dusek et al. 2022). Intra-annual sea level change (SLC) is heavily forced by the annual warming/cooling cycle; warming, expanding, and gaining water from melting sea and land ice in the summer and early autumn, to contracting and losing water as sea and land ice refreezes in the winter and early spring. The effect on MSL is especially strong in the Northern Hemisphere (Commonwealth Scientific and Industrial Research Organisation). Also, an earlier start in the annual melting of sea ice as global mean temperatures warm (at rates that are amplified in the Arctic (Gutiérrez et al. 2021; Griffith and Kozick-Kingston 2022)), less multi-year ice (ice that remains solid for at least one summer), delayed freeze-up in the winter (Zheng et al. 2021), as well as cascading effects on global ocean circulation (thermohaline circulation) (Thibodeau et al. 2018) cause changes in seasonality relating to intra-annual MSL.

To address the lack of existing near-future projections in HTF events, and the lack of extreme sea level projections with yearly and monthly granularity, this thesis presents the first publicly accessible and available projections of continuous, combined yearly and monthly granularity HTF frequencies. In addition, this is also the first study to directly conduct projections for popular travel destinations specifically at the most risk of potential SLR. The capability of the methods applied in this dissertation is show-cased by conducting projections for the top ten major global metropolises at the most risk of potential SLR across the period of the next nodal (19 year) cycle. Also, projections of future frequencies in HTF events have previously not been made outside the United States, nor do most simulations of extreme sea levels and return periods of extreme high-tide flooding events take into account the combined effects of SLR and modulations by precessions in the Moon's orbital path around the Earth (Thompson et al. 2021). Furthermore, changing seasonality in the melting and freezing of sea ice and the effect on intra-annual SLC is accounted for here by a novel method involving the projection of trends in SLC by month, to capture the

effect at each respective location. This kind of look into future conditions, specifically with respect to individual years and seasons of greatest risk, provides a valuable early warning indication for coastal cities to plan for tide-driven flooding increasing in consistency and severity through advances in flooding countermeasures and reorganization of water and waste-management systems, among other mitigation and adaptation strategies to coastal flooding (Ward et al. 2015).

This thesis also utilizes a novel method considering the correlation of astronomical tides with sea level variability (Devlin et al. 2017) by conducting dedicated harmonic analysis on tide gauge data binned by month, as well as including a representation of seasonal extremes in MSL in a second projection of SLC. In addition, seasonal predictions of sea level components attributable to surge, wave setup, and wave swash are included at each location.

The analysis required extensive Matlab programming with more than four-thousand lines of proprietary code and respective data science, applying numerous novel methodologies to realize the following analysis of the chosen GESLA-3 tide gauge data sets. Unlike all other known published approaches to projecting HTF frequencies, this code allows continuous monthly granularity predictions and seasonal event patterns for the first time. HTF events can now be predicted at monthly and yearly resolutions, thus enabling improved early warning capabilities globally.

Aim

The aim of this thesis is to create a novel projection framework and early warning system able to model localized HTF frequency into the near future (over the next nodal cycle), with the specific and unique ability to identify years and seasons of the greatest predicted HTF frequencies, and thus inform locals and travelers, while galvanizing decision makers to implement appropriate mitigation and adaptation measures within appropriate time frames. The model is required to be versatile; able to be adaptable to locations of different tidal cycles, seasonal weather, and coastline/harbor geometry, while retaining the ability to update projections alongside new tide gauge data. Therefore, this thesis seeks to answer the following research questions:

1. How will HTF frequency change in the near future for popular travel destinations at the greatest risk from potential SLR?
2. During which seasons/months will HTF be the most frequent?
3. How large are differences in intra-annual SLC trends?
4. How strong is the modulation of the highest tides by lunar precession?

To answer research questions 1 & 2, HTF projections over the next nodal (~19-year) cycle are made for the world's popular travel destinations at the most risk from potential SLR according to the 2050 Climate Change index. Further details on the calculation of the index are given in the methods. To answer question 3, seasonality and trends in mean monthly sea level are assessed, while the modulation of the highest tides by the nodal and perigean cycles is calculated at each location analyzed to answer question 4.

Background

Sea level at a given coastal location is driven by interactions between astronomical tides, surge, wave set-up, wave swash, and variability in MSL (fig. 1). These components themselves are affected by local coastal geometry, seabed topography, and intra-annual cycles in climate and ocean circulation (for example the El Niño-Southern Oscillation), that bring about changes in sea water temperature, salinity content, weather and wind (Vitousek et al. 2017; Idier et al. 2019).

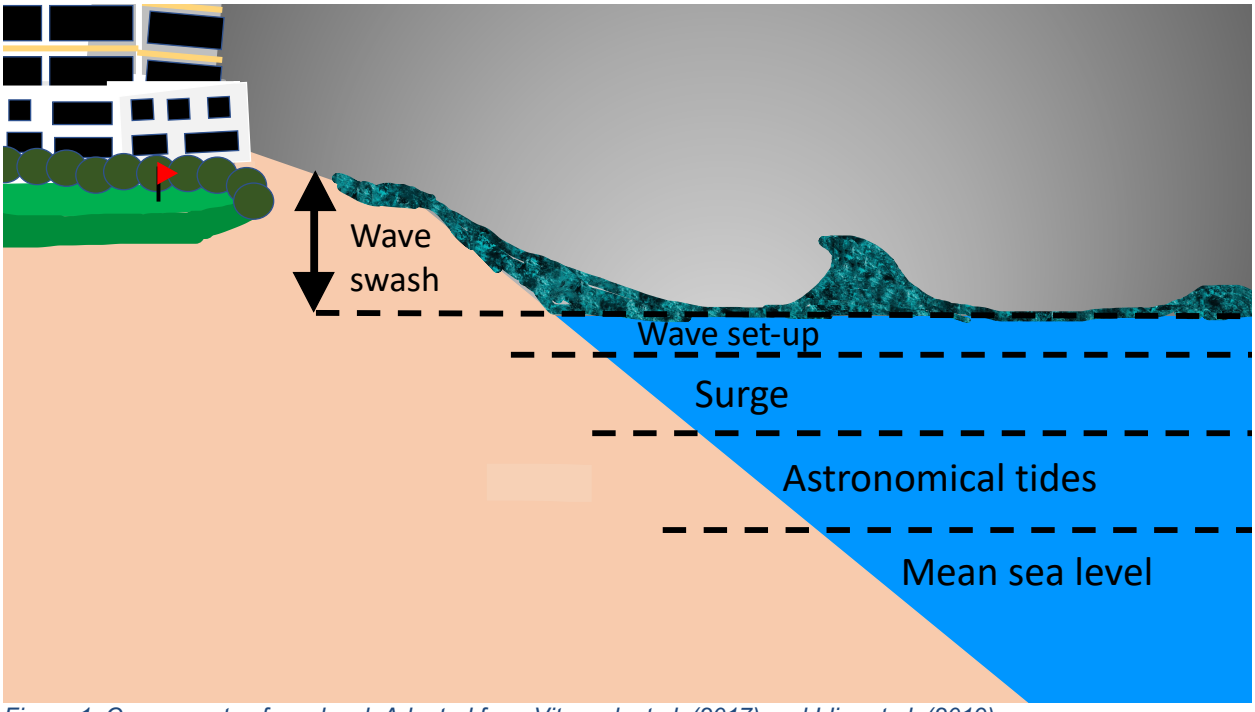

Figure 1: Components of sea level. Adapted from Vitousek et al. (2017) and Idier et al. (2019).

Seasonal changes in MSL are due to cycles in climate; warming and expansion of oceans in the summer, along with melting of sea ice and snow, cooling, and contraction in the winter, along with freezing of sea water and snowfall. These seasonal shifts in climate drive ocean currents and thermohaline circulation, which together with movements of weather events further affect changes in seasonal MSL. Intra-annual to decadal fluctuations in MSL are driven by irregular oscillations in ocean-atmosphere interaction phenomena, including for example El Niño/La Niña events, the North Atlantic Oscillation, the Pacific Decadal Oscillation, and the Indian Ocean Dipole (Commonwealth Scientific and Industrial Research Organisation). Melting sea ice, glaciers, and ice sheets Greenland and Antarctica, as well as thermal expansion as sea surface temperature increases are the main factors contributing to trends in SLR over longer time frames. The interactions between oceans and the Greenland and Antarctica ice sheets represent the largest potential driver affecting potential changes in sea level, although historically glaciers have contributed more to SLR (Commonwealth Scientific and Industrial Research Organisation; Oppenheimer et al. 2019).

Astronomical tides are driven by gravitational forces of the Sun and the Moon pulling on the oceans, or rather the difference in attraction to the attracting bodies (Sun and Moon), across an ocean's surface. As the distance to an attracting body becomes farther away from a location on the

Earth's surface, its gravitational force on the Earth decreases by inverse square (Souchay et al. 2012). Surge is created by storms causing the rise of water above the astronomical tides as strong winds push an accumulating amount of water toward the shore, combining to form a storm tide (Commonwealth Scientific and Industrial Research Organisation). When a storm tide occurs during normal high tide, this is what has the potential to create the most dangerous coastal flooding (Caldwell et al. 2009; Barnard et al. 2015; National Oceanic and Atmospheric Administration of the United States (NOAA) (b)). Wave set-up refers to the temporary increase in water level brought by breaking waves, as opposed to wave set-down, which refers to the temporary decrease in water level during the shoaling process of the wave as water accumulates in the wave, but declines in front of the wave (Bowen et al. 1968; Kireczi et al. 2020; Liu et al. 2020). Swash refers to the motion of water up a beach after a wave breaks (Fairbridge, 1968). Its magnitude is sensitive to geological characteristics, such as beach slope, and it can contribute to coastal flooding by overtopping seawalls (Vitousek et al. 2017); especially during storms, when wave height and frequency increase (Fairbridge, 1968). Harbors and rivers, however, are offered a certain degree of protection, although not immunity, from wind, waves and currents. This means that surge and wave setup components are typically dampened, while swash is not applicable unless the tide gauge is directly on a beach (Thompson & Hadley 1995).

A fluctuation in one of these components can have a range of effects on the others. For example, although SLR tends to increase the frequency, duration, and severity of coastal flooding (Sweet et al. 2014), an increase in water depth due to SLR can have varying effects on tidal range and surge, depending upon multiple factors. The ratio of the local tidal forcing frequency to the period of the respective ocean basin is one example; if this ratio is close to one, meaning the tidal forcing frequency is similar to the period of the basin, then there is a resonance between the two, which creates the largest tidal amplitudes. SLR can either push the ratio closer, or farther away from resonance, resulting in either a greater, or lesser tidal range, respectively. The effectiveness of wind forcing also declines on the larger volume of water, leading to a reduced wave set-up at a similar order of magnitude (Guerreiro et al. 2015; Idier et al. 2019). Storm surges have been found to affect the timing and magnitude of maximum tidal range (Lewis et al. 2017), while waves have been shown to affect tidal energy by up to 20% for extreme wave conditions (Hashemi et al. 2015). For a complete understanding of the mechanisms present in the interactions between sea level components and their orders of magnitude, readers are encouraged to refer to Idier et al. (2019) and Woodworth et al. (2019). The influence of each mechanism is once again affected by local coastal geography and seabed topography.

The orders of magnitude that main sea level components contribute to the total water level at the coast vary according to location. Vitousek et al. (2017) found tides to be the dominant single contributor to total water level at the coasts on average globally, controlling more than half of the variation in total water level, although when combining wave set-up and swash, this was found to be even more influential. Resio & Westerink (2008) found surge to be the main modulator of coastal flooding events (Muis et al. 2016), while Idier et al. (2019) and Woodworth et al. (2019) found that tides and surge tend to dominate globally. Examples of the varying contribution of astronomical tides to total sea level, and contributions attributable to surge, wave set-up and swash at locations examined in this paper are shown below in Figure 2.

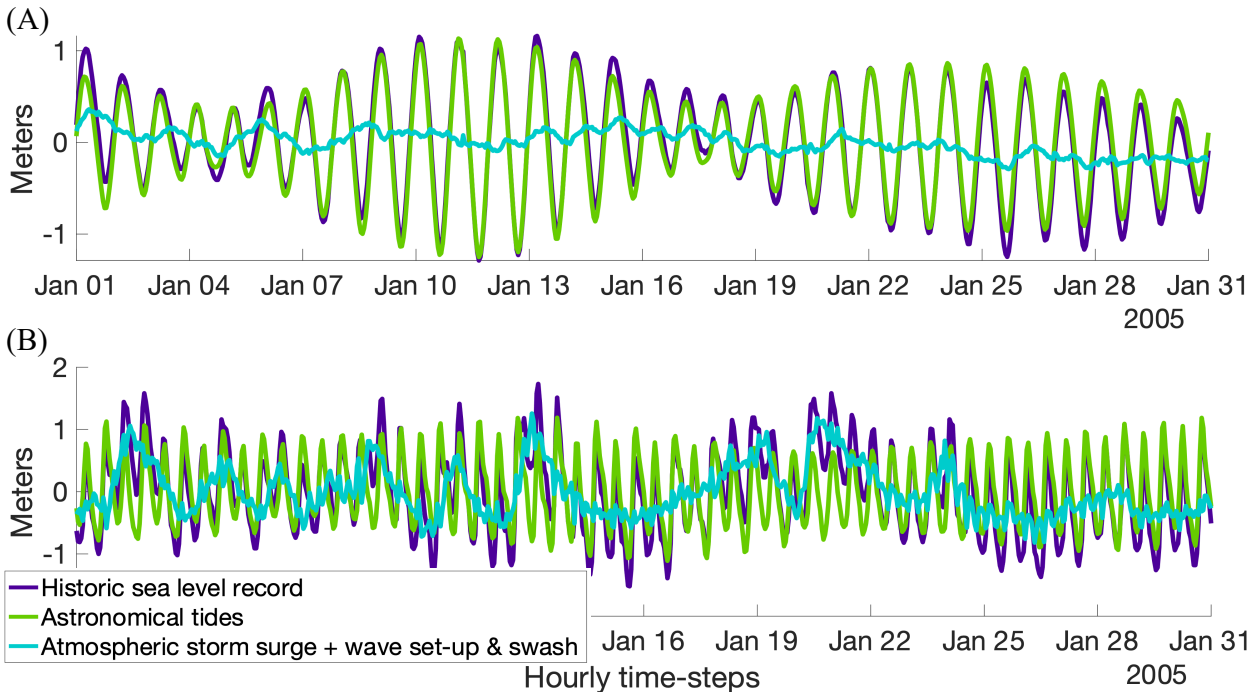

Figure 2: Example showing the varying influence of astronomical tides on coastal sea level at different locations when compared to the combined influence attributed to surge, wave set-up and swash. A) Components of sea level in Bangkok, Thailand. B) Components of sea level in Amsterdam, the Netherlands.

Astronomical tides dominate sea levels in Bangkok, Thailand, while the orders of magnitude are more even to surge, wave set-up, and wave swash in Amsterdam, the Netherlands.

Harmonic Analysis of Astronomical Tides

To determine the phases and amplitudes of astronomical tides from within a sea level record, harmonic analysis is applied to the respective known frequencies of different tidal constituents. Thus, harmonic analysis itself is a kind of signal processing, by which signals are reconstructed

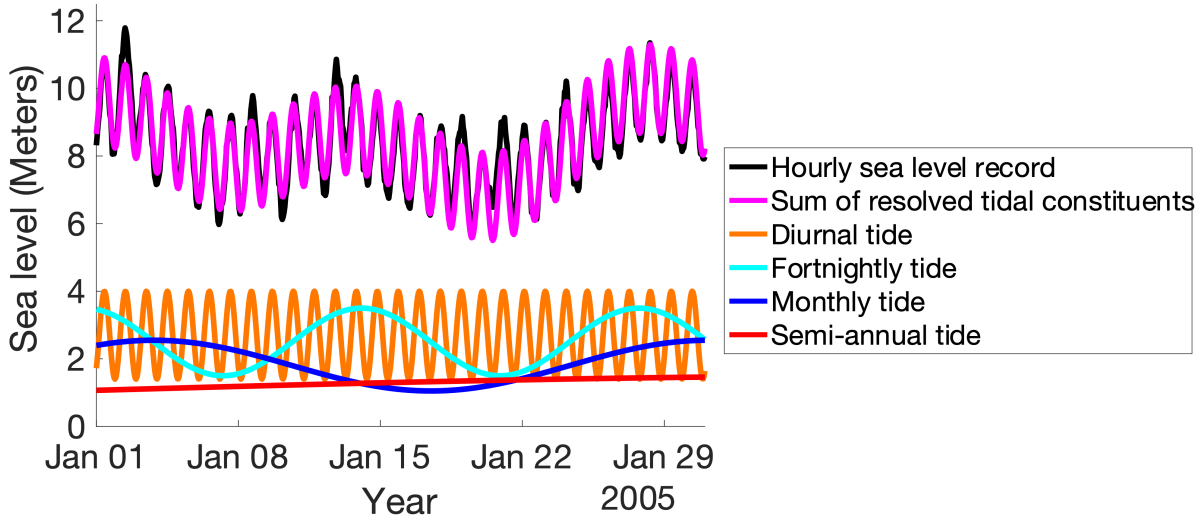

Figure 3: Simplified representation of the harmonics of main tidal constituents resolved over sea level data. The black fluctuations around the superposition of resolved tidal constituents are attributable to surge, wave setup and swash.

by the superposition of waves. For example, the fundamental frequencies of astronomical tides are driven by the "pull" of the gravitational forces of the Sun and the Moon on the oceans as the Earth rotates on its axis. The fundamental frequencies are the lengths in time of the mean lunar day, tropical month, tropical year, the cycle of lunar perigee and the lunar nodal cycle, as well as the cycle of solar perigee, although with its period of 20900 years, the cycle of solar perigee can be deemed to be negligible over the time span examined here (German Federal Waterways Engineering and Research Institute). These frequencies in various combinations make up the main constituents of tides. For a complete overview of the compositions of main tidal constituents, readers are encouraged to refer to the German Federal Waterways Engineering and Research Institute's information on the harmonic analysis of water level. Figure 1 shows a simplified representation of four main tidal constituents resolvable from a sea level record. Once the amplitude and phase of a particular tidal constituent at a respective location is known, this can be projected into the future. Additional frequencies driven by local bathymetric properties known as shallow water constituents can also be resolved through harmonic analysis. Shallow water constituents describe the effect of local coastal bathymetric properties on the motion of water as it approaches the shore (German Federal Waterways Engineering and Research Institute). The frequencies of shallow water constituents are in turn composed of various combinations of main tidal constituents. Components of the sea level record that are unresolvable through harmonic analysis (shown in Figure 1 as the fluctuation of the sea level record above and below the sum of the resolved main tidal constituents), are attributable to the influence of day-to-day weather, including storms (Tebaldi et al. 2012). The fundamental frequencies for gravitational tides are given below in terms of mean solar days (MSD), the standard 24-hour time frame it takes for Earth to perform one full rotation on its axis:

Table 1: The fundamental frequencies of gravitational tides. From the Bundesanstalt für Wasserbau (German Federal Waterways Engineering and Research Institute).

Frequency	***Astronomical time constant***
mean lunar day	1.04 MSD
tropical month	27.32 MSD
tropical year	365.24 MSD
cycle of lunar perigee	period: 8.85 years
lunar nodal cycle	period: 18.61 years
cycle of solar perigee	period: 20900 years

The mean lunar day refers to the time it takes for a point on the Earth to rotate once fully on its axis with respect to the Moon. The tropical month is the time it takes for the Moon to revolve once fully around the Earth, while the tropical year is the time it takes for the Earth to revolve once fully around the Sun. The cycle of lunar perigee refers to a precession of the slightly elliptical path of the Moon's orbit around the Earth; the major axis of which rotates once fully every 8.85 years, affecting tides as a quasi-approximately 4.425-year cycle however, as the major axis of the Moon's slightly elliptical orbit around the Earth lines up with the Earth and the Sun twice during this cycle (Figure 4, the alignment when tidal range is the greatest, and Figure 5, other possible alignments) (Haigh et al. 2011).

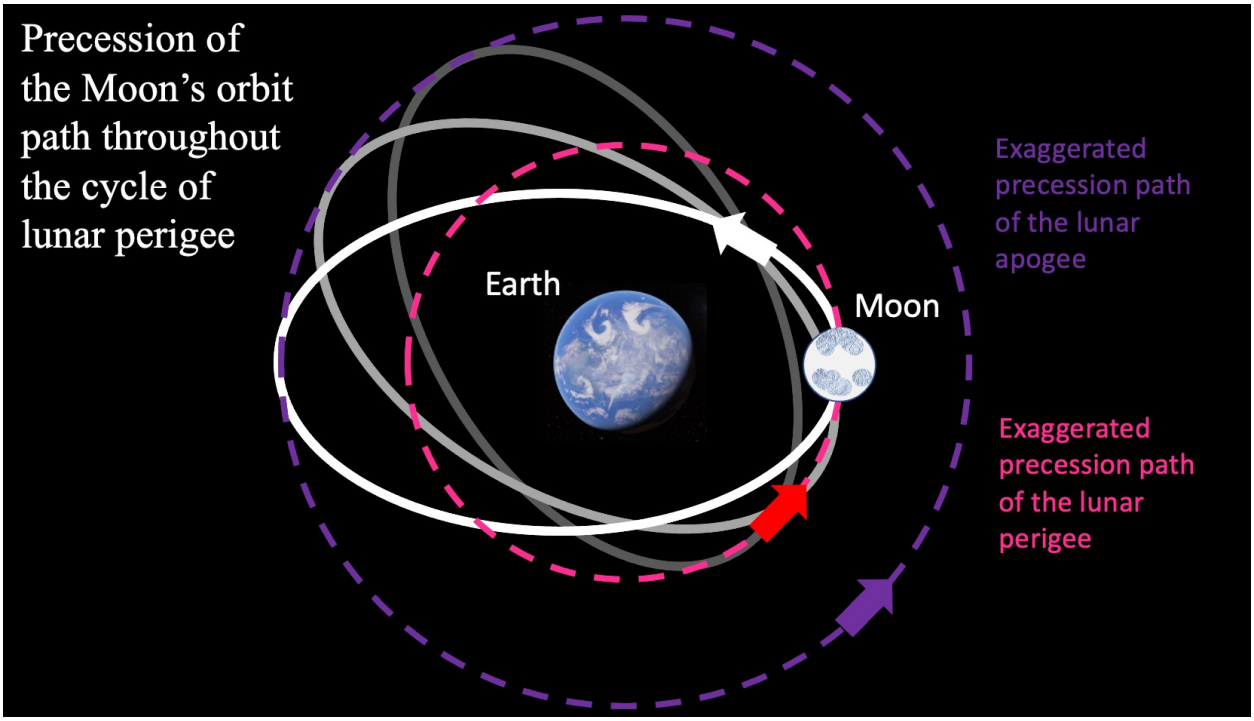

Figure 4: Schematic for the precession of the Moon's orbit described as the "cycle of lunar perigee"; the cycle of the point in the Moon's orbit closest to the Earth. The cycle of lunar perigee thus is the term for the "horizontal" precession of the Moon's orbital path; horizontal being with respect to the plane of the Moon's orbit around the Earth. It takes 8.85 years for the lunar perigee to perform one full revolution around the Earth. Earth is shown from the "top", from the North Pole, with the precession path rotating counterclockwise. The Moon's orbit around the Earth is also counterclockwise. The white ellipse represents the most recent orbital path, and the Moon is at its most recent point of lunar perigee. The ellipsoids representing the lunar orbit are strongly exaggerated. Figure not to scale. Modified from [Orbit of the Moon by Rfassbind]. Wikimedia Commons (https://en.wikipedia.org/wiki/Orbit_of_the_Moon#/media/File:Moon_apsidal_precession.png). In the public domain. *Figure not to scale. The satellite image of the Earth is from Google Earth (Google Earth (a)).*

The alignment of the Earth, Sun, and major axis of the Moon's slightly elliptical orbital path occurs approximately every 4.425 years, and is why the cycle of lunar perigee affects high tide levels at this frequency, as opposed to the full 8.85 years it takes for the major axis of the Moon's elliptical orbit path to perform one full rotation (Haigh et al. 2011; Ray and Merrifield 2019). As the frequencies of the cycle of lunar perigee, the tropical year, and the tropical month are out of phase; meaning that the length of time between an alignment of Sun, Earth, and major axis of the Moon's elliptical orbit occurs at non-consistent time intervals; Ray and Merrifield (2019) have found the mean time period between these alignment events creating the greatest tidal ranges to have been 4.42 years, with a standard deviation of 0.41 years.

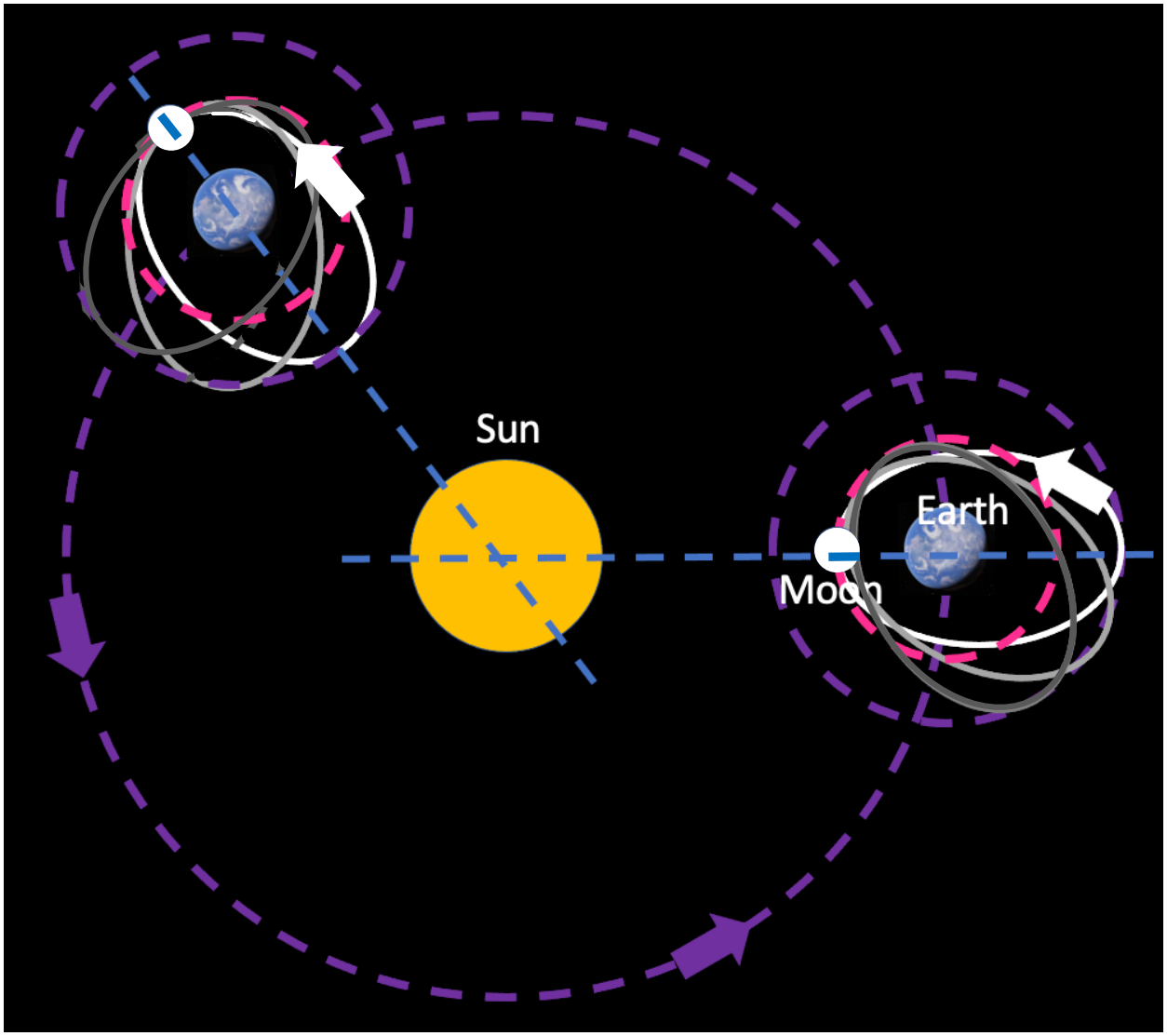

Figure 5: Schematic showing the dynamics of the Sun, Earth, Moon system, and two possible alignments of the major axis of the Moon's elliptical orbit around the Earth with the Earth and the Sun. The Moon orbits in a counterclockwise direction around the Earth, and the Moon's elliptical orbit also rotates in a counterclockwise direction (Souchay et al. 2012). The Earth continues its orbit around the Sun, also in a counterclockwise direction. The dashed, blue lines show the alignment of Earth, Sun, and Moon. Note: the ellipsoids representing the lunar orbit are strongly exaggerated. Modified from [Ray and Merrifield, 2019]. Figure not to scale. The satellite image of the Earth is from Google Earth (Google Earth (a)).

While the cycle of lunar perigee refers to an oscillation in the horizontal boundaries of the Moon's orbital plane around Earth, as shown in Figures 4 and 5, the nodal cycle refers to the vertical "wobble" of the plane, and itself describes an 18.61-year period of precession in the lunar orbit during which the "pitch" of the Moon's orbital plane varies between an inclination and declination of 5°9' respectively to the plane of Earth's orbit around the sun, shown itself in Figure 6 below:

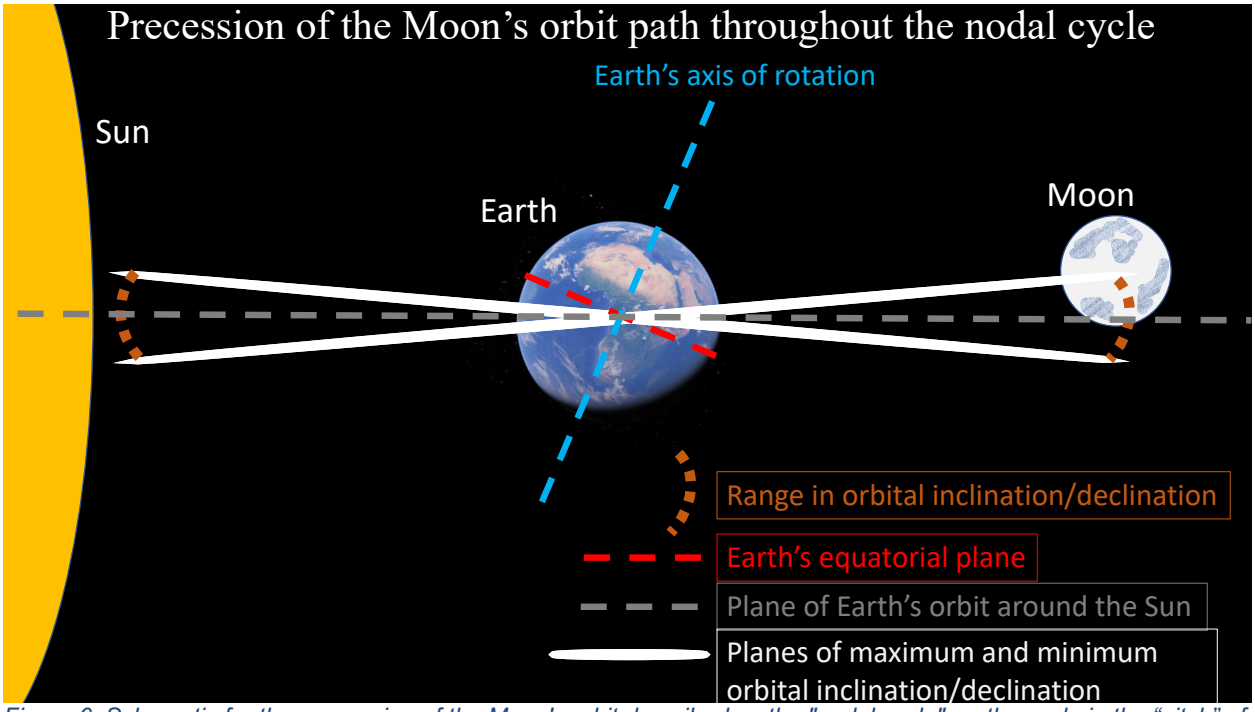

Figure 6: Schematic for the precession of the Moon's orbit described as the "nodal cycle", or the cycle in the "pitch" of the lunar orbital plane relative to the plan of Earth's orbit around the Sun. The nodal cycle thus is the term for the "vertical" precession of the Moon's orbital path; vertical being with respect to the plane of Earth's orbit around the Sun. It takes 18.61 years for the "pitch" in the Moon's orbit relative to the plane of Earth's orbit around the Sun to complete a full cycle. Modified from [Lunar standstill by Another Matt]. Wikimedia Commons (https://en.wikipedia.org/wiki/Lunar_standstill#/media/File:Lunar_standstill.GIF). CC0 (http://creativecommons.org/publicdomain/zero/1.0/). *Figure not to scale. The satellite image of the Earth is from Google Earth (Google Earth (b)).*

The cycle of lunar perigee and the nodal cycle describe the precession, or "wobble" of the Moon's orbit around Earth, which creates a unique pattern of influence at every coastal location; each coast has its own unique tidal signature related to local coastal geometry, seabed topography, latitude, longitude, and other factors (German Federal Waterways Engineering and Research Institute). These cycles in the lunar orbit periodically serve to dampen and amplify tidal range at a respective location and modulate the magnitude of the highest tides (Haigh et al. 2011), which makes them important when it comes to HTF predictions. Notably, modulation by the nodal cycle is projected to outpace the rate of SLR in certain coastal regions of the United States by the 2040's (Thompson et al. 2021). Figure 7 shows the spatial distribution in the magnitude of modulation of the highest tides by both lunar cycles separately.

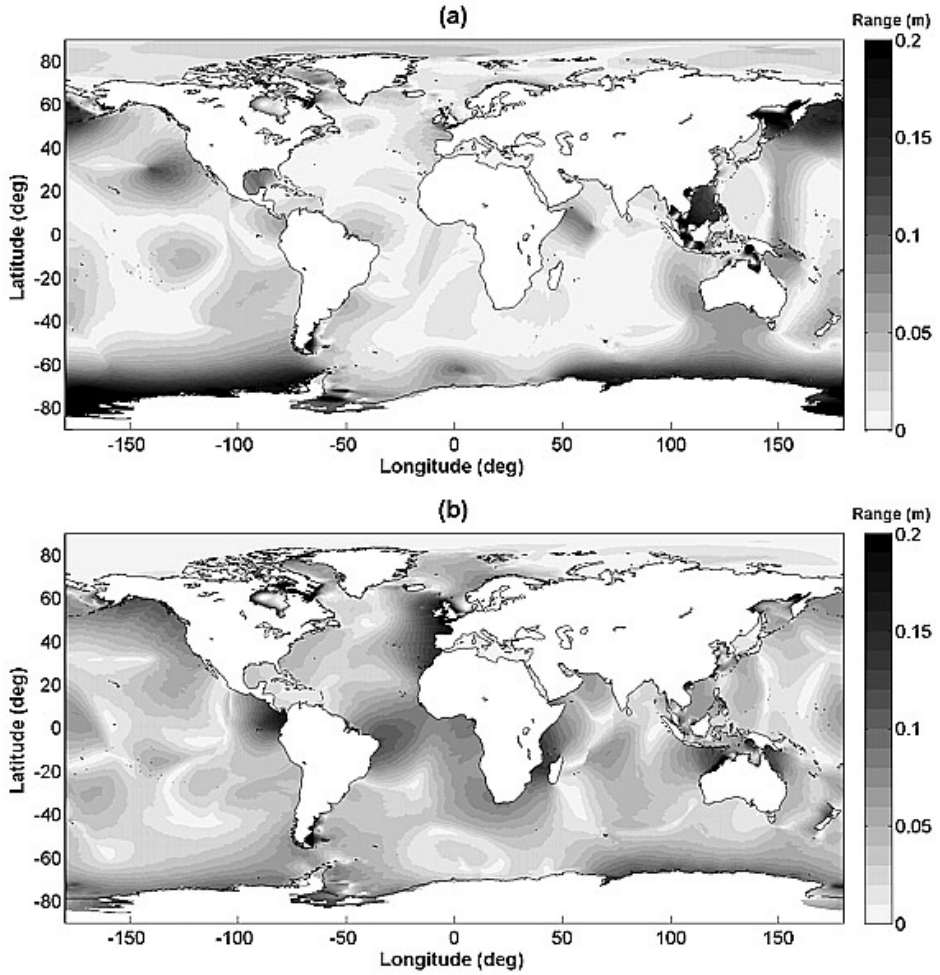

Figure 7: Global modulation range in the 99.9th percentile tidal level by (a), the nodal cycle, and (b), the cycle of lunar perigee (Haigh et al. 2011). Dark areas thus represent the greatest modulation by a lunar cycle. Reprinted with permission from Dr. Ivan D. Haigh.

The cycle of lunar perigee tends to dominate in regions with semidiurnal tidal cycles (meaning two high tides and two low tides daily), while the nodal cycle tends to dominate in regions with diurnal tidal cycles (one high tide and one low tide daily), although this is not always the case, and regions may experience influences from both cycles (Haigh et al. 2011). The cycle of lunar perigee tends to dominate high tide levels along most coasts, with the nodal cycle dominating a lesser sum of coastline, notably in the Gulf of Mexico, the South China Sea and in the Gulf of Thailand (Haigh et al. 2011). A global spatial distribution of the dominating lunar cycle modulating high tide levels from Haigh et al. 2011 is shown below in Figure 8:

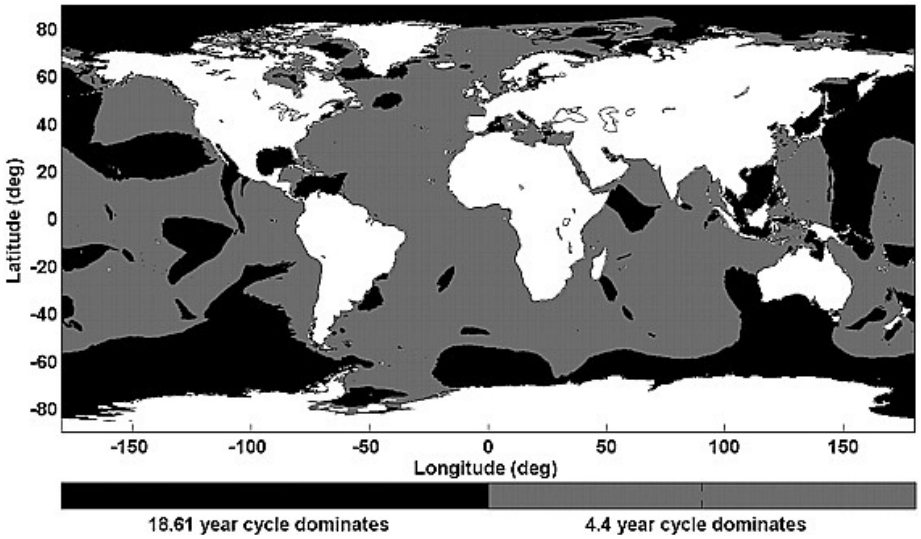

Figure 8: Global distribution of the dominant lunar cycle modulating high tide levels (Haigh et al. 2011). Note: here the the nodal cycle is referred to as the "18.61 year cycle", and the cycle of lunar perigee is referred to as the "4.4 year cycle. Reprinted with permission from Dr. Ivan D. Haigh.

Most coastal regions are influenced at least to a greater degree by the cycle of lunar perigee, while notably the Gulf of Mexico, the Caribbean Sea, the South China Sea, the Gulf of Thailand, the Sea of Japan, the Sea of Okhotsk, and large parts of the Pacific Ocean are modulated to a greater degree by the nodal cycle.

Harmonic analysis nowadays follows the still relevant tidal potential theory first presented by Doodson in 1921, which describes the frequency of each tidal constituent as a linear superposition of the six fundamental frequencies of astronomical tides shown above in Table 1, from which the positions of the Sun and Moon relative to a point on the Earth's surface, tide generating force, and thus tidal potential at that point, can be calculated for any specific time. For an in-depth derivation of the tide generating potential, readers are encouraged to refer to Rahman et al. (2017). Tidal records with data over a complete nodal cycle then allow for the calculation of the modulation (phase and amplitude) at a specific location and allows for their projection into the future (Haigh et al. 2011). For a comprehensive overview of harmonic analysis techniques and its application to tides, readers are encouraged to refer to Foreman and Henry (1989).

Flooding Risks and Adaptation Strategies in Selected Cities

As coastal flood risks show an increasing trend in many regions due to socioeconomic growth, land subsidence, and increasingly, SLR, it is becoming increasingly interesting for coastal cities to conduct cost-benefit analyses of implementing flood defense systems (Dupuits et al. 2017; Amadio et al. 2022). Flood defense systems can consist of multiple lines of defense, with a storm surge barrier in the front, and a levee or dike behind it (Dupuit et al. 2017). However, their construction is often costly, with the strengthening of dikes costing between an estimated 15.5 and 22.4 million Euros per kilometer of length and meter raised in urban areas in the Netherlands at 2009 price levels, although figures of a few million Euros are cited for different types of flood defenses such as levees and concrete flood barriers, with labor costs dictating much of the cost (Jonkman et al. 2013; Cioffi et al. 2022).

Below are brief summaries of implemented and/or planned coastal flooding defense systems of the cities examined in this thesis.

Bangkok, Thailand
Flooding during monsoon rain events is common, and HTF periodically overwhelms drainage capacity, so the more than 30 agencies for water management set up in the wake of extreme flooding in 2011 are required to employ stop-gap solutions to provide relief during flood events, while construction of long-term defense systems is thus delayed. A flood prevention system in the form of flood barriers installed along all waterways in Bangkok is planned, however remains a work in progress. Flood gates and water pumping stations to drain water into the Chao Phraya River are active, while another water pumping station is under construction, and several are planned, as high tides often overwhelm current drainage capacity. In addition, exponential urban growth and unenforced planning laws are cited as factors leading to increased risk in the future, as wetlands offering natural water retention and flooding buffers continue to be lost to buildings and infrastructure (Thai PBS World (a) 2022; Thai PBS World (b) 2022).

Amsterdam, the Netherlands
Holland is the gold-standard when it comes to flood management and coastal engineering. A system of dams, dikes and storm barriers are the adaptive measures that have been taken to allow the country to coexist with the sea, and with its tides. In addition, a nature-based solution of adding a "ramp" of grass-covered clay to the seaward side of dikes has also been implemented, which dampens wave impact during storms, and protects the dikes against erosion (Van Loon-Steensma and Vellinga 2019).

Cardiff, United Kingdom
Flooding in Wales due to heavy rainfall, rapid snowmelt, and storm surge has become more common. In response, the Welsh Government in collaboration with the Cardiff council is set to approve a new flood defense system to protect properties in south-east Cardiff from SLR and one in 200-year flooding events until the end of the century. The defense system will include rock barriers and embankments along the coast as well as sheet piling in select locations, and is scheduled to be completed in 2025 (Cardiff News Room 2022).

Manila, the Philippines
The Manila Bay is already very affected by HTF, with the islands in the Bulacan Province being inundated by every high tide. Land subsidence further exacerbates the problem, with groundwater pumping resulting in a declining water table and compression of soils, effectively adding to rising sea levels. The loss of protective mangrove forests due to both natural causes such as extreme weather, as well as human-driven removal to make way for farming and aquaculture have further increased vulnerability to flooding (Goldberg et al. 2020). Mangrove forests dissipate waves and storm surges; reducing wave energy by two-thirds within the first one-hundred meters of forest width, while protecting vulnerable coastal soils from erosion (Menéndez et al. 2020). This combined with the on average twenty annual typhoons affecting the city, as well as expected urban growth bringing the total population to nearly twenty million people by 2050 results in a real task for planners and the Government of the Philippines (Delano 2022).

The Philippines Department of Public Works and Highways built a seawall along the coastline of the Manila Bay as a part of the Manila Bay Integrated Flood Control, Coastal Defense & Expressway project, although there remain gaps and communities unprotected by the seawall (Delano 2022). Furthermore, the National Economic and Development Authority (NEDA) together with the Government of the Kingdom of Netherlands (through the Ministry of Foreign Affairs) initiated the formulation of Manila Bay Sustainable Development Masterplan (MBSDM) in 2018, and completed it in 2021, aiming to relocate residents, settlers and their businesses away from areas that are prone to flooding. In addition, the North Manila Bay Flood Protection Strategy has been outlined in 2022, including sustainable, nature-based flood protection measures, and the recommendation of pilot locations for their implementation to reduce flooding exposure particularly in the northern coastal area. A combination of geospatial data and stakeholder interviews have led to a comprehensive plan to combat the risks from storm surges and fluvial flooding while restoring natural habitat and transforming and adapting the livelihoods of locals and especially those that are encouraged to move out of hazard-prone areas (Royal HaskoningDHV, 2022). Tablazon et al. (2015) have also created probability-based storm surge inundation maps of the capital region of the Philippines; Metro Manila, by employing frequency distributions of different storm surge heights above maximum astronomical tidal heights in relation to a digital terrain model.

London, United Kingdom

The water level in the Thames river flowing through London is tide-driven, with a tidal range of up to seven meters; tidal flooding from the North Sea has been a growing risk (Lavery and Donovan 2005; EnvironmentAgencyTV 2022). The construction of the Thames Barrier, eight other flood barriers, hundreds of kilometers of flood walls and embankments as well as flood gates and pumps provide a good standard of flood defense. The adaptive Thames Estuary 2100 Plan also has provisions for securing land to improve and raise flood defenses from 2035 to 2050 (Environment Agency 2012).

Hamburg, Germany

Hamburg lies on the Elbe river, which is a tidal waterway with a mean tidal range of 3.66 meters (Port of Hamburg, 2022). Storms can cause surges that cause flooding in parts of the city. Hamburg is protected by linear flood defenses such as sea and estuarine dikes, coastal dunes and flood defense walls, as well as more recent, innovative designs such as artificial sand terraces to loft new structures high above the high-water line (Yeung 2021). This is important, as a study by Naulin et al. (2015) investigated the reliability of flood defenses in Hamburg through breach modeling with probability-based storm surge scenarios and sea states, finding that extreme conditions can cause dikes to fail by wave overtopping and even overflow and overloading of dike slopes during such events.

Philadelphia, United States

Although Philadelphia is not located directly on the coast, tidal modulation of water levels in the Delaware and Schuylkill Rivers can create flood conditions around the city. Philadelphia is projected to suffer more than two hundred HTF days by 2045; in response, the city plans to introduce wetlands to buffer the city from the sea (Union of Concerned Scientists 2016). Higher baseline river levels may permanently flood parts of the city, while increases in precipitation coupled with coinciding storm surges and high tides can increase the frequencies and severities of

flooding events, with extreme storm events having already become more common in the 21st century (Flood Risk Management Task Force, City of Philadelphia 2014). A report from NOAA confirms that Philadelphia will see an increase of flood days by 2050 (Sweet et al. 2019).

To improve Philadelphia's flood mitigation planning, a forum hosted by the American Society of Civil Engineers called for the strengthening of existing flood defense systems and innovation in reducing vulnerability to future flooding, while encouraging coordination between agencies involved in flood risk management nationally (Flood Risk Management Task Force, City of Philadelphia 2014).

New York City, United States
New York City has faced climate change and resulting extreme events; the impact of Hurricane Sandy in October of 2012 claimed lives, caused billions of dollars in damage, damaged water and sewer infrastructure, and affected economic activity. SLR is already causing a greater frequency in HTF events in Atlantic and Gulf Coast cities in the United States, while SLR projections in New York exceed the global average, with HTF expected to flood twenty percent of Lower Manhattan's streets and affect ten percent of its properties by the end of the century if adaptation is not adequate (New York City Economic Development Corporation 2019).

The city has implemented a climate adaptation program encompassing policies to anticipate risk from and improve resilience to SLR (Aerts and Wouter Botzen 2011), while the "Big U" project designed to prevent flooding began in 2018; itself a sixteen-kilometer barrier wrapping around the southern part of Manhattan. The barrier itself is not a traditional barrier, but is made up of pavilions, museums, and public spaces, thus being a holistic strategy to flood protection (Hobson 2014; Howarth 2018).

Jacksonville, United States
The East Coast of the United States is experiencing record-breaking tides, with tides trending higher and higher due to a combination of SLR, tropical storms and astronomical high tides, which is expected to only get higher and more frequent. In Jacksonville, the National Weather Service of the United States is issuing more coastal flood advisories than during past years (Voyles Pulver 2019).

Jacksonville city leaders in collaboration with local organizations and the Environmental Defense Fund advocating climate resilience for all communities are implementing measures increasing resilience to sea level rise and flooding in the form of natural barriers and buffers such as the protection and planting of mangrove forests and the restoration of creeks and wetlands around the urban core of the city (Environmental Defense Fund Florida 2023).

Hong Kong, SAR China
Flood risk in Hong Kong is increasing due to SLR, climate change induced frequency of tropical cyclones and strong storm surges, and subsidence of land, while a continued influx of workers and investment further increases the number of people vulnerable to such events (Bailey 2011; Seto 2011; Qiang et al. 2021). When storm events coincide with astronomical high tides, low-lying areas are flooded (Lui 2018).

In response, Hong Kong has incorporated Flood Risk Management practices with engineering-based methods. The city has an underground stormwater drainage system, while alteration of natural waterways to increase discharge capacity has also been pursued extensively (Qiang et al. 2021) This together with walls and breakwaters attains a protection standard of one-in-one-hundred to one-in-two-hundred year flooding events. Furthermore, the Town Planning Board must be approached with a Drainage Impact Assessment by representatives involved in development plans in Hong Kong to ensure that flooding risk to the area does not increase under proposed projects. Preparedness and awareness of communities in regard to flooding is also prioritized, with tide and storm surge early warning provided to residents. Emergency response drills in areas prone to flooding are also conducted once annually. Channel embankments have also been reinforced through the planting of vegetation, while wetland introduction providing a flooding buffer has also occurred, further complementing engineered drainage infrastructure (Chan et al. 2018).

Despite this, Hong Kong is not immune to flood events, which do still occur during heavy storms. In addition, the Planning Department in Hong Kong does lack authority beyond the consideration of drainage ordinance in new projects. For example, it is not authorized to restrict projects in flood zones: spatial plans for Hong Kong in 2030 include proposed ambitious expansion into flood-vulnerable areas on reclaimed land (Chan et al. 2018).

Methods

Selection of Cities

The cities selected for analysis were initially chosen to be the top 10 popular travel destinations at the greatest threat of flooding from projected SLR. Rankings come from the 2050 Climate Change City index, which ranks the threat to popular major global metropolises by vulnerability to climatic shifts likely to occur in the future. Flooding from projected SLR is one of three risk criteria, along with climate shift, and water stress. Potential SLR impact scores are based on a calculation of how much of each city (area) would be affected by rising sea levels and coastal flooding under a "Business as usual" SLR scenario by Kopp et al. 2014, in relation to a digital elevation model of a respective city.

All cities included in the analysis were required to have consistent, quality-controlled sea level data in the GESLA-3 database over at least a full (~19 year) nodal cycle. Tide gauge data was required to be recent enough to project at least ten years into the future. Of the top 10 major global cities expected to suffer the most flooding due to SLR, several lacked the consistency and/or recency in data needed to conduct a projection of future HTF. Shown below is an overview of popular global metropolises ranked by their potential SLR impact score.

Table 2: Ranking of the world's 85 most popular travel destinations by threat of potential SLR by 2050. Rankings come from the 2050 Climate Change City Index. The data range represents the most recent available data covering a full nodal cycle (19 years) at each location, and the projection period is the next full nodal cycle for which HTF events were projected. An "x" denotes unsatisfactory data availability. The number in parentheses next to the ranking represents the new ranking taking into account data accessibility.

Ranking	*City*	*Country*	*Potential SLR Impact Score*	*Data range*	*Projection period*
1	Bangkok	Thailand	100	2000 - 2018	2019 - 2037
2	Amsterdam	Netherlands	89.56	1999 - 2017	2018 - 2036
3	Ho Chi Minh City	Vietnam	88.67	x	x
4 (3)	Cardiff	UK	45.88	2002 - 2020	2021 - 2039
5	New Orleans	US	37.37	x	x
6 (4)	Manila	Philippines	37.01	1996 - 2014	2015 - 2033
7 (5)	London	UK	28.49	2002 - 2020	2021 - 2039
8	Shenzhen	China	28.06	x	x
9 (6)	Hamburg	Germany	24.48	2001 - 2019	2020 - 2038
10	Dubai	United Arab Emirates	20.84	x	x
11	Belfast	UK	20.39	x	x
12 (7)	Philadelphia	US	18.34	2002 - 2020	2021 - 2039
13	Dublin	Ireland	16.88	x	x
14 (8)	New York City	US	16.09	2000 - 2018	2019 - 2037
15 (9)	Jacksonville	US	15.94	2002 - 2020	2021 - 2039
16 (10)	Hong Kong	SAR China	15.27	2000 - 2018	2019 - 2037

Tide gauge records with denoted data ranges and projection periods met the data requirements, while tide gauge records missing these specifications lacked sufficient recency, data quality, and/or length. The first 10 popular cities at the most risk of SLR meeting the data requirement were chosen for the analysis.

Shown below are the locations of the cities included in this thesis by region, along with the tide gauges chosen at each location. Tide gauges were chosen by (1) data quality, (2) proximity, and (3), similarity in coastal geometry to at the location of the city. If no tide gauge within the sphere of similar coastal geometry at a respective city fulfilled the data requirements, then HTF was not projected for the city. A global map of cities examined in this thesis is shown below in figure 9. The most at-risk cities in the US are shown in Figure 10 with the location of their corresponding

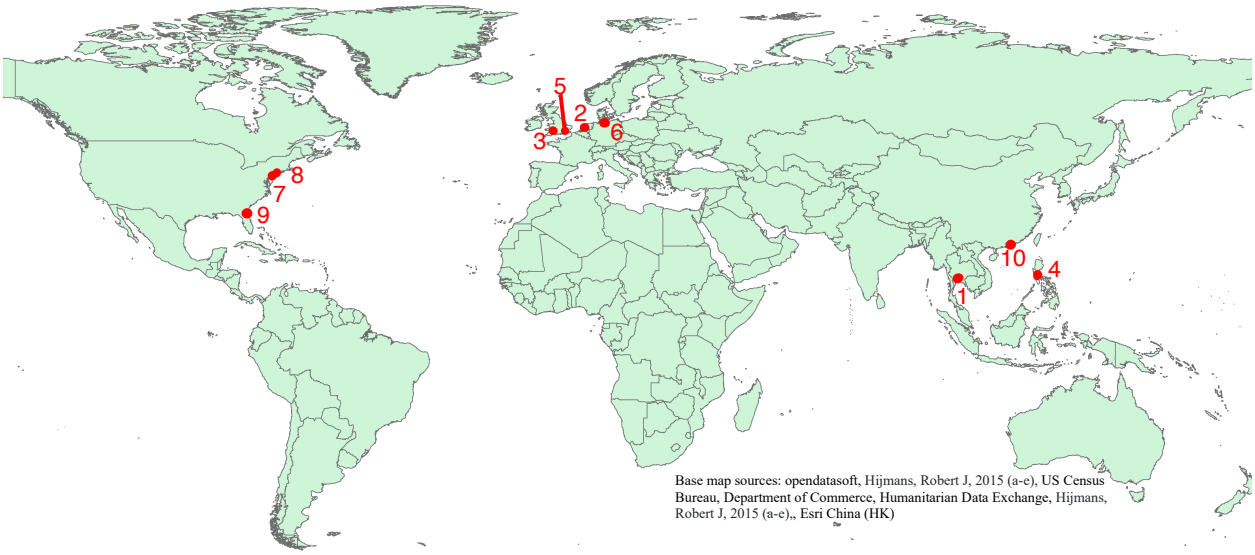

Figure 9: Map of chosen coastal cities for which HTF projections were conducted in this thesis. Cities are numbered according to their ranking from Table 2.

available tide gauges. Philadelphia and New York City had tide gauges with sufficient data local to the city, while for Jacksonville the closest tide gauge fulfilling data requirements was near the mouth of the St. Johns River, which flows through Jacksonville, emptying into the Atlantic Ocean. The most at-risk cities in Europe with acceptable data are shown alongside in Figure 10. Sea level data for Amsterdam was represented by the Ijmuiden-Buitenhaven tide gauge at the harbor entry.

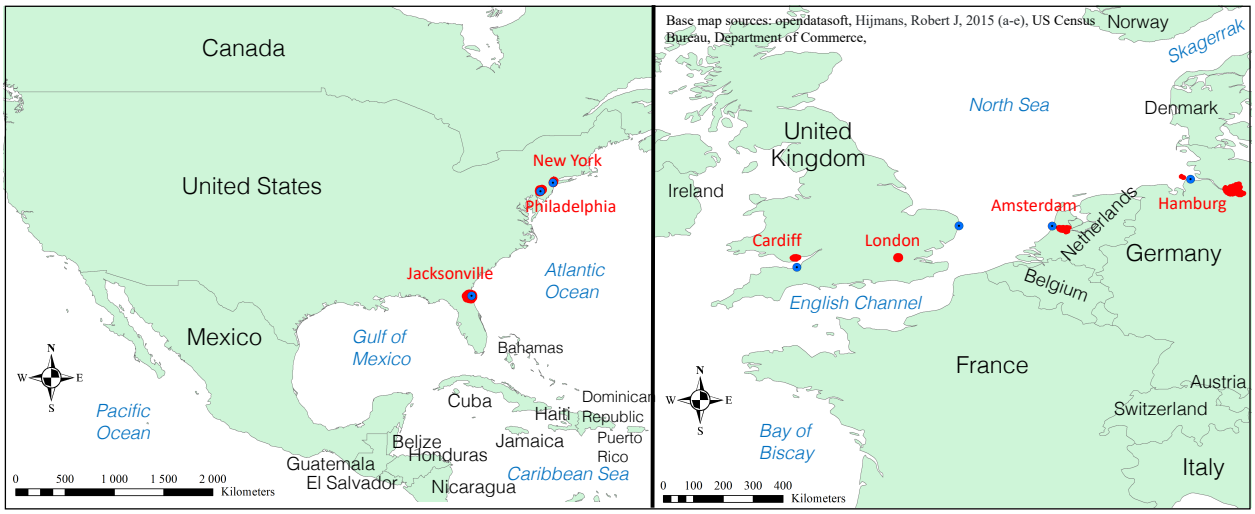

Figure 10: Map showing coastal cities examined in the US (left) and Europe (right), in red, along with respective locations of tide gauges with sufficient data, in blue.

For Cardiff, the nearest station meeting the data requirements was at Hinkley Point, roughly 25 kilometers across the Bristol Channel from Cardiff. For London, the nearest station meeting data requirements was at Lowestoft, roughly 170 kilometers north-east of London. For Hamburg, no riverine tide gauges were available on the Elbe River, so the tide gauge at Cuxhaven-Steubenhoft, near the mouth of the Elbe, was chosen.

The most at-risk cities in Asia for which tide gauge data of acceptable quality was found are shown in Figure 11. Tide gauges meeting the data requirements were available locally for Hong Kong and Manila, while the nearest tide gauge meeting data requirements for Bangkok was available from Ko Lak, 200 kilometers south south-west from Bangkok itself.

Figure 11: Map showing coastal cities examined in Asia, in red, along with respective locations of tide gauges with sufficient data, in blue.

Projection of Future HTF Days

The projection method was based upon a monthly dedicated reconstruction of tidal constituents resolvable from the tide gauge record, and a deterministic, monthly prediction of surge, wave setup, wave swash, and tidal constituents unresolvable from the tide gauge record, as well as extrapolation of underlying monthly trends in SLC.

Tide gauge records stemmed from version 3.0 of the Global Extreme Sea Level Analysis project's (GESLA) dataset released in November of 2021, which features consolidated, quality-controlled tide gauge data from around the world of at least hourly resolution (Caldwell et al. 2015; Woodworth et al. 2017; Haigh et al. 2021). Coastal cities selected for analysis were popular travel destinations designated to be at the most risk from potential future SLR by the 2050 Climate

Change City Index, which ranks the top 85 global travel destinations by risk to different climate change indicators. Sea level records over the last full nodal cycle available from respective tide gauges were analyzed, which resolved each fundamental frequency of gravitational tides at least once, (except for the cycle of solar perigee, assumed to be negligible over the period examined here). Tide gauge locations were checked in Google Maps and on the Permanent Service for MSL to verify their location (Woodworth and Player, 2003; Holgate et al. 2011), and all months included in the analysis were required to have at least 40 percent quality-controlled data; months missing more than this were excluded from the initial analysis.

The tide gauge records were first filtered to remove unreliable data, and then binned by month, thus forming twelve separate datasets. Each dataset was then detrended by monthly mean sea level (MMSL). From the MMSL values, linear trends were fitted to each dataset and extrapolated, forming future mean sea level projections. An estimation of the extreme range of MMSL anomalies was included by adding maximum historical residuals in MMSL to the linear projections. From the detrended data, the dominating astronomical tidal constituents were calculated separately by harmonic analysis for each dataset. From this, the dominating astronomical tidal constituents were projected into the future by their detected phases and amplitudes and superimposed upon each other. Furthermore, a percentile time series analysis of annual 99th percentile astronomical tidal heights was conducted, to which the harmonics of both lunar precessions described earlier were fitted. Then, terms describing the phases and amplitudes of modulations of tidal heights by lunar precession were superimposed upon the main tidal constituents, while historical values of sea level components surge, wave setup, and swash were calculated by observing fluctuations in tide gauge records around the detected tidal constituents. The projected detectable tidal constituents and their variation in amplitude across the twelve, monthly datasets were then added to their respective historical values of surge, wave setup, and swash, and separately to the two MMSL projections previously described to calculate monthly and annual HTF counts (days with minor and/or moderate HTF threshold exceedances). This created, for the first time, a detailed, continuous projection of HTF events on a monthly granularity, as well as a seasonal description of which months can be expected to see the greatest number of these events.

The projection method is described and motivated in detail below:

Detrending by MSL

Each dataset was binned by month to isolate the effects of seasonal cycles in climate and their cascading influence on interactions between sea level components described in the background under Figure 1, as well as resulting seasonal changes in the geometry of harbors and estuaries; specifically changes in the depth and width of channels, which leads to altered tidal velocities and resonance (described in the background on page 11), which affect tidal amplitudes (Friedrichs and Aubrey 1994; Winterwerp & Wang 2013; Guerreiro et al. 2015; Talke et al. 2021). Then, each of the twelve tide gauge records binned by month was detrended by subtracting the MMSL to separate the astronomical tides from non-astronomical components influencing MSL, including SLR. Tebaldi et al. (2012) employ detrending of raw data prior to their extreme value analysis of high-water events, while Thompson et al. (2021) also detrend prior to estimating tidal constituents. This created a less cluttered signal for harmonic analysis by allowing for a more accurate representation of the sea level patterns of tidal components non-related to changes in MSL, and indeed the

amplitude of each resolvable tidal constituent, as tidal amplitude is correlated with changes in MSL due to factors such as altered frictional effects, and the local ocean basin's resonance response (Pelling and Green 2014; Devlin et al. 2017).

Tidal amplitude is also known to be correlated to changes in coastal geometry; notably changes in harbor structure and river channel geometry, as well as seasonal differences in weather (Tebaldi et al. 2012; Talke et al. 2021, Thompson et al 2021). Variability in coastal geometry and weather have a direct influence on atmospheric storm surge, wave setup and swash where applicable (tide gauges located in a harbor are offered a certain degree of protection, although not immunity, from wind, waves and currents (Thompson & Hadley 1995)), along with tidal amplitude (Idier et al. 2017, Kirezci et al. 2020). While it is difficult to account for all uncertainty related to these factors and their influence on high-tide levels in the future, detrending by monthly MSL and performing harmonic analysis on monthly binned tide gauge records, as well as capturing seasonal differences in surge, wave setup and swash, river discharge where applicable (Devlin et al. 2017), and the resulting forcings on interactions between sea level components captured seasonal differences in the above-mentioned factors that were also then implicit in the projected sea level.

Deriving Major Tidal Constituents

The phases and amplitudes of tidal constituents acting at a given location were derived by harmonic analysis of the detrended, monthly-consolidated tide gauge record over the latest complete nodal cycle (19 years) available from tide gauge data. Harmonic analysis was conducted separately for each monthly-consolidated sea level record in order to account for seasonal cycles in MSL and related effects on the amplitudes of tidal constituents. Harmonic analysis was conducted in Matlab via an implementation of UTide, using the iteratively-reweighted least-squares method to limit sensitivity to outliers in tide gauge data when estimating tidal constituents (Codiga 2011). Only major constituents with signal-to-noise ratios (SNR) greater than two were included in the analysis, which is standard practice in harmonic analysis (Codiga 2011, Thomspon et al. 2021). The SNR is the squared ratio of the amplitude of a possible detected tidal constituent, to the error in the amplitude (noise around the signal) (Pawlowicz et al. 2002). Tides are dominated by only a few constituents at a respective location, while others are minute and difficult to detect. Thus, there are typically a handful of constituents with a clear a signal, and many that are barely detectable (Godin 1986).

Following harmonic analysis, the amplitudes and phases of the dominating tidal constituents and their seasonal variability were known, and these were then superimposed on each other seasonally to reconstruct the tidal record with the detectable tidal constituents. From this, the sea level components attributable to weakly influential tidal constituents, as well as surge, wave setup and swash were isolated. A deterministic prediction of sea level components mainly attributable to seasonal cycles and weather was made by taking the difference between the superimposed amplitudes and phases of tidal constituents detected through harmonic analysis, and the tide gauge record. This part of tide gauge record historically driven by seasonal cycles in climate and weather was estimated by month to capture seasonal differences, while the harmonic analysis; also done by month, captured interactions between surge and waves typical of a certain season and tidal energy.

Secular Local Mean Sea Level Rise Projections

In projecting sea level rise into the future, twelve linear trends of localized mean monthly sea level over the historical period were extrapolated into the future to serve as a baseline for the future projection. As the harmonic analysis was carried out by month to account for seasonal cycles in climate, so too were linear trends in MSL extrapolated for each month individually to account for seasonal patterns modulating mean, non-tidal sea level variability. Changes in the patterns of sea ice melting (earlier start in the melting of sea ice in the year due to rising temperatures as global mean temperatures warm (at rates that are amplified in the arctic (Gutiérrez et al. 2021; Griffith and Kozick-Kingston 2022)), less multi-year ice (ice that remains solid for at least one summer) and delayed freeze-up in the winter (Zheng et al. 2021) cause cascading effects on global ocean circulation (thermohaline circulation) (Thibodeau et al. 2018), which in turn cause feedback loops in complex interactions occurring between different parts of the hydrological cycle, ocean-atmosphere interactions, and ocean properties causing different patterns and trends during the different seasons creating varying trends in the net effect on MSL (Commonwealth Scientific and Industrial Research Organisation) that need to be accounted for. SLR models continue to be plagued by gaps in observations, data-poor regions, as well as uncertainty in interactions of relevant processes and high sensitivities to processes which are not yet fully understood (Oppenheimer et al. 2019). Instead, interactions between the above-mentioned processes implicit in the tide gauge data for the city in question and in trend analysis over different seasons and months when projecting into the future were the chosen method here.

Extrapolating linear trends over time-series of tide gauge data spanning fifty years is a common way to project rates of SLR into the future (Tebaldi et al. 2012). Here, a time-series over the latest 19 years of data covering the latest full nodal cycle was used in order to balance (1), observing more recent trends in SLC than those observed over fifty years, (2) performing harmonic analysis on a tide gauge dataset with each major frequency of gravitational tides being resolved at least once (the cycle of solar perigee is deemed to be negligible), and (3), being able to conduct an analysis for the cities expected to be most at risk from potential SLR, even if long-standing, tidal records that go back many decades are not available. Using historical MMSL information allowed for local interdecadal oscillations and the variation in winds, currents, sea surface temperatures, and other dynamic factors that they drive to be resolved multiple times throughout the historical period, effectively cancelling out biases present in shorter time-series.

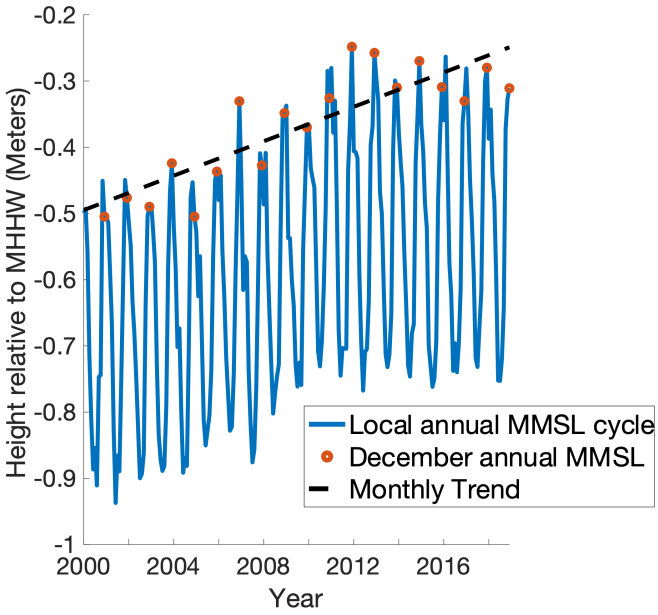

Figure 12: Annual cycles in the historical MMSL record between 2000 and 2018 used to represent Bangkok, Thailand. Sea level is relative to the local mean higher high water (MHHW) index defined below in the section "Projecting counts of HTF days". The linear trend shown for MMSL during December is shown, highlighting the high MMSL during that month when compared to the rest of the record.

Figure 12 shows an example of seasonal cycles present in MMSL, with the month of December clearly showing consistently high mean sea levels.

In projecting tidal variability into the future, extrapolating linear trends of MSL per month under a detrended tidal analysis also accounted for the general, local relationship between MSL and the amplitude of tidal constituents, which is also related to water depth and stratification (Thompson et al. 2021).

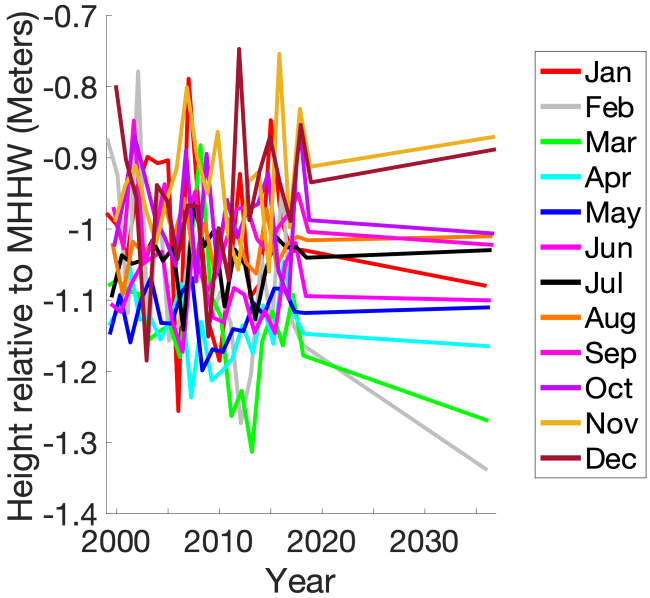

Figure 13: Historical MMSL in Amsterdam, the Netherlands and extrapolated linear trends showing the seasonal variation.

Thermal expansion of water, vertical land movement along the coast due to glacial isostatic adjustment, depletion of ground water, gravitational and rotational effects of melting glaciers and ice sheets and other drivers contributing to variation and uncertainty in local projections of sea level rise were also implicitly represented in the linear trend over 19 years of tide gauge data (Tebaldi et al 2012; Thompson et al. 2021). The IPPC's chapter on SLR and Implications for Low-Lying Islands, Coasts and Communities states that numerical models simulating SLR continue to be hampered by observational gaps and under-sampled regions, as well as uncertainty in factors related to the measurement of thermal expansion, subsidence and high sensitivity to different possible responses of the Antarctic Ice Sheet to future climate, while ice sheet models lack realistic representations of certain physical processes (Oppenheimer et al. 2019). While local SLR scenarios do exist for parts of the world, notably those from the NOAA for the coastal regions of the United States (Sweet et al. 2017), SLR tends to be given by fixed amounts per decade, which does not account for seasonal differences existing for example in Amsterdam, shown in Figure 13, or periodic extremes in sea level variability shown below in Figure 14.

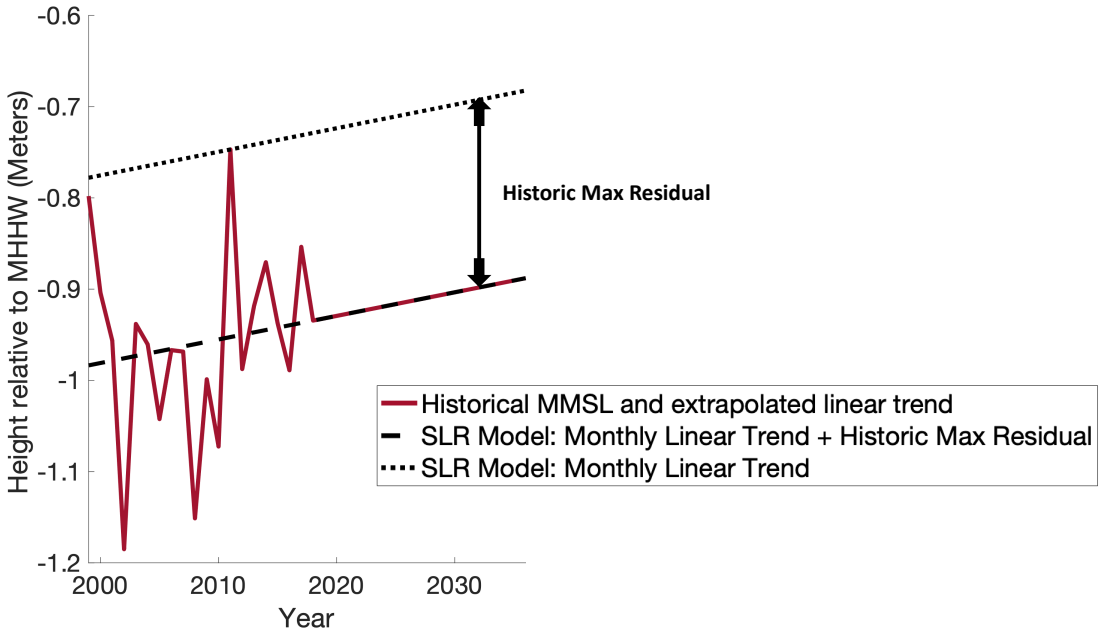

Figure 14: Schematic of the SLR model made to represent maximum positive historical residuals in MMSL. Extreme years in MMSL are missed by a linear trend; In the year 2011 the MMSL was much higher than it would otherwise be projected to be in 2030.

To account for a portion of the variability in local mean monthly sea level and differences in rates of seasonal SLR, the local linear rate of SLR over the historical period was calculated for each month individually and extrapolated into the future at each location. In addition, another SLR model including maximum historical residuals in MMSL to quantify the predicted MMSL component with overshoots of linear trends of the same magnitude as recorded over the historical period was implemented to represent future mean sea levels if an overshoot of the same magnitude were to occur in future years.

This accounted for variability in MMSL, specifically representing the upper projection range of possible mean sea levels.

Projecting Counts of HTF Days

To construct the projection of future total sea level, the amplitudes and phases detected at the frequencies of the dominating tidal constituents were translated across the next nodal cycle with UTide's nodal/satellite correction capability to account for modulation by the nodal and perigean cycles in the orbit of the Moon (Codiga, 2011). Nodal/satellite corrections are done by accounting for the instantaneous positions of the Moon and the Sun relative to a position on the Earth and the resulting impact on potential tidal force. This is done by continuously calculating (1) mean lunar time, (2) mean longitude of the Moon, (3) mean longitude of the Sun, (4) mean longitude of the lunar perigee, (5) longitude of the Moon's ascending node (related to the nodal cycle), and (6) mean longitude of the solar perigee, occurring at the fundamental frequencies of gravitational tides shown in table 1, to correctly project tidal constituents into the future.

The influence of both the lunar perigean and lunar nodal cycles on the highest tides at each location was then checked through the fitting of the frequencies of both harmonics to the 99th percentiles of annual astronomical tidal heights across the latest nodal cycle (example shown in Figure 15) available from the tide gauge data. The phases and amplitudes of detected lunar precessions were projected into the future to show the timing in years of increased modulation by these cycles on high tides, and thus increased risk of HTF frequency.

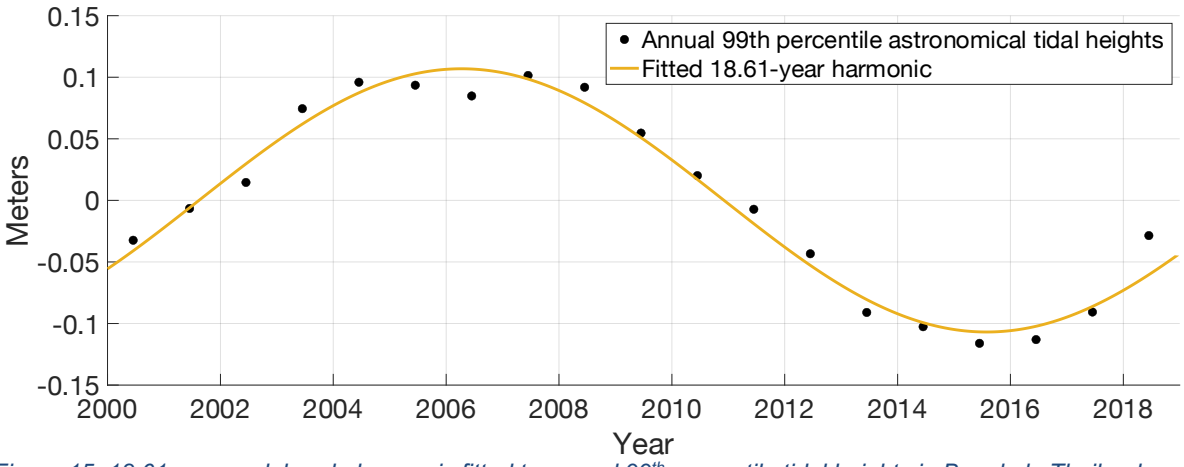

Figure 15: 18.61-year nodal cycle harmonic fitted to annual 99th percentile tidal heights in Bangkok, Thailand.

The projected detected tidal constituents were then combined with the deterministic, seasonal prediction of surge, wave setup and swash. One projection was made with the extrapolated linear trends in MMSL from the historical period added to the main tidal constituents and deterministic prediction of the other components, and another with the historical maximum residual added to the extrapolated linear projections, to duplicate the historical exception in MSL to the future, as a representation of the highest scenario of future MMSL.

Coastal flood events are typically graded by exceedance of a flooding threshold, which itself is typically linked to the local mean higher high water (MHHW) tidal datum height (Sweet et al. 2017; Thompson et al. 2021). The local MHHW tidal datum represents the average of the higher high-water height (the highest tide recorded) over each tidal day during the last Tidal Datum Epoch, which is normally calculated over twenty-year intervals, the latest being 2000 to 2020

(Sweet et al. 2017). Here it was calculated over the last nodal cycle (19 year) period available from respective tide gauge records.

Minor and moderate flooding thresholds were taken from the lower bounds of those used in Thompson et al. (2021), which originate from the American National Oceanic and Atmospheric Administration, and represent 0.5, and 0.8 meters above the local MHHW tidal datum respectively. These are values tailored to coastal regions of the United States that were applied here to the rest of the world, due to the lack of defined thresholds at other locations.

Total counts of days exceeding minor and moderate flooding thresholds were calculated per month; the sea level was required to reach above a flooding threshold at least once during a day to count as a flooding event.

HTF events were summed by month in order to give an understanding of which seasons historically experience the greatest number of flooding events, and how this is expected to change over the next nodal cycle. HTF events were also summed annually to further visualize projected future coastal flooding frequencies to historical frequency.

As new tide gauge data becomes available, projections can easily be made over the updated period of the nodal cycle.

Deriving Lunar Nodal and Perigean Modulations

Modulations in high tide levels by lunar precession were calculated by the percentile time series analysis method common in sea level research (Woodworth and Blackman 2004; Haigh et al. 2011; Thompson et al. 2021). The 99^{th} percentile of gravitational tidal heights was calculated annually, which equated to roughly the seven highest hourly tides every month. Haigh et al. (2011) measure even higher at the annual 99.9^{th} percentile level, which equates to the highest eight hourly tides annually. Here, a more conservative level was used to estimate the influence of the nodal and perigean cycles on more consistent tidal levels as opposed to only the highest ones. Haigh et al. (2011) specifically conduct a global assessment of the influence of the precessions in the lunar orbit (nodal and perigean cycles) on the highest tides, while here the goal was to look at the frequency in flooding, and so the focus was not on extreme events, but on the modulation of consistent high tide levels and their frequency.

A sine curve was fitted to the time series of the historical 99^{th} percentile annual gravitational tidal heights by non-liner least squares regression (Figure 15) to find the phases and amplitudes of the nodal and perigean harmonics at a respective location. The detected phases and amplitudes of the tide-modulating precessions in the lunar orbit path were then projected over the next nodal cycle to visualize the years when the nodal and perigean cycles will amplify high tides. This was then combined and compared with the magnitude of local rates of SLR described by linear models.

Results

HTF Projection

HTF projections are presented in the order of cities expected to be most at risk from potential SLR as ranked by the 2050 Climate Change Index. Bangkok is listed as the top city at risk from rising sea levels.

Top 1: Bangkok, Thailand

A projection of future annual HTF counts affecting Bangkok (Figure 16) showed a clear, sudden increase with HTF frequencies three to four times higher than during the 2000's and 2010's becoming common in the 2020's. In addition, projections in Figure 18A showed that the frequency of HTF days per month will effectively double during the 2020's when compared to the prior two decades, surpassing twenty HTF days per month during the most affected months.

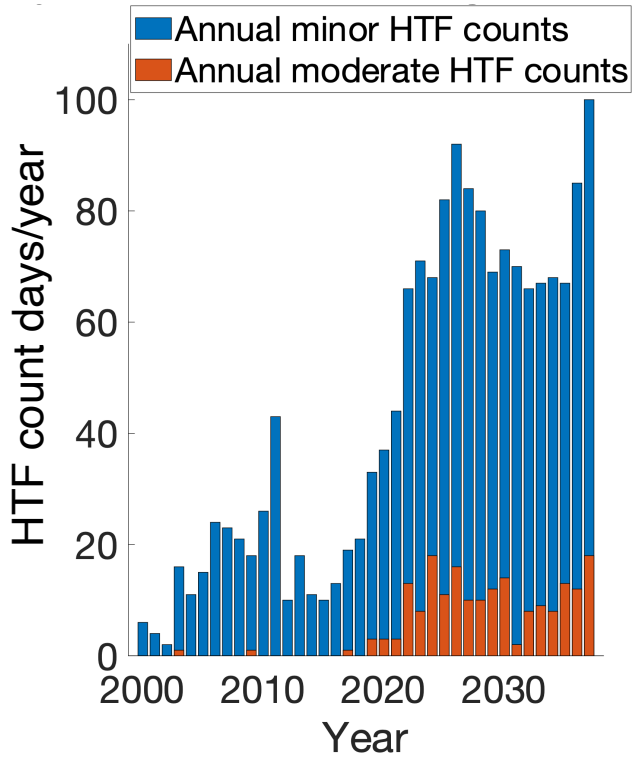

Figure 16: Historic and projected annual counts of HTF in Bangkok, Thailand. Annual projections in HTF days were based on the linear trend model for MMSL and did not take into account historic residuals in MMSLs.

Increases in the frequency of HTF events were also projected to be clustered during one season as opposed to being evenly distributed throughout the year (Figure 17), with the vast majority of HTF days expected to be during the northern hemisphere's winter, with January and December projected to be especially affected. An average December and January until 2037 was projected to have triple the amount of HTF days as between 2000 and 2018.

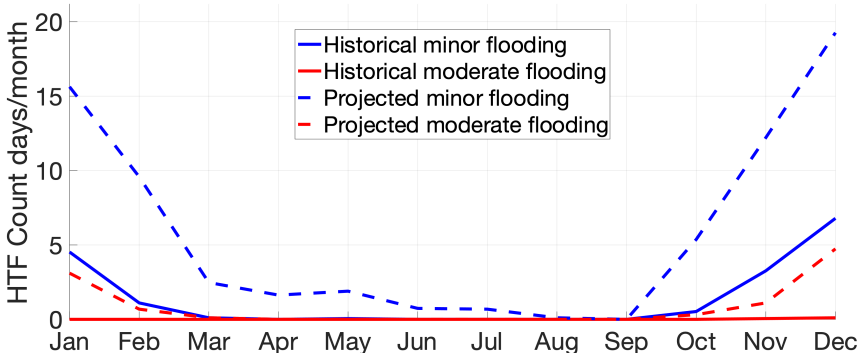

Figure 17: Average historical and average projected seasonal cycles in the frequency of HTF events in Bangkok, Thailand. Average historical seasonal HTF frequency was calculated over the latest nodal cycle available from tide gauge data, and the average future projected seasonal HTF was calculated over the next full nodal cycle.

A sea level rise scenario incorporating the magnitude of historical overshoots in the linear trends in MMSL was projected to further add to clusters of both minor and moderate flooding events (Figure 18B), with especially pronounced moderate flooding of ten days per month or more between 2025 and 2030, and again from 2035.

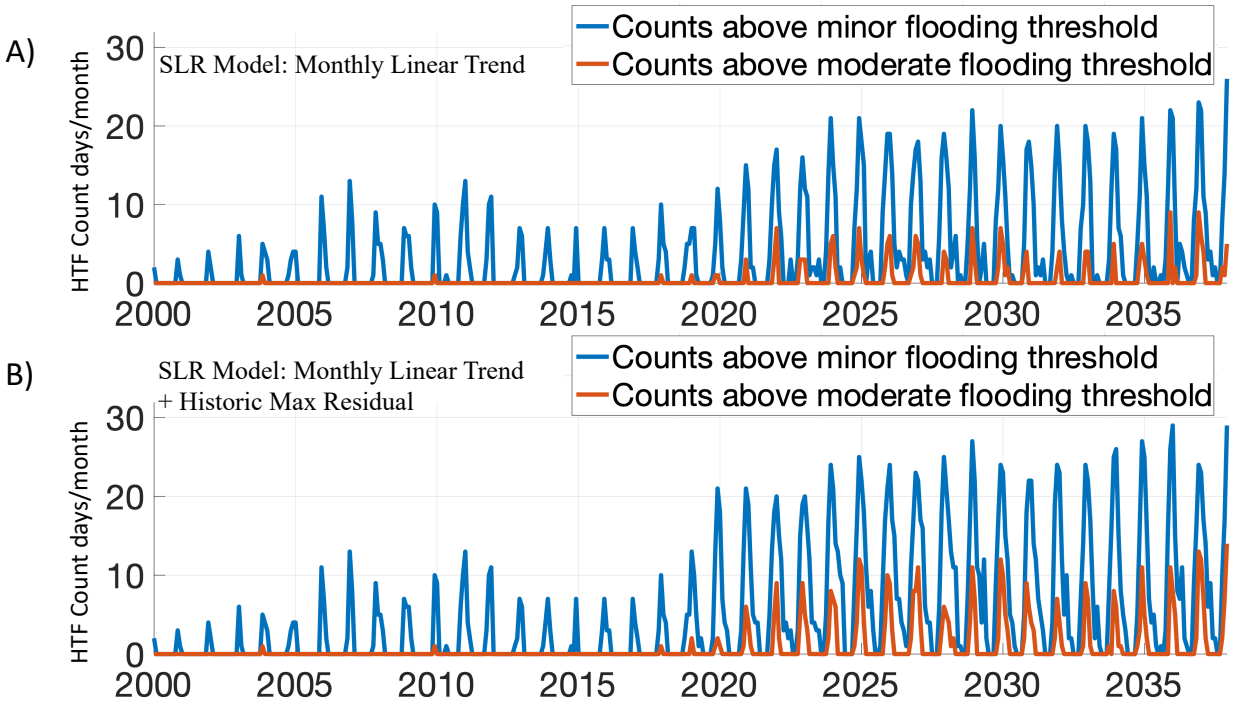

Figure 18: Time series of the historical and projected HTF event frequency in Bangkok, Thailand. Figure A assumes a linear form in the trends of MMSL, while Figure B accounts for maximum residuals in MMSLs.

Modulation of HTF by lunar precession was visible in annual (Figure 16) and monthly (Figures 18A and 18B) granularity projections, coinciding with the combined harmonic signals of lunar precession shown in Figure 19A and 19B. The nodal cycle was projected to amplify high tide levels in the 2020's, and dampen high tides in the 2030's, effectively canceling out much of the projected SLR during the first half of the 2030's. Figure 18 shows the clear uptake in HTF frequency in the 2020's amplified by lunar precession, and a stagnation in increasing projected HTF in the first half of the 2030's dampened by lunar precession, followed by another uptake towards the end of the projection, when the nodal cycle will begin to move towards the half of its

cycle amplifying high tides again. The nodal cycle was found to be the dominating precession in the lunar orbit modulating high tide levels in Bangkok (figure 19). The amplitude in the modulation of high tide levels by the nodal cycle was found to be 10.7 cm; high tide levels in Bangkok were found to be amplified by a maximum of 10.7 cm by the nodal cycle. Maximum amplification of

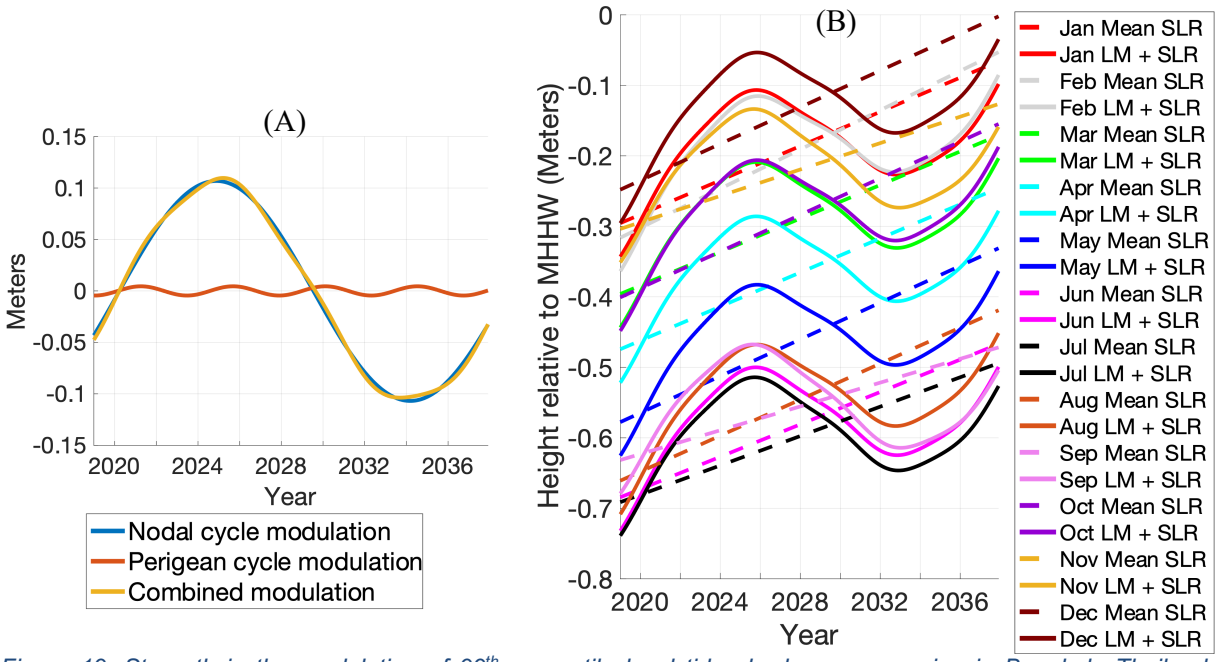

Figure 19: Strength in the modulation of 99th percentile level tides by lunar precession in Bangkok, Thailand. A) Separate and combined modulation in strength and signal for the nodal and perigean cycles. B) Combined effect of lunar precession on the highest tides and seasonal SLR. SLR projections represent the linear extrapolation from historical data.

high tides by the perigean cycle by comparison was found to be negligible. Rates of SLR by month were found to range from 8.0 (September) to 13.2 (February) cm per decade, by comparison. Historical measures of MMSL and their extrapolated linear trends are illustrated below in Figure 20, showing overall SLR during all months at a rapid rate. Variability in MMSL was found to be low, with only small fluctuations; average residuals in MMSL were found to be between three and five centimeters.

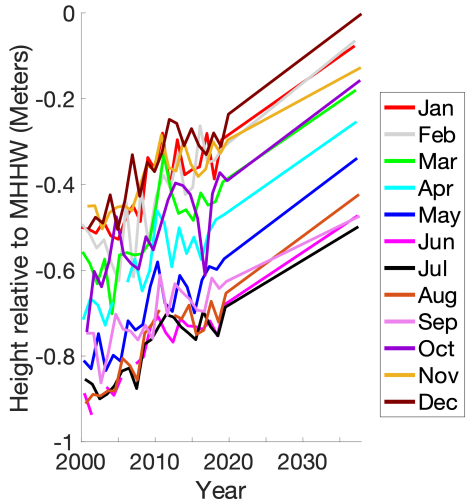

Figure 20: Historical MMSL in Bangkok, Thailand and extrapolated linear trends.

Top 2: Amsterdam, the Netherlands

Amsterdam is number two on the list of cities most at risk from rising sea levels. A time-series of historical and projected total annual HTF events showed, however, that annual frequency in both minor and moderate flooding events will remain similar, and even decline until the mid 2030's (Figure 21).

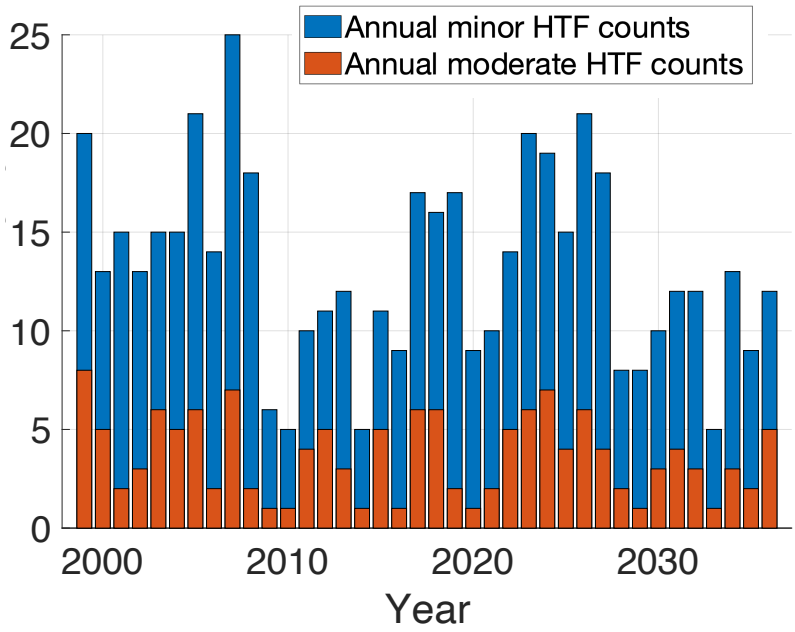

Figure 21: Historic and projected annual counts of HTF in Amsterdam, the Netherlands. Annual projections in HTF days were based on the linear trend model for MMSL and did not take into account historic residuals in MMSLs.

The seasonal distribution of HTF events will also remain similar, with the majority of HTF projected to continue occurring in the winter, with low frequencies of minor flooding events in spring and fall, and almost none in summer, as illustrated in Figure 22. A slight shift of HTF events from January and February to November and December was projected.

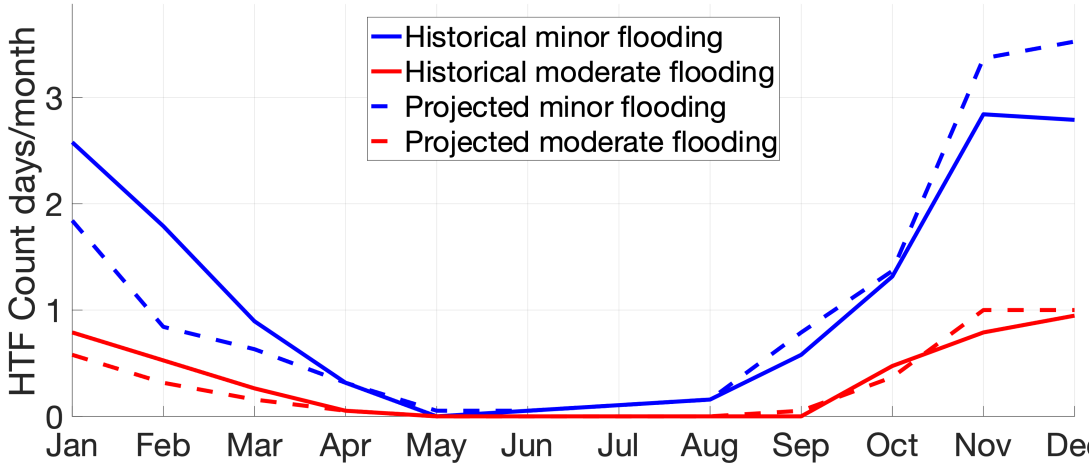

Figure 22: Average historical and average projected seasonal cycles in the frequency of HTF events in Amsterdam, the Netherlands. Average historical seasonal HTF frequency was calculated over the latest nodal cycle available from tide gauge data, and the average future projected seasonal HTF was calculated over the next full nodal cycle.

A time series of past and projected HTF counts shown in Figure 23A showed a similar result. Frequencies in monthly HTF were projected to remain similar over the next nodal cycle as to between 1999 and 2017, following a linear projection of SLR in MMSL. When historical maximum residuals, or extreme years in MMSL were taken into account (Figure 23B), winters between 2022 and 2027/2028, as well as the winter of 2031/2032 were projected to see higher frequencies in HTF days than during the previous nodal cycle.

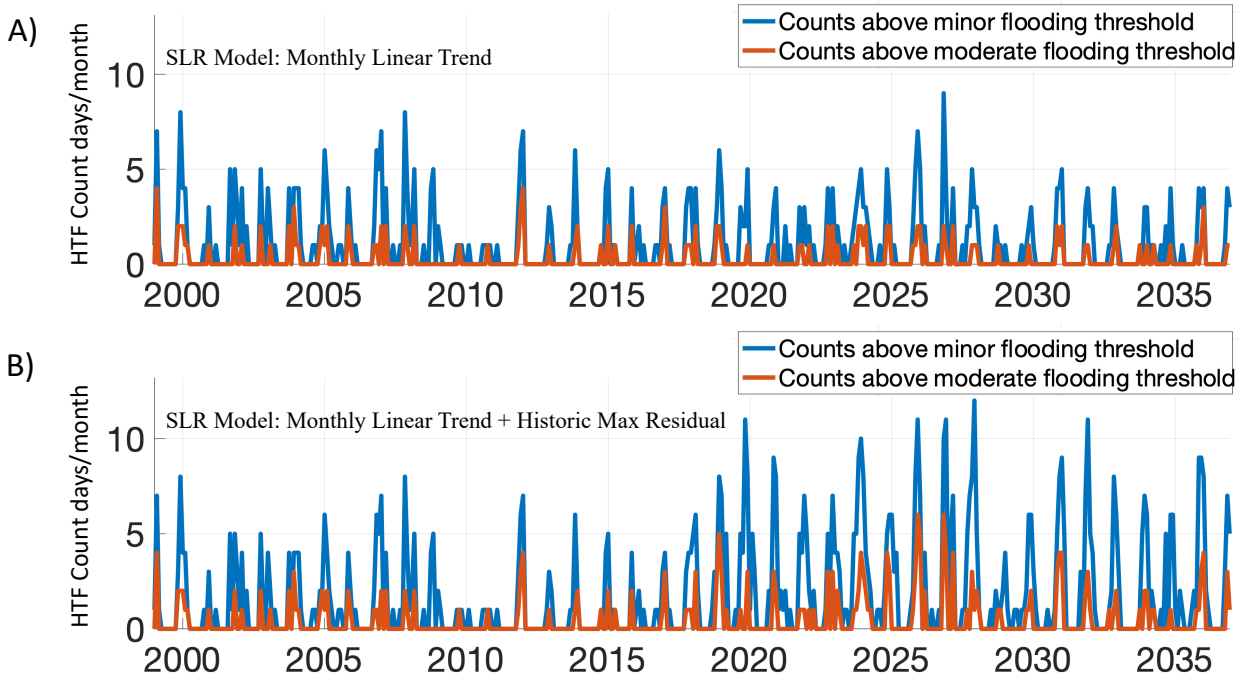

Figure 23: Time series of the historical and projected HTF event frequency in Amsterdam, the Netherlands. Figure A assumes a linear form in the trends of MMSL, while Figure B accounts for maximum residuals in MMSLs.

Figure 24 shows that modulation of astronomical tides by lunar precession in Amsterdam was found to be relatively weak. The nodal cycle was found to amplify local tides by only around 1.2 cm. The perigean cycle was found to modulate astronomical tides by less than a cm. Both cycles were projected to combine to slightly dampen high tides until 2030, before slightly amplifying high tides from 2034 to 2036.

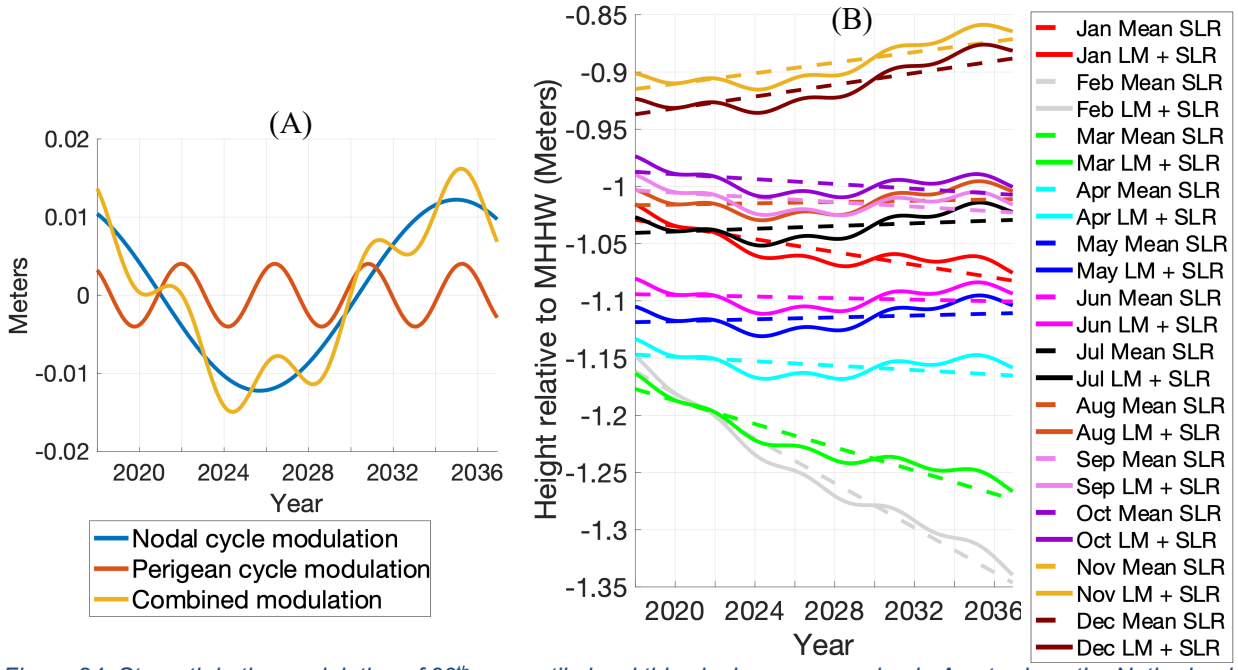

Figure 24: Strength in the modulation of 99th percentile level tides by lunar precession in Amsterdam, the Netherlands. A) Separate and combined modulation in strength and signal for the nodal and perigean cycles. B) Combined effect of lunar precession on the highest tides and seasonal SLR. SLR projections represent the linear extrapolation from historical data.

The nodal cycle was found to be the dominant precession in the lunar orbit modulating local high tide levels. Weak high tide modulation by lunar precession combined with minimal projected SLR during November and December, similar seasonal cycles in HTF for much of the year, and declining trends in MMSL during February and March, showed that HTF frequency will likely remain similar, or decline slightly during the early 2030's.

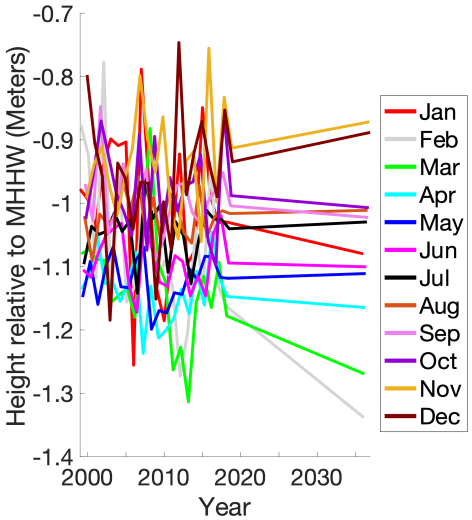

Figure 25: Historical MMSL in Amsterdam, the Netherlands and extrapolated linear trends.

Figure 25 shows historical measures of MMSL with varying trends in SLC, with clear decreases in MMSL projected during January, February and March, and slight positive trends in November and December. The average residual in MMSL was found to be the highest between December and February, around eight to nine centimeters, with three to six centimeters during other months.

Top 3: Cardiff, UK

The third-highest ranked city at risk from potential impacts by SLR by the 2050 Climate Change City Index was projected to see a temporary dip in minor HTF frequency during the 2020's, followed by an increase in minor HTF events in the early to mid-2030's, as shown in Figure 26. Moderate flooding events were projected to remain similar in frequency to recent historical events temporarily during the 2020's, and to increase during the early to mid 2030's.

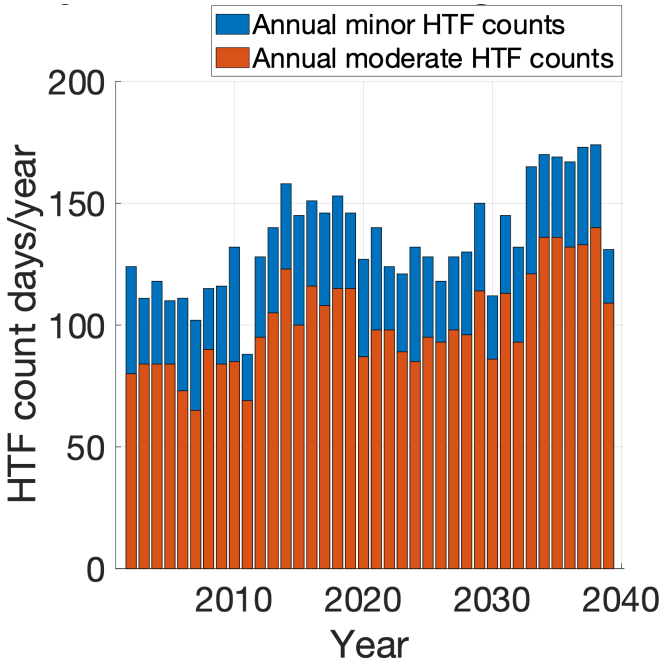

Figure 26: Historic and projected annual counts of HTF in Cardiff, UK. Annual projections in HTF days were based on the linear trend model for MMSL and did not take into account historic residuals in MMSLs.

Seasonal cycles in HTF frequency were projected to remain similar (Figure 27), with increases being well spread out throughout the year, although spring and fall were projected to remain the seasons with the highest frequencies in HTF. Both minor and moderate HTF events were projected to experience slight increases on the order of one additional day during each month in the winter, with very marginal increases in HTF frequency during other seasons.

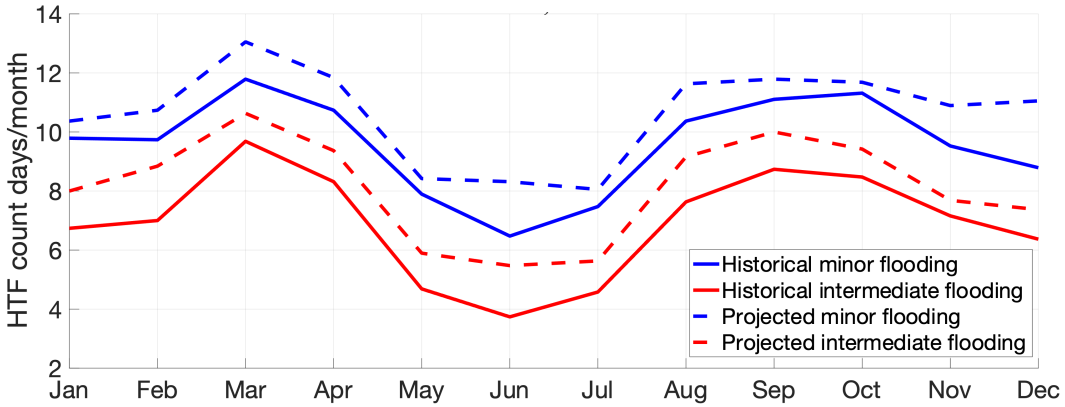

Figure 27: Average historical and average projected seasonal cycles in the frequency of HTF events in Cardiff, UK. Average historical seasonal HTF frequency was calculated over the latest nodal cycle available from tide gauge data, and the average future projected seasonal HTF was calculated over the next full nodal cycle.

A projection of total monthly HTF frequency over the next nodal cycle showed similar event frequency in both minor and moderate flooding until 2031, followed by more consistent occurrences of higher counts in HTF as the tide-amplifying phase of the nodal cycle shown in Figure 29 is reached (Figure 28A). When taking into account historical anomalies in MMSL, specifically large positive residuals are projected to cause several more days of HTF events per month, reaching twenty HTF days during the most affected months (Figure 28B).

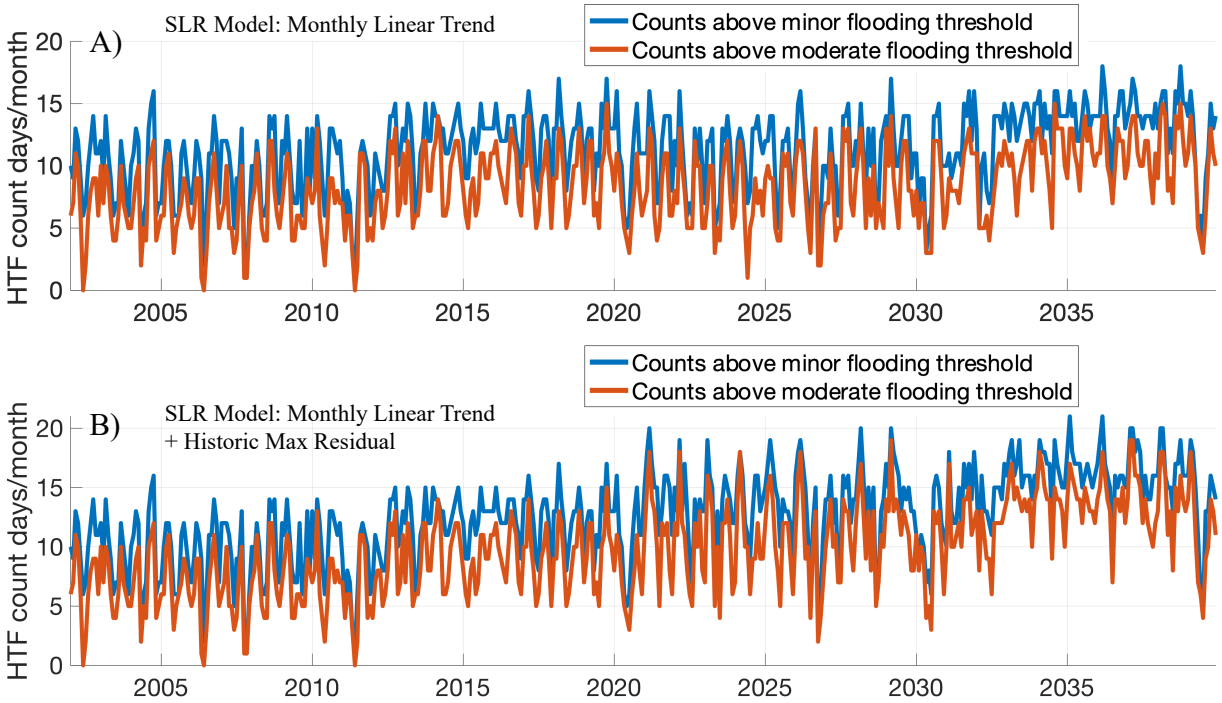

Figure 28: Time series of the historical and projected HTF event frequency in Cardiff, UK. Figure A assumes a linear form in the trends of MMSL, while Figure B accounts for maximum residuals in MMSLs.

Modulation in annual 99th percentile level tides by lunar cycles was found to be relatively strong, with amplitudes of 10.8 cm by the nodal cycle, and 3.4 cm by the cycle of lunar perigee, shown in Figure 29. The 2020's were projected to see dampening of the highest tides, followed by a sudden inflection from 2030 to 2032 as the nodal cycle reaches its tide-amplifying phase, combining with projected sea level rise. Modulations of high tide levels by the nodal cycle were found to outpace projected rates of SLR (figure 29B): between 2030 and 2034 the nodal cycle was projected to create a sudden 10 cm increase in sea level between two and three times the rate of projected sea level rise over the same period of time. The modulation by lunar precession on projected HTF frequency is visible in Figure 26, with the early to mid 2030's showing a jump coinciding with the tide-amplifying phase of the nodal cycle.

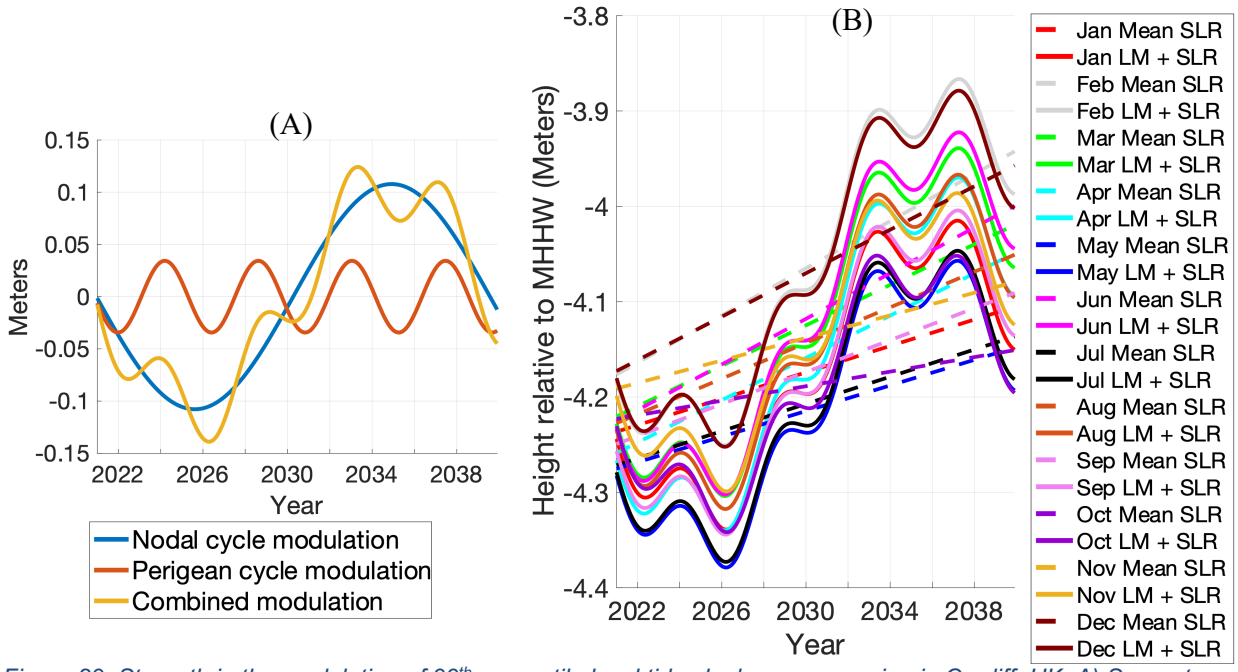

Figure 29: Strength in the modulation of 99th percentile level tides by lunar precession in Cardiff, UK. A) Separate and combined modulation in strength and signal for the nodal and perigean cycles. B) Combined effect of lunar precession on the highest tides and seasonal SLR. SLR projections represent the linear extrapolation from historical data.

Figure 30 shows local rates of mean monthly SLR, although there was a period of missing data from January of 2011 to November of 2012, followed by a large spike during several months. Rates of SLR were found to be the highest in February through April, June and December, with rates exceeding 10 cm per decade. Average residuals in MMSL were found to be the greatest from January to March; 10, 16, and 11 cm respectively. Average residuals were found to be between 4 and 9 cm during other months.

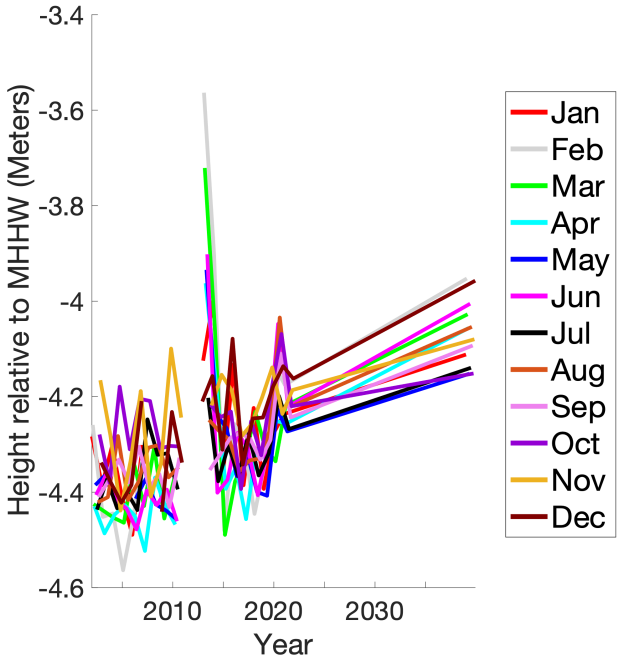

Figure 30: Historical MMSL in Cardiff, UK and extrapolated linear trends.

Top 4: Manila, the Philippines

Tide gauge data for Manila was only available until 2014, which resulted in a shorter projection period until 2033, during which minor flooding events were projected to become far more common, clustering mainly during summer months (Figure 32). Figure 31 shows an unprecedented rise in annual minor HTF frequency that was projected to be in effect from the early 2020's, and continue until the mid 2020's, which is followed by a plateau and a decline until the final year of the projection 2033, when a higher annual total in HTF events was projected.

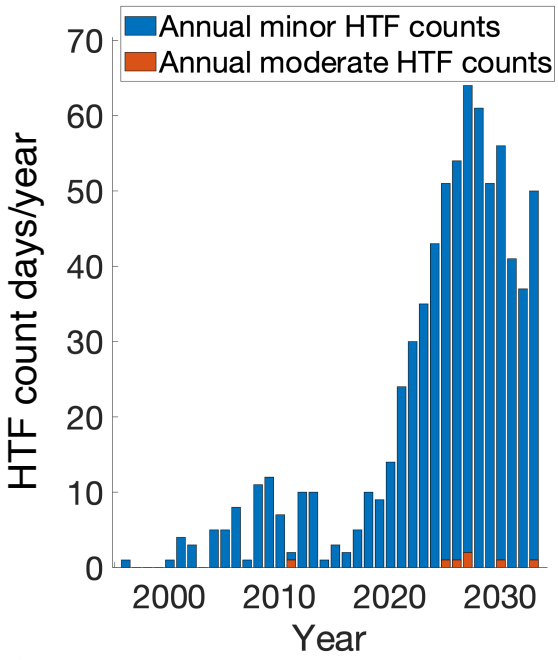

Figure 31: Historic and projected annual counts of HTF in Manila, the Philippines. Annual projections in HTF days were based on the linear trend model for MMSL and did not take into account historic residuals in MMSLs.

Minor HTF events were projected to cluster during the summer, with seven events per month projected to occur on average until 2033. Minor HTF events in the fall and winter were projected to occur at low counts (Figure 32).

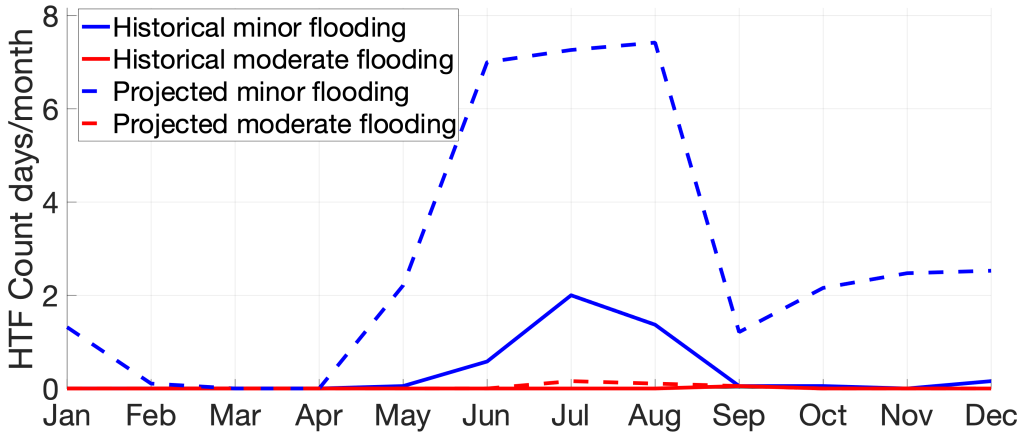

Figure 32: Average historical and average projected seasonal cycles in the frequency of HTF events in Manila, the Philippines. Average historical seasonal HTF frequency was calculated over the latest nodal cycle available from tide gauge data, and the average future projected seasonal HTF was calculated over the next full nodal cycle.

A clear uptake in total annual minor HTF events was projected, with frequencies projected to peak in the mid 2020's, decline briefly thereafter, and increase again in 2032, and 2033 (Figure 33A). When taking into account maximum historical residuals in MMSL, frequencies in minor HTF events were projected to reach 15 counts during summer months, and to spread more into the fall and early winter. Maximum frequencies in minor high-tide flooding, taking into account historical extremes, were projected to remain at around 15 days per month from the mid 2020's until 2033 (Figure 33B).

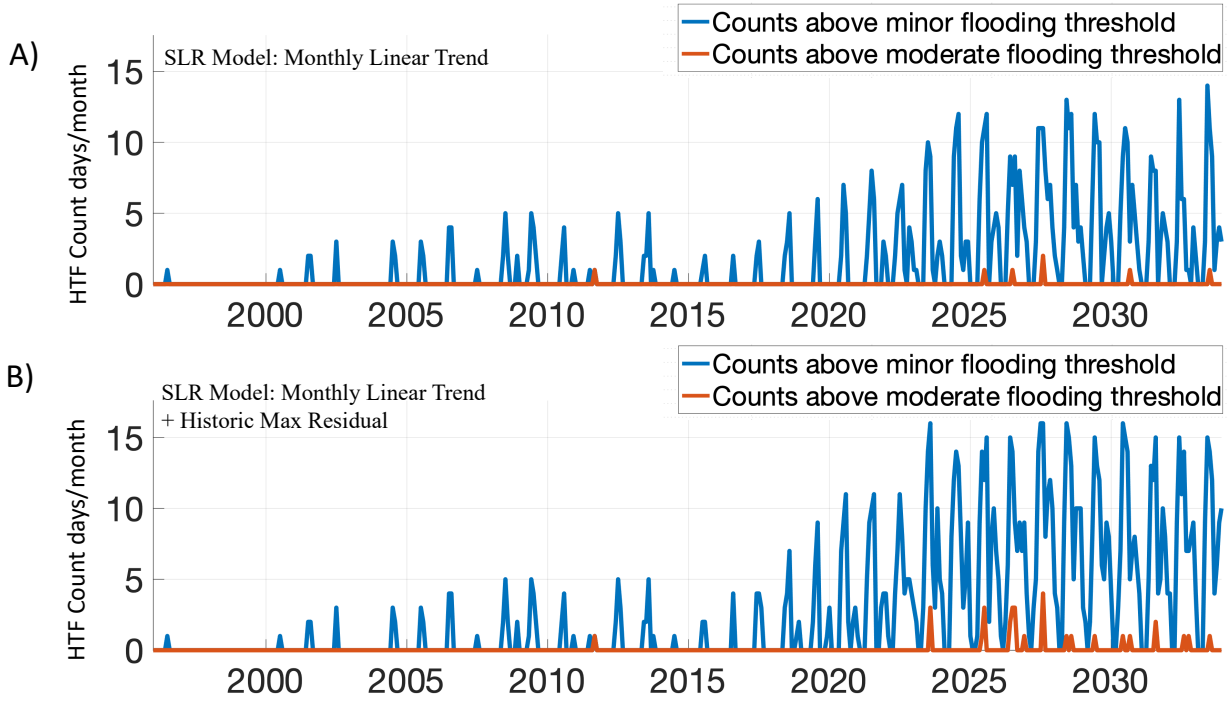

Figure 33: Time series of the historical and projected HTF event frequency in Manila, the Philippines. Figure A assumes a linear form in the trends of MMSL, while Figure B accounts for maximum residuals in MMSLs.

Modulations in high-tide levels by precessions in the lunar orbit were found to be dominated by the nodal cycle, which was found to amplify local high tides by up to 6.7 centimeters (Figure 34). Due to this modulation, high tides were projected to be the highest between 2022 and 2028. The perigean cycle was found to have a negligible effect on high tide levels. The modulation in high tides by the nodal cycle was found to currently be in its amplifying phase. After 2030, the nodal cycle was projected to dampen high tides, although rates of SLR by MMSL were projected to push high tides higher.

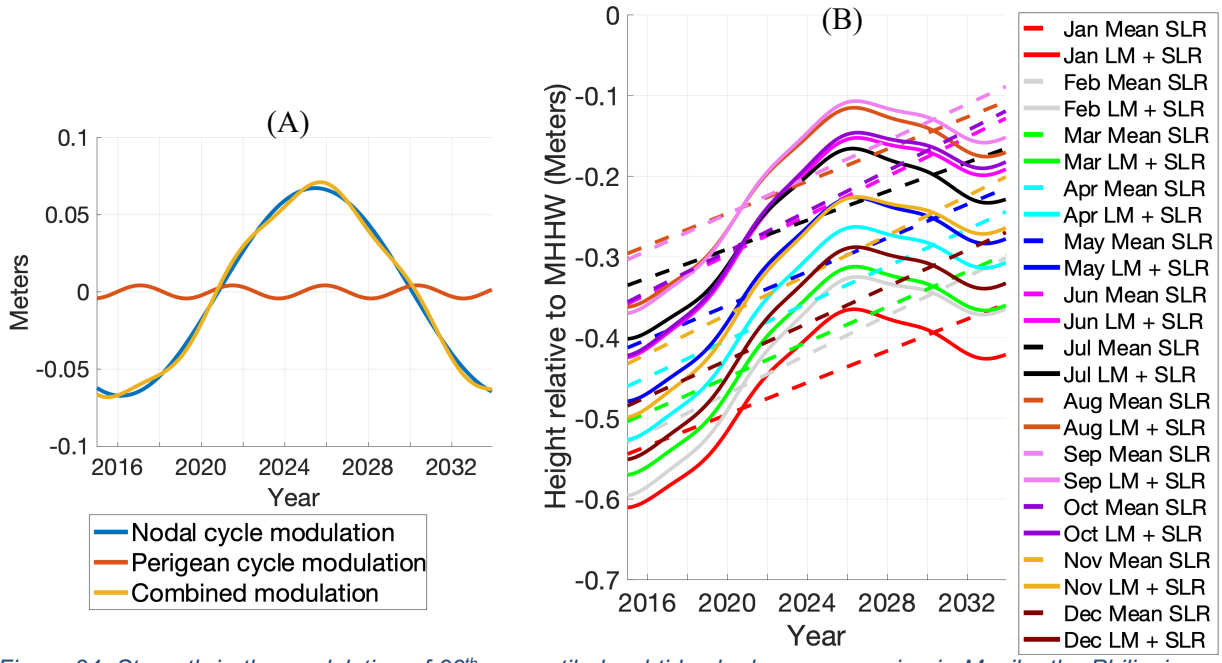

Figure 34: Strength in the modulation of 99th percentile level tides by lunar precession in Manila, the Philippines. A) Separate and combined modulation in strength and signal for the nodal and perigean cycles. B) Combined effect of lunar precession on the highest tides and seasonal SLR. SLR projections represent the linear extrapolation from historical data.

Figure 35 shows the historical profile in MMSL and extrapolated linear trends thereof. All months were projected to increase in MSL at similar rates. Historical variability in MMSL was found to have fluctuated within an average residual of 3 to 6 cm.

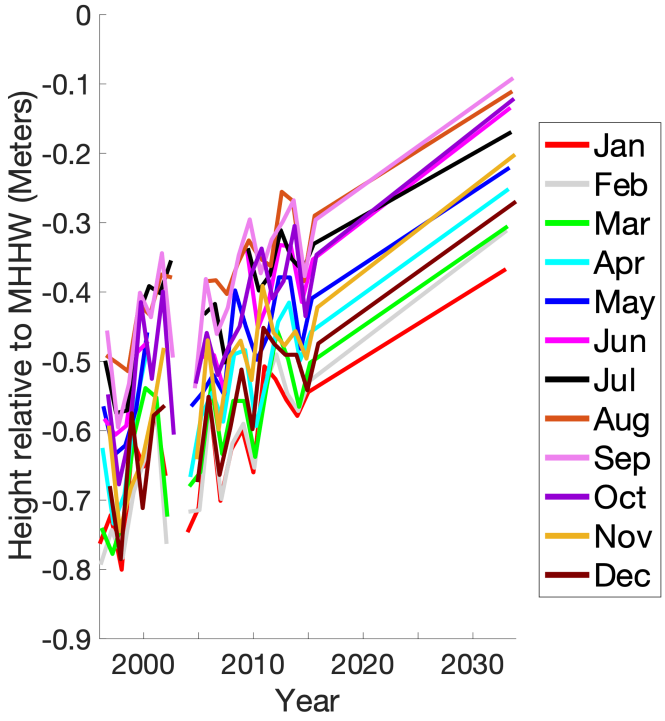

Figure 35: Historical MMSL in Manila, the Philippines and extrapolated linear trends.

Top 5: London, UK

A comparison of historical and projected annual HTF frequency in Figure 36 showed that years with frequencies of minor flooding events above 15 HTF events will increase in the future, with the highest counts expected between 2024 and 2027, and again between 2034 and 2039. Moderate HTF frequency was projected to remain similar, although a maximum of 9 moderate HTF days were projected in 2024.

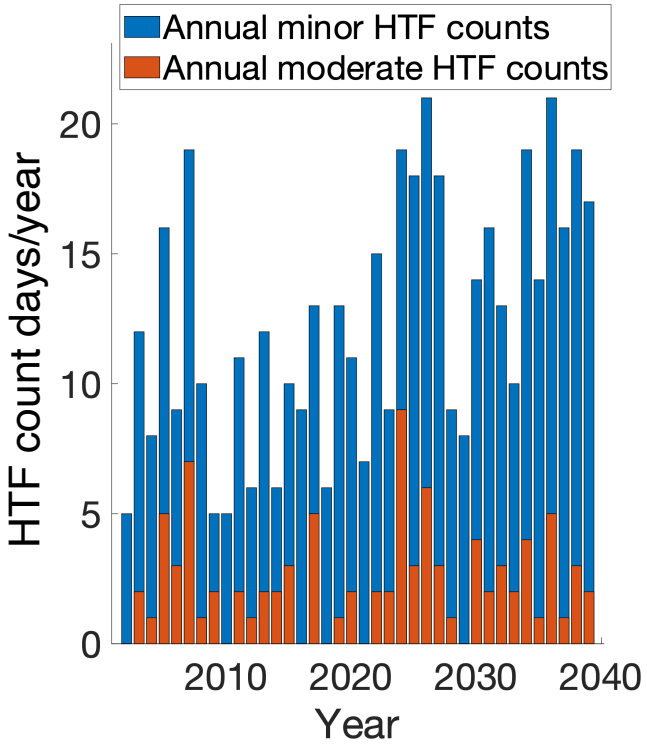

Figure 36: Historic and projected annual counts of HTF in London, UK. Annual projections in HTF days were based on the linear trend model for MMSL and did not take into account residuals in MMSLs.

Increases in HTF frequency were projected to cluster in fall and winter as shown in Figure 37, with minor counts in HTF frequency projected to double in December from less than two to four in an average year over the projected nodal cycle. Spring and summer were projected to remain similar in HTF frequency, with few events projected to occur during these seasons.

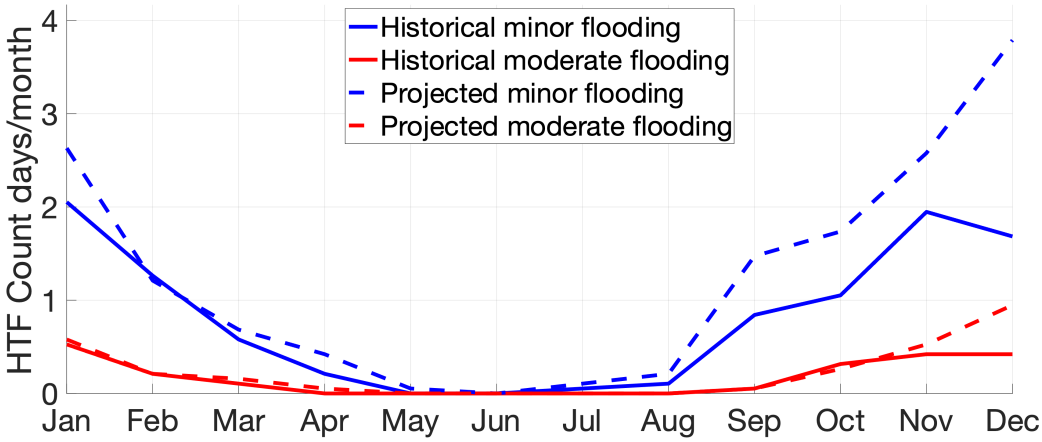

Figure 37: Average historical and average projected seasonal cycles in the frequency of HTF events in London, UK. Average historical seasonal HTF frequency was calculated over the latest nodal cycle available from tide gauge data, and the average future projected seasonal HTF was calculated over the next full nodal cycle.

Maximum frequencies in minor monthly HTF days over the projected nodal cycle were projected to remain similar, as shown below in Figure 38. The frequency and consistency in moderate HTF days was also projected to remain similar. When historical maximum residuals in historical MMSL were included in the projections, months with higher frequencies in minor HTF were projected to occur more consistently, while months with more than one day of moderate flooding were also projected to occur more consistently.

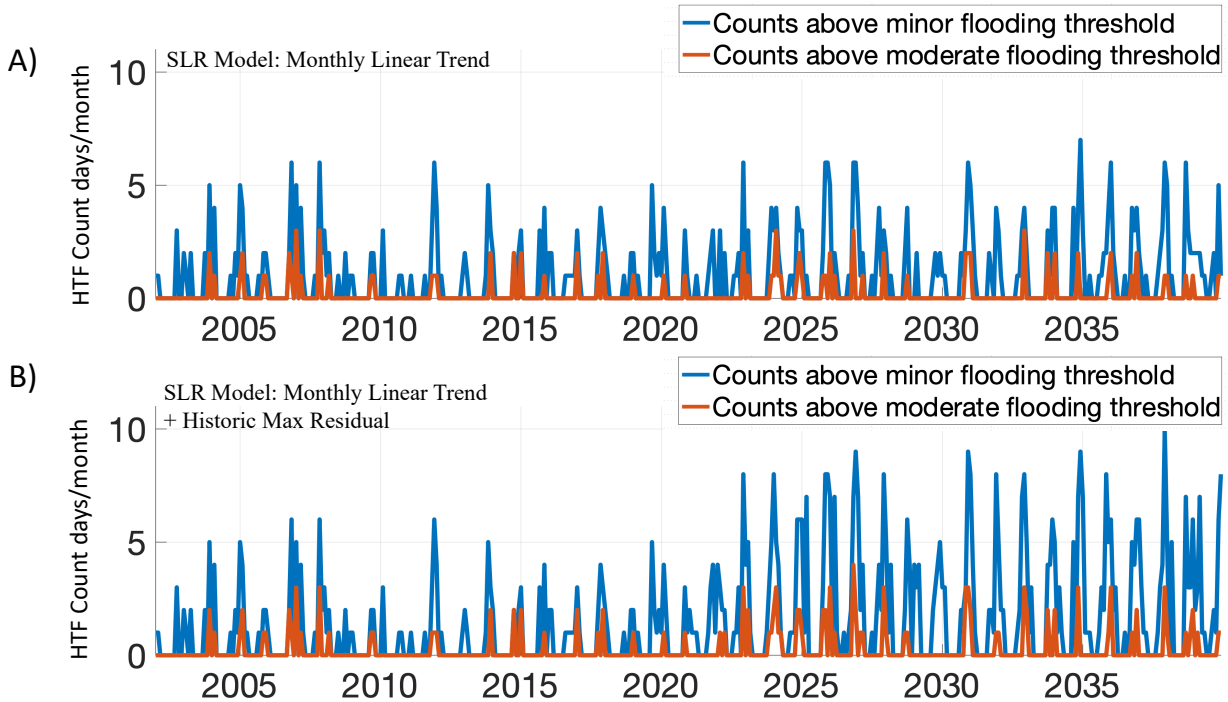

Figure 38: Time series of the historical and projected HTF event frequency in London, UK. Figure A assumes a linear form in the trends of MMSL, while Figure B accounts for maximum residuals in MMSLs.

High tides in London were found to be weakly modulated by lunar precession, with maximum amplifications of only 1.5 cm and 0.4 cm respectively by the nodal and perigean cycles. The

amplifying phase of the nodal cycle was projected to begin in 2029, while the amplifying phases of both cycles were projected to align from 2033 to 2034, as shown in Figure 39A.

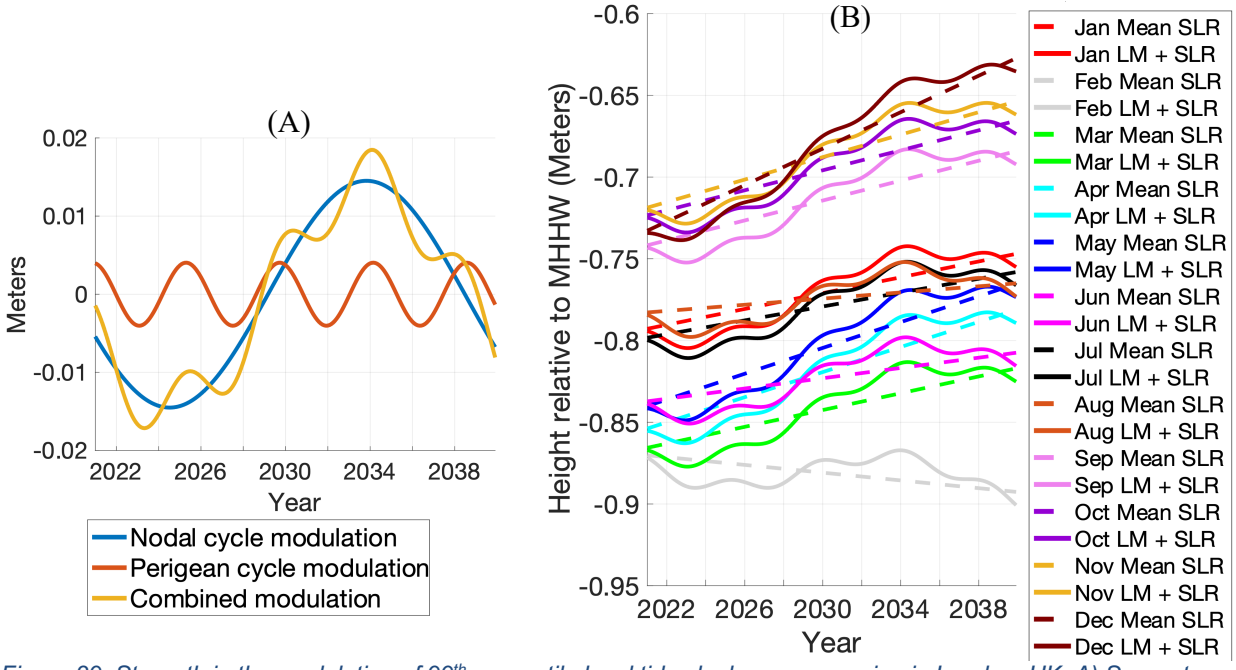

Figure 39: Strength in the modulation of 99th percentile level tides by lunar precession in London, UK. A) Separate and combined modulation in strength and signal for the nodal and perigean cycles. B) Combined effect of lunar precession on the highest tides and seasonal SLR. SLR projections represent the linear extrapolation from historical data.

Historical measures in MMSL and extrapolated linear trends are shown in Figure 40. All months except February showed increasing trends in MSL. Average residuals in MMSL were found to be the highest between November and March, with values between 4 and 5 cm. Average residuals in MMSL were between 2 and 4 cm during other months.

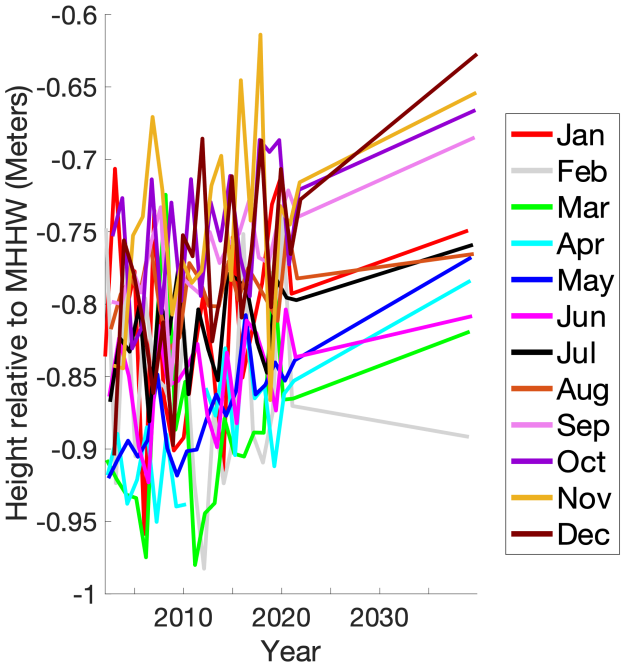

Figure 40: Historical MMSL in London, UK and extrapolated linear trends.

Top 6: Hamburg, Germany

HTF frequency by total events annually was projected to remain similar until 2038, with one breakout year being 2027, when minor HTF events were projected to occur more often than during all other years (Figure 41). Moderate flooding was projected to occur more often in 2024, and in 2026.

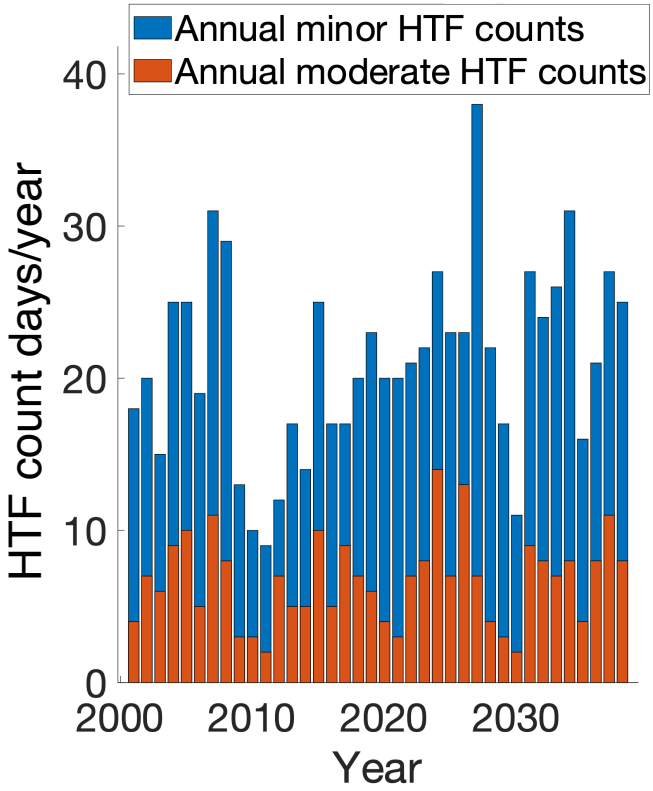

Figure 41: Historic and projected annual counts of HTF in Hamburg, Germany. Annual projections in HTF days were based on the linear trend model for MMSL and did not take into account historic residuals in MMSLs.

Seasonal cycles in HTF were projected to remain similar as shown in Figure 42, with nearly all increases in HTF projected to occur in December, when minor and moderate HTF events were projected to more than double in frequency on average over the projected nodal cycle as compared to between 2000 to 2019.

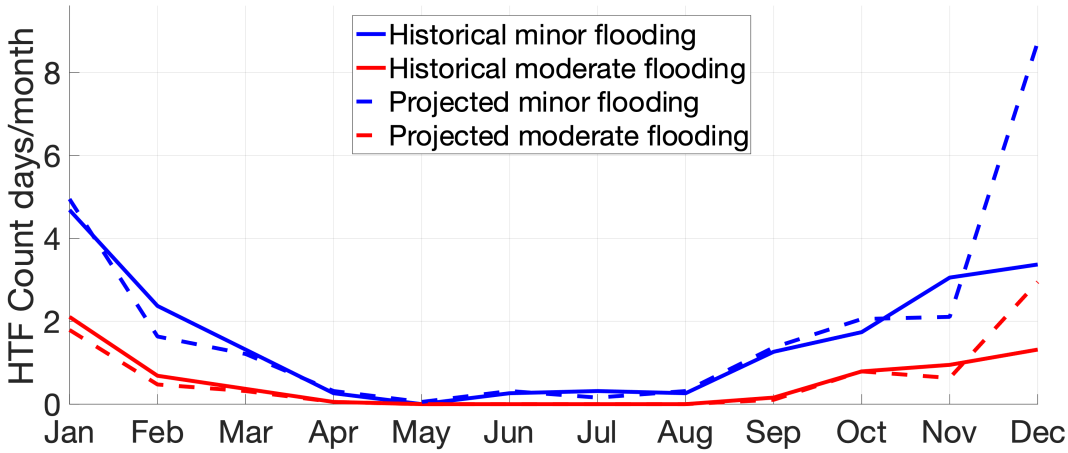

Figure 42: Average historical and average projected seasonal cycles in the frequency of HTF events in Hamburg, Germany. Average historical seasonal HTF frequency was calculated over the latest nodal cycle available from tide gauge data, and the average future projected seasonal HTF was calculated over the next full nodal cycle.

Signatures in total counts of monthly HTF events were projected to remain similar (Figure 43A), although when taking into account historical extreme MMSLs, years with sudden jumps doubling past minor flooding frequencies, and increases in the frequency in moderate flooding, were projected as shown in Figure 43B.

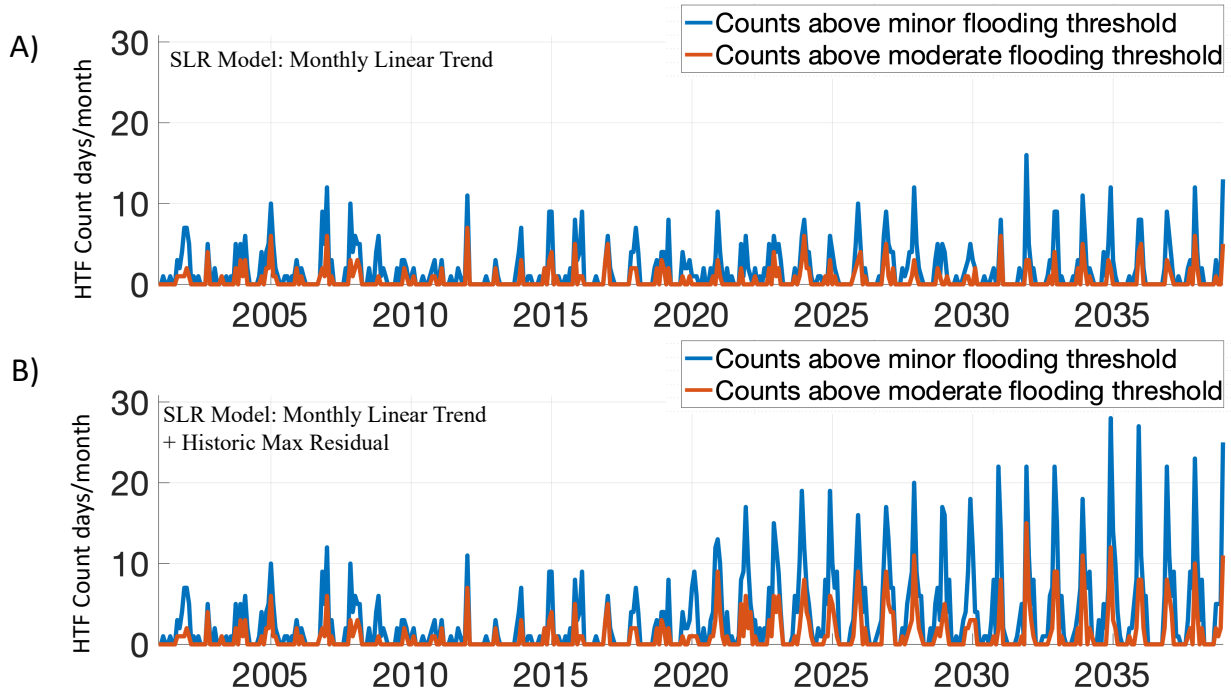

Figure 43: Time series of the historical and projected HTF event frequency in Hamburg, Germany. Figure A assumes a linear form in the trends of monthly sea level, while Figure B accounts for maximum residuals in MMSLs.

Lunar modulations of the highest tides affecting Hamburg were found to be comparatively weak, with a maximum potential amplification of only 1 cm when the amplifying phases of both cycles coincide. The strongest tide-dampening of around 1 cm was projected for 2026/2027, while the next tide-amplifying phase of the nodal cycle was projected to begin in 2032, as shown in Figure 44.

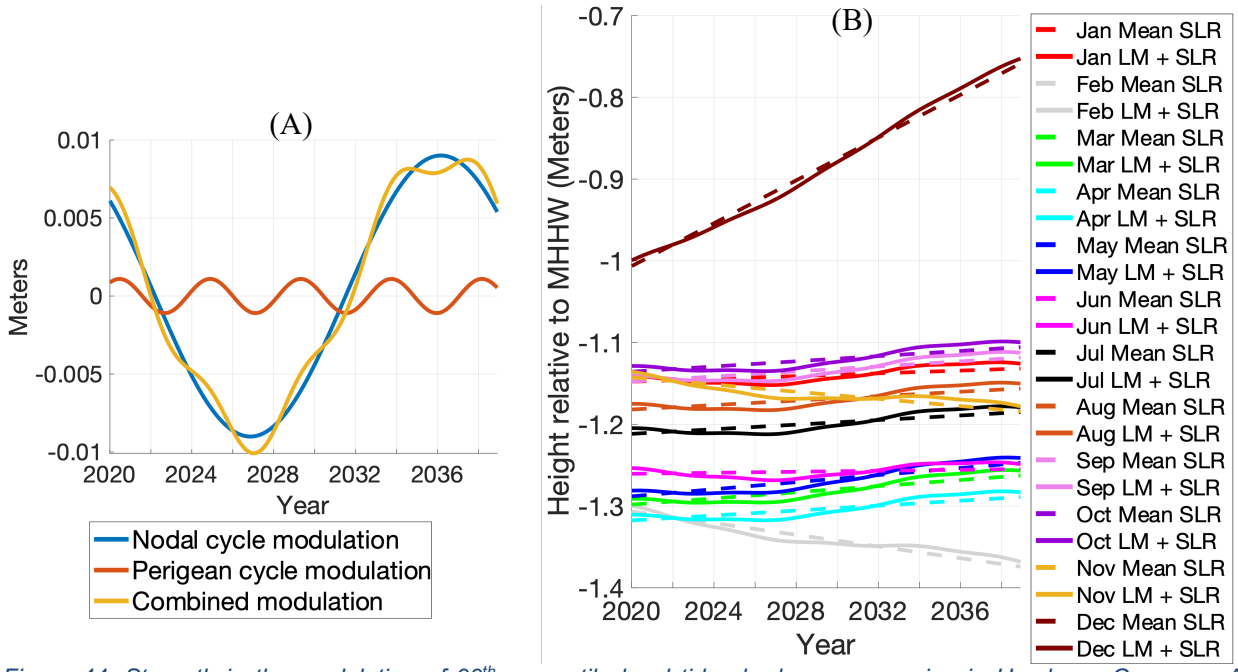

Figure 44: Strength in the modulation of 99th percentile level tides by lunar precession in Hamburg, Germany. A) Separate and combined modulation in strength and signal for the nodal and perigean cycles. B) Combined effect of lunar precession on the highest tides and seasonal SLR. SLR projections represent the linear extrapolation from historical data.

The month of December was found to have a much higher rate of SLR (13 cm per decade) than the other months, shown in Figure 45. Trends in MMSL were found to be negative in November and February, while the remaining months were found to follow slight positive trends. Average residuals in MMSL were the greatest between November and March, with values from 9 to 13 cm, while average residuals in remaining months were between 3 and 7 cm.

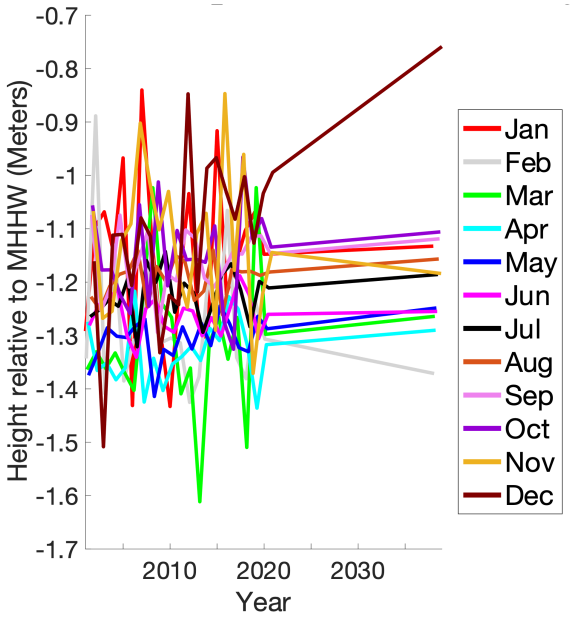

Figure 45: Historical MMSL in Hamburg, Germany and extrapolated linear trends.

Top 7: Philadelphia, Pennsylvania, USA

Philadelphia was projected to continue to have overarchingly low numbers of minor and moderate HTF events during the 2020's, as shown in Figure 46. During the 2030's, minor flooding events were projected to become more numerous, with 2037 projected to have 25 such minor flooding events.

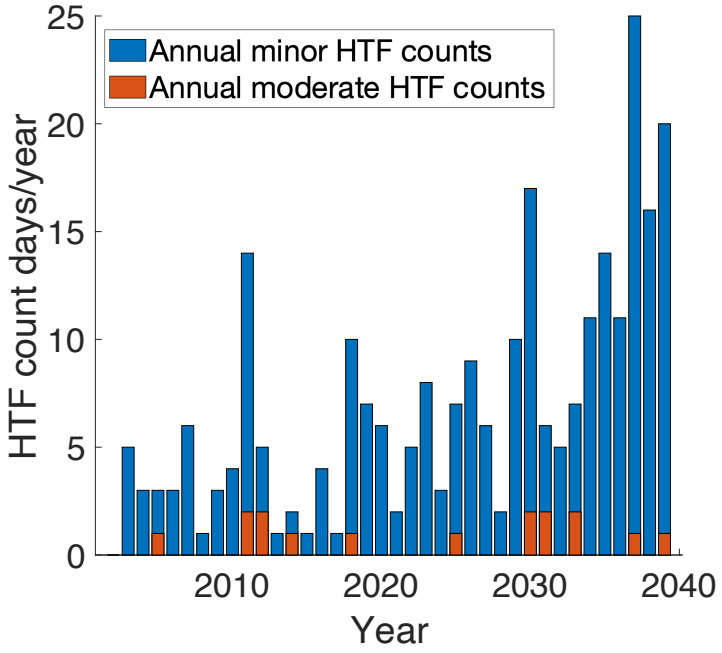

Figure 46: Historic and projected annual counts of HTF in Philadelphia, Pennsylvania, USA. Annual projections in HTF days were based on the linear trend model for MMSL and did not take into account historic residuals in MMSLs.

Average HTF counts were projected to remain around one per month during even the highest-incidence months until 2039 as shown in Figure 47, with HTF events projected to occur on average between April and October.

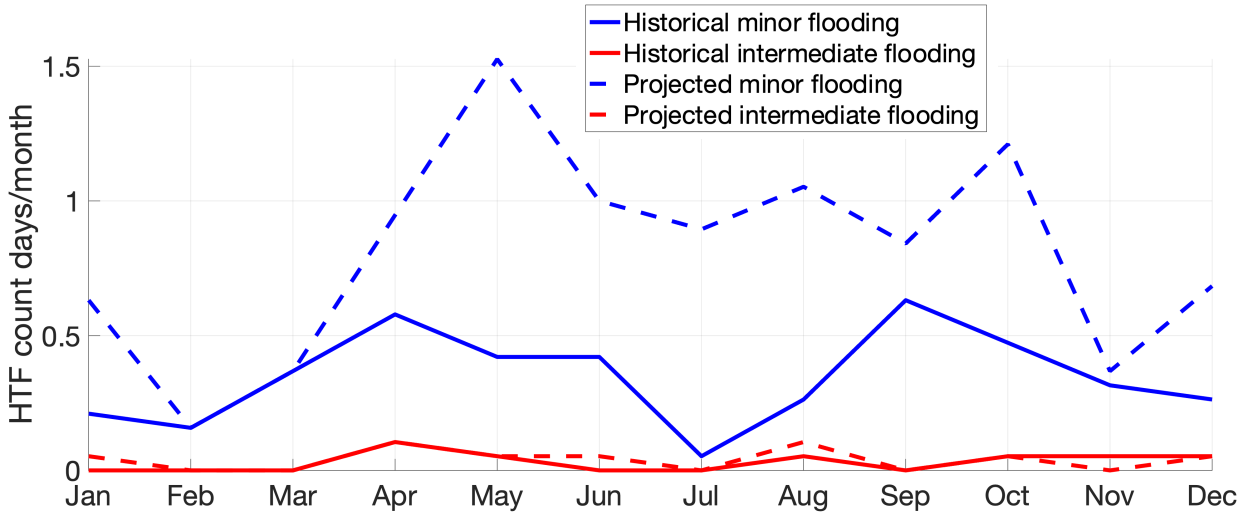

Figure 47: Average historical and average projected seasonal cycles in the frequency of HTF events in Philadelphia, Pennsylvania, USA. Average historical seasonal HTF frequency was calculated over the latest nodal cycle available from tide gauge data, and the average future projected seasonal HTF was calculated over the next full nodal cycle.

Unless extreme MMSLs on the order of those that have occurred between 2001 and 2020 recur, HTF events were projected to become more consistent, however remain low in frequency. During years with MMSLs exceeding the linear trends by magnitudes seen for breakthrough data points between 2001 and 2020, minor HTF events were projected to reach above ten during high-incidence months, with flooding spreading to more parts of the year as well (shown in Figure 48B), however. If sea levels follow the historical trend, HTF events will remain low in frequency.

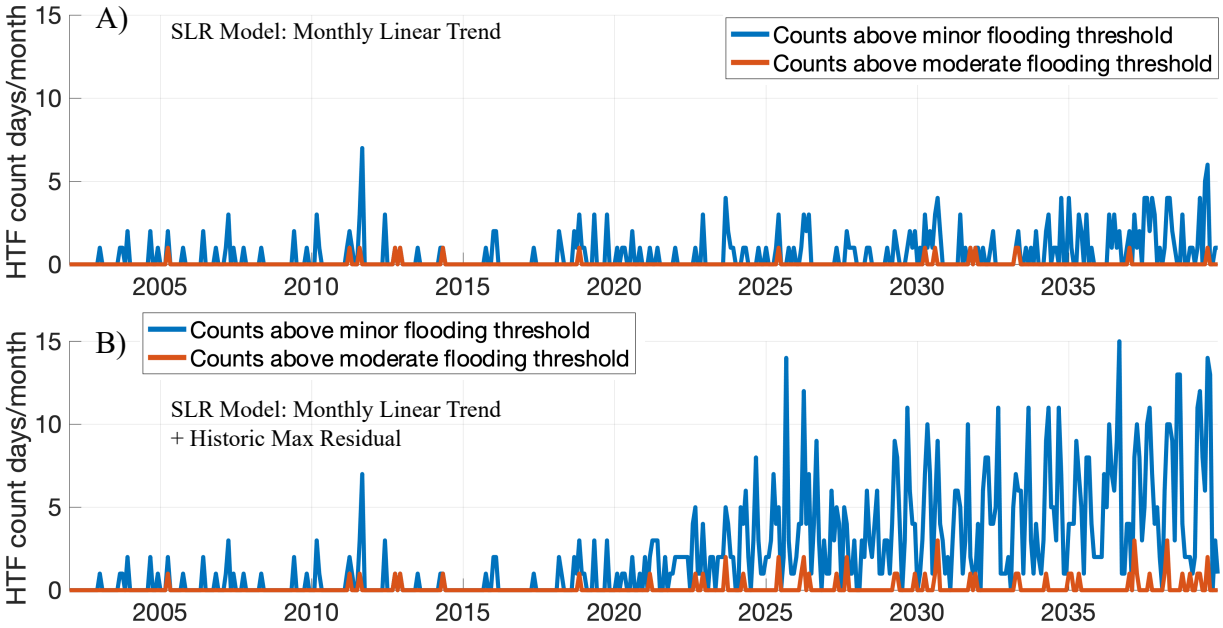

Figure 48: Time series of the historical and projected HTF event frequency in Philadelphia, Pennsylvania, USA. Figure A assumes a linear form in the trends of MMSL, while Figure B accounts for maximum residuals in MMSLs.

Modulations of high tide levels by lunar precession were found to be less than 2 cm by the nodal cycle, and less than 1 cm by the perigean cycle, with consistent, small fluctuations projected. The next phase of tide-amplification driven by the nodal cycle was projected between 2032 and 2037 as shown in Figure 49.

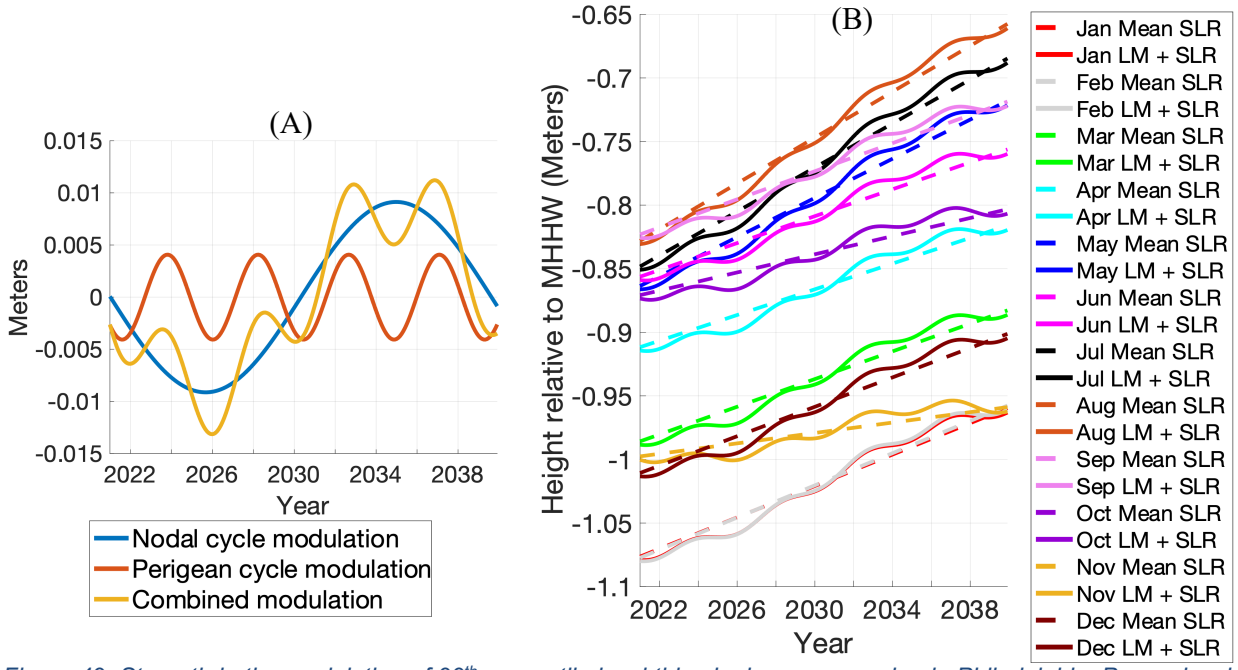

Figure 49: Strength in the modulation of 99th percentile level tides by lunar precession in Philadelphia, Pennsylvania, USA. A) Separate and combined modulation in strength and signal for the nodal and perigean cycles. B) Combined effect of lunar precession on the highest tides and seasonal SLR. SLR projections represent the linear extrapolation from historical data.

All months showed positive trends in MSL (Figure 50). Average residuals in MMSL ranged from 3 to 9 cm.

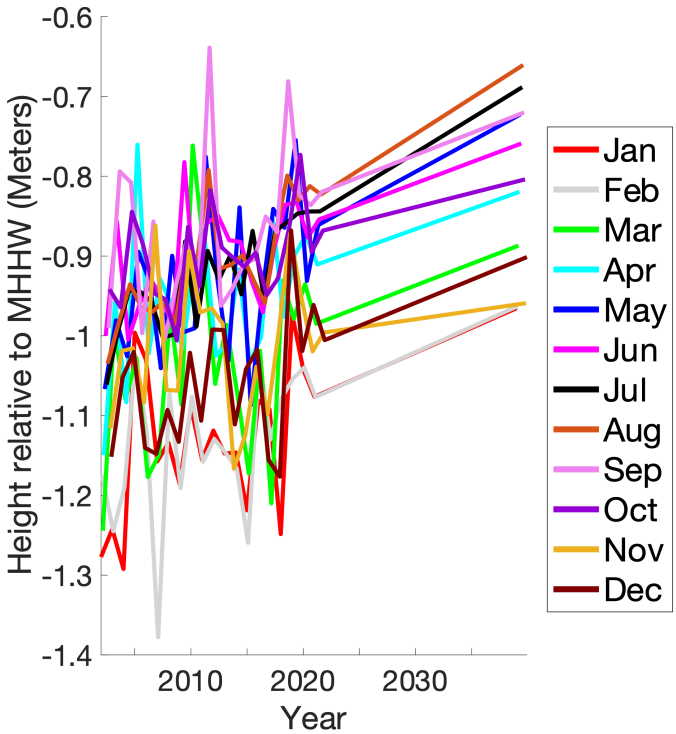

Figure 50: Historical MMSL in Philadelphia, Pennsylvania, USA and extrapolated linear trends.

Top 8: New York City, New York, USA

New York City was projected to begin to suffer higher frequencies in minor HTF days in the late 2020's, with frequencies increasing into the 2030's (Figure 51). Moderate flooding was projected to occur more consistently during the 2030's as well.

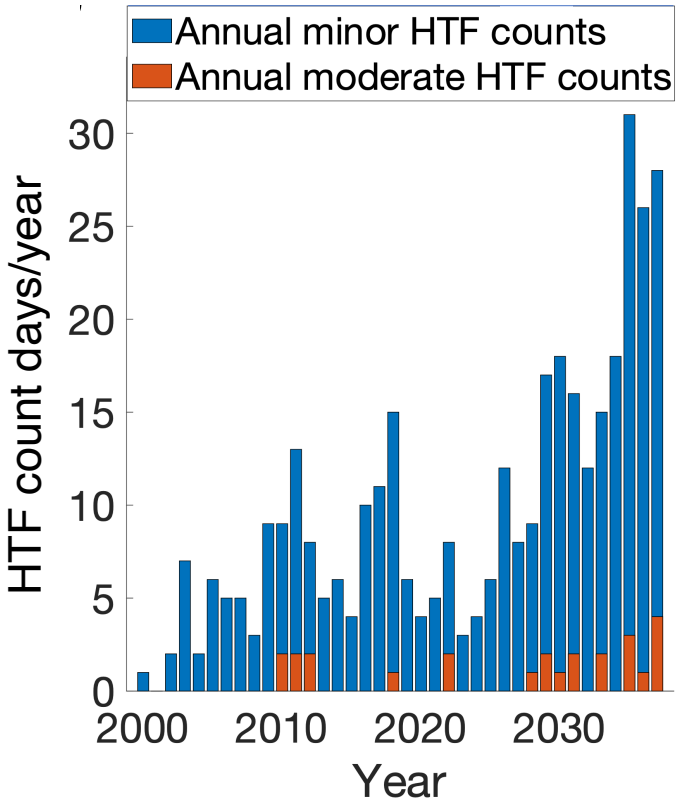

Figure 51: Historic and projected annual counts of HTF in New York City, New York, USA. Annual projections in HTF days were based on the linear trend model for MMSL and did not take into account historic residuals in MMSLs.

HTF frequency was projected to increase the most during fall on average, especially in October (Figure 52). Modest increases were projected throughout other parts of the year.

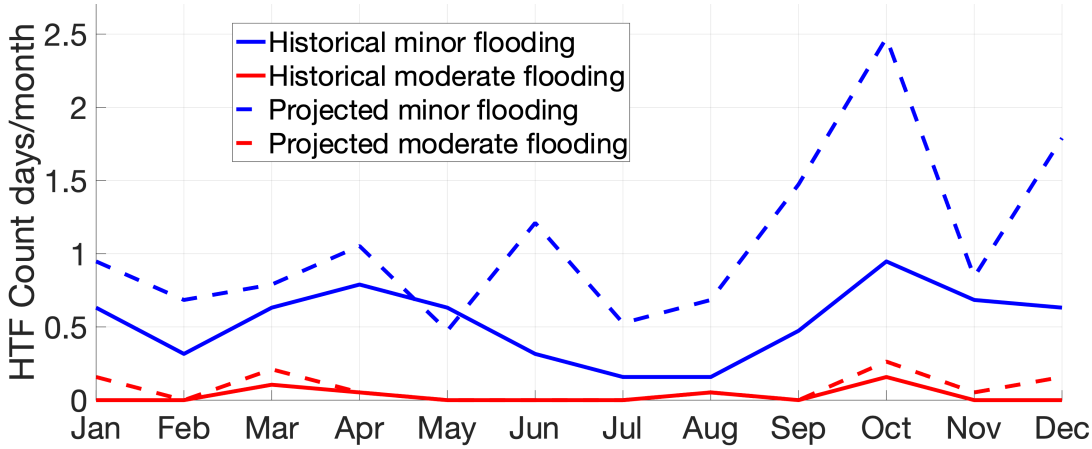

Figure 52: Average historical and average projected seasonal cycles in the frequency of HTF events in New York City, New York, USA. Average historical seasonal HTF frequency was calculated over the latest nodal cycle available from tide gauge data, and the average future projected seasonal HTF was calculated over the next full nodal cycle.

A monthly aggregation of projected minor and moderate HTF showed increases in frequency during the 2020's and 2030's, especially during the second half of the 2030's (Figure 53). Moderate flooding especially will become more common from 2030 onwards. During periods of MMSLs with exceptionally high values on the order of magnitude seen since the year 2000, higher frequencies in HTF were projected almost year-round (Figure 53B).

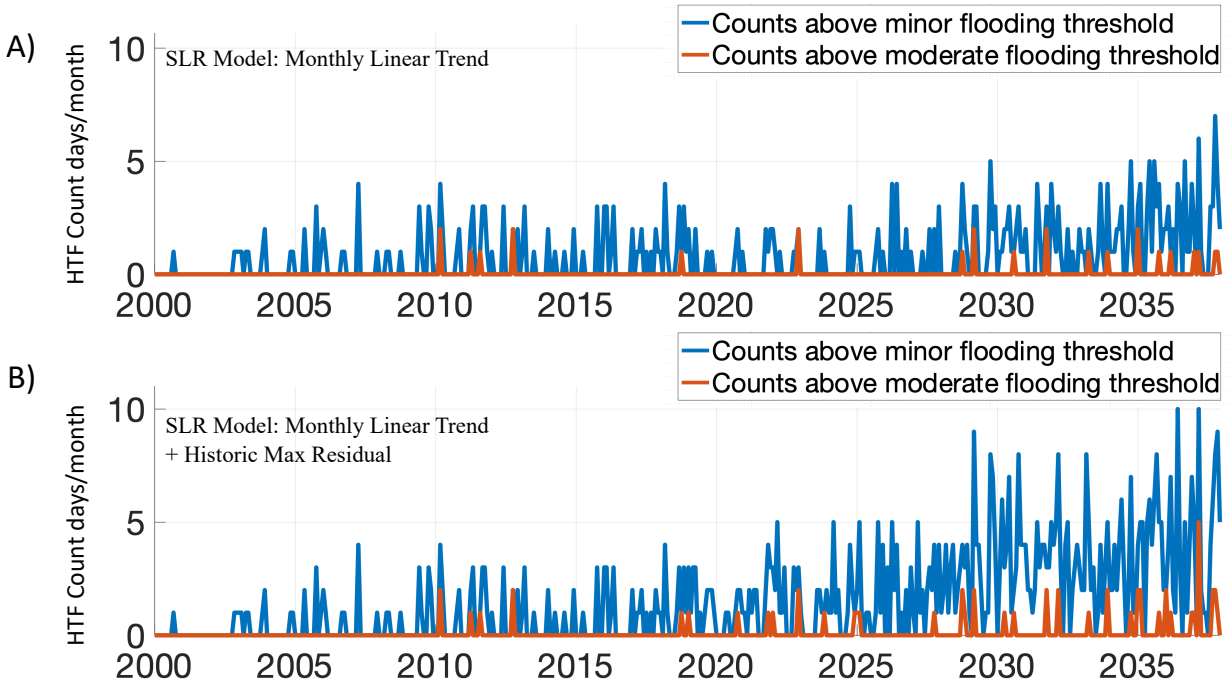

Figure 53: Time series of the historical and projected HTF event frequency in New York City, New York, USA. Figure A assumes a linear form in the trends of monthly sea level, while Figure B accounts for maximum residuals in MMSLs.

The nodal cycle was found to be the dominating precession in the lunar orbit modulating high tide levels in New York City, amplifying levels by a maximum of 1.4 cm, shown in Figure 54. The perigean cycle was found to amplify high tide levels by a maximum of 0.8 cm. High tide amplification was projected to occur from 2030 to 2034, when the nodal cycle will reach its amplifying phase, shown in Figure 54. The tide-amplifying phases of the nodal and perigean cycles were projected to coincide between 2032 and 2034.

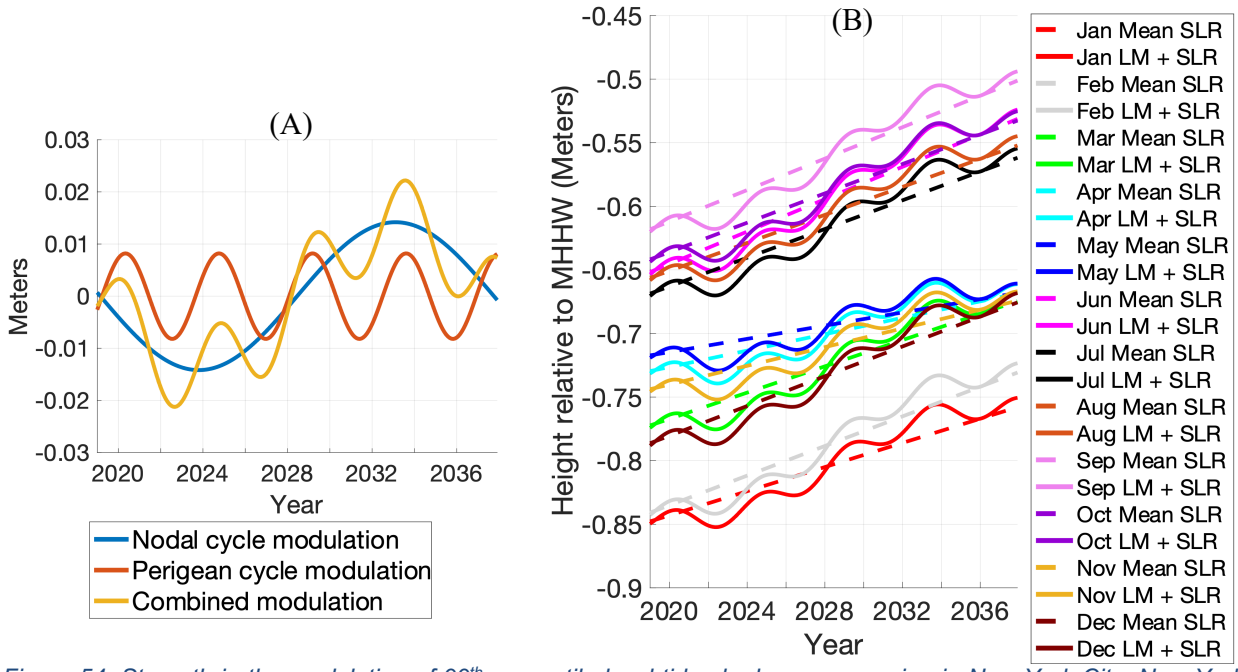

Figure 54: Strength in the modulation of 99th percentile level tides by lunar precession in New York City, New York, USA. A) Separate and combined modulation in strength and signal for the nodal and perigean cycles. B) Combined effect of lunar precession on the highest tides and seasonal SLR. SLR projections represent the linear extrapolation from historical data.

All months showed increasing trends in MMSL, with sea levels typically found to be highest in the summer and early fall, and lowest in the winter (Figure 55). Average residuals in MMSL were between 3 and 8 cm.

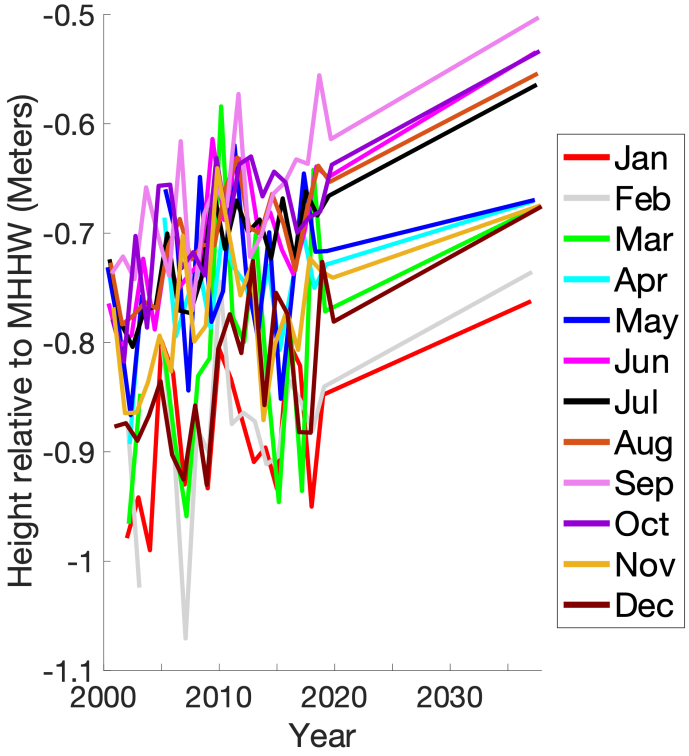

Figure 55: Historical MMSL in New York City, New York, USA and extrapolated linear trends.

Top 9: Jacksonville, Florida, USA

HTF in Jacksonville was projected to slowly build during the 2020's, before increasing dramatically during the 2030's, although HTF events were projected to remain overarchingly minor (Figure 56.)

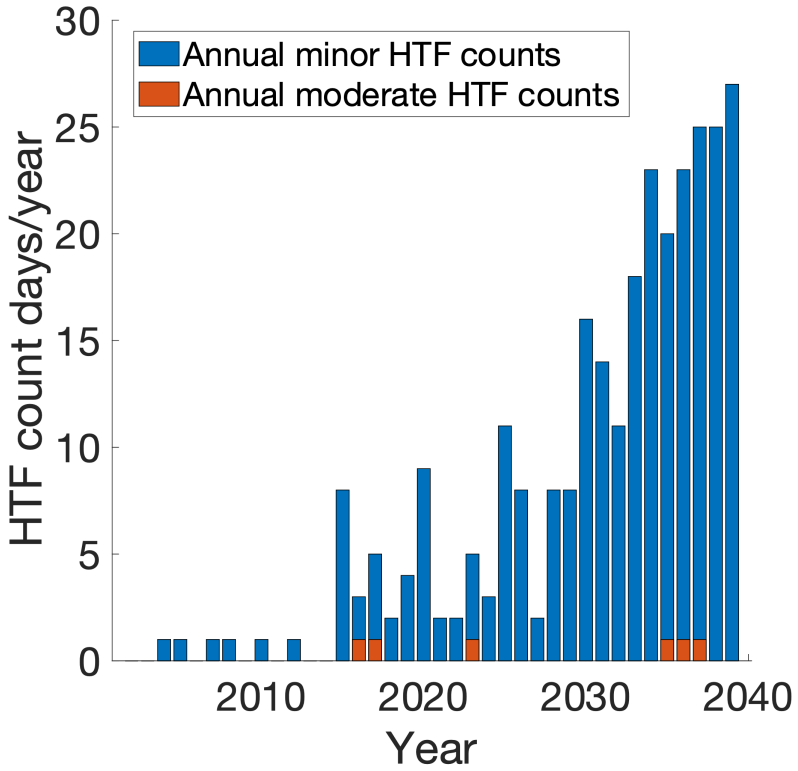

Figure 56: Historic and projected annual counts of HTF in Jacksonville, Florida, USA. Annual projections in HTF days were based on the linear trend model for MMSL and did not take into account historic residuals in MMSLs.

HTF events were projected to increase and cluster mainly during autumn and December, with very few events throughout the rest of the year (Figure 57).

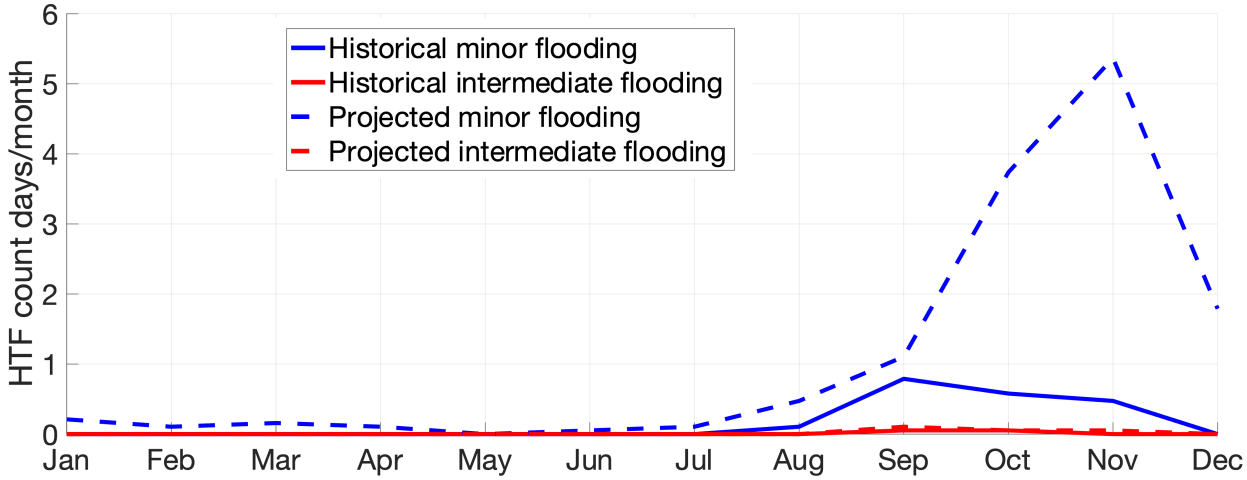

Figure 57: Average historical and average projected seasonal cycles in the frequency of HTF events in Jacksonville, Florida, USA. Average historical seasonal HTF frequency was calculated over the latest nodal cycle available from tide gauge data, and the average future projected seasonal HTF was calculated over the next full nodal cycle.

Figure 58 again shows a slow building of minor HTF events during the 2020's, followed by a more stark increase during the 2030's. Moderate HTF events were projected to remain rare. When taking into account the highest historical residuals in MMSLs, HTF events were projected to occur during more parts of the year, and at higher frequencies (Figure 58B).

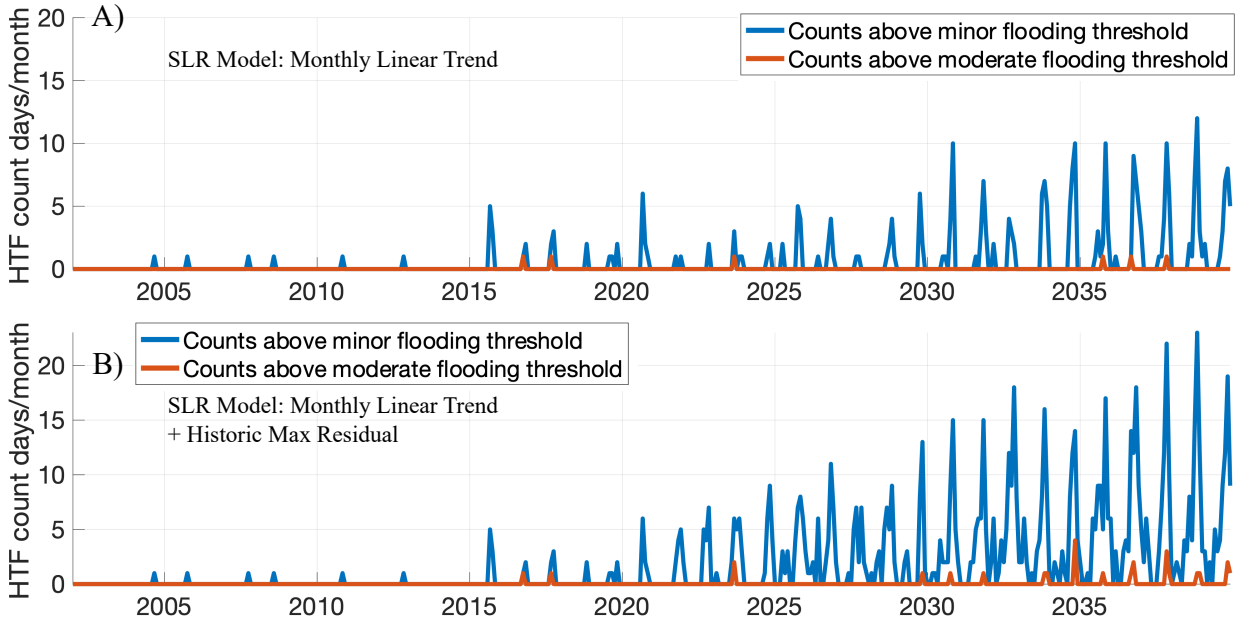

Figure 58: Time series of the historical and projected HTF event frequency in Jacksonville, Florida, USA. Figure A assumes a linear form in the trends of monthly sea level, while Figure B accounts for maximum residuals in MMSLs.

The nodal cycle was found to modulate high tides in Jacksonville by 3.6 cm, while the perigean cycle was found to hardly be influential, with a total modulation of less than 0.5 cm (Figure 59). The nodal cycle was projected to go into its tide-amplifying phase in 2031, which was projected to continue until the end of the projection in 2039. Tide amplification of just under 2 cm by coinciding tide-amplifying phases of the nodal and perigean cycles was projected in 2033 and 2037.

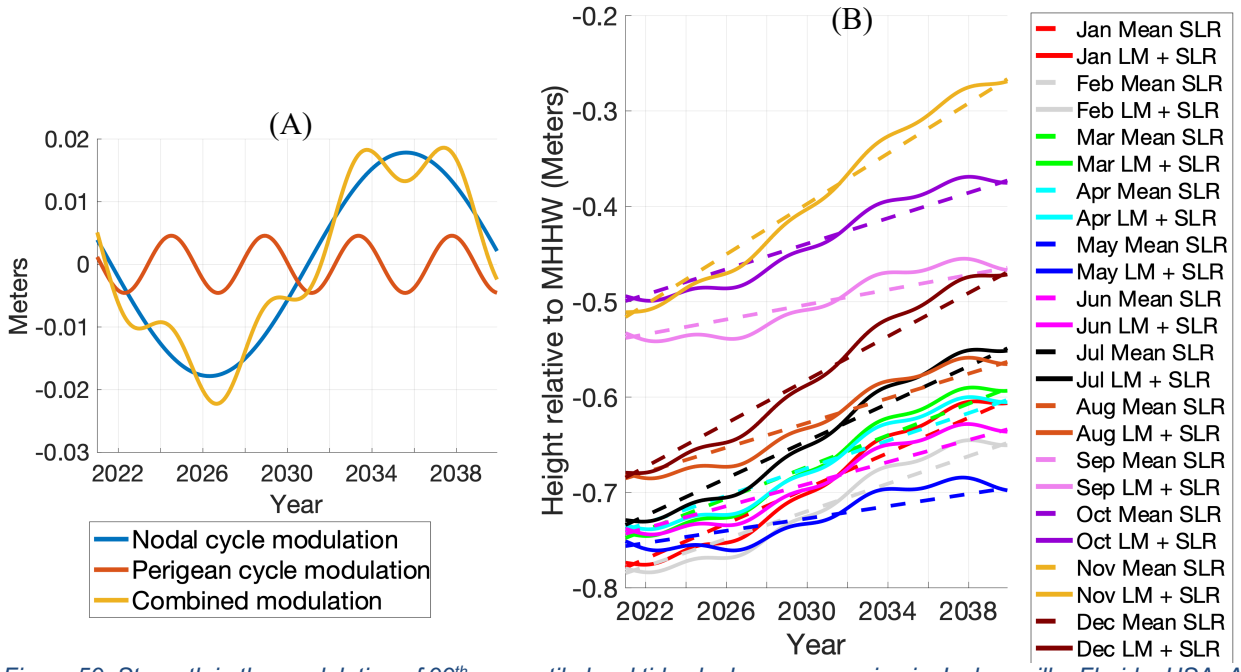

Figure 59: Strength in the modulation of 99th percentile level tides by lunar precession in Jacksonville, Florida, USA. A) Separate and combined modulation in strength and signal for the nodal and perigean cycles. B) Combined effect of lunar precession on the highest tides and seasonal SLR. SLR projections represent the linear extrapolation from historical data.

All months showed a positive trend in sea level, with mean sea levels being the highest in summer, and the lowest in winter (Figure 60). Average residuals in MMSL were found to be between 4 and 8 cm.

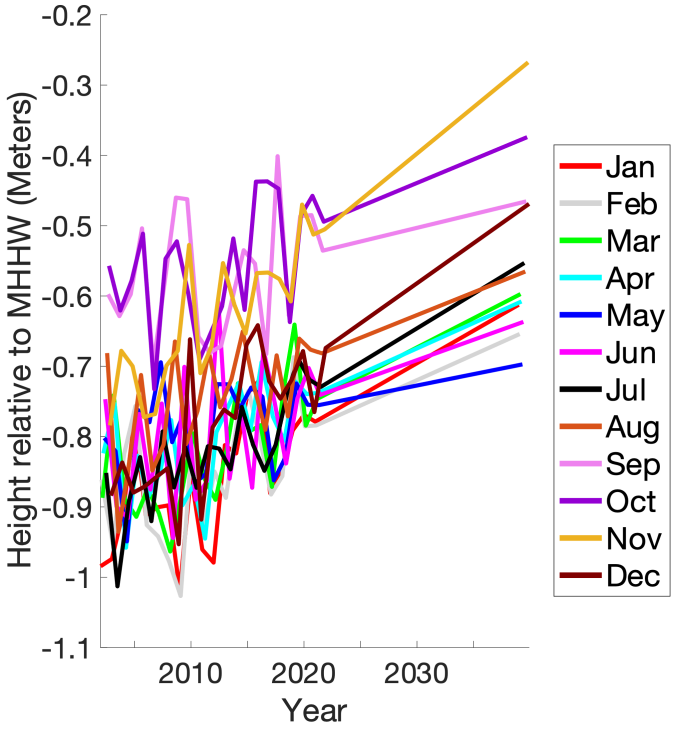

Figure 60: Historical MMSL in Jacksonville, Florida, USA and extrapolated linear trends.

Top 10: Hong Kong, SAR China

Higher frequencies in minor HTF in Hong Kong were projected to become more consistent from the late 2020's, with at least ten days annually projected every year until 2037, with thirty counts of HTF projected in 2028, and in 2037 (Figure 61). Moderate HTF was projected to remain rare.

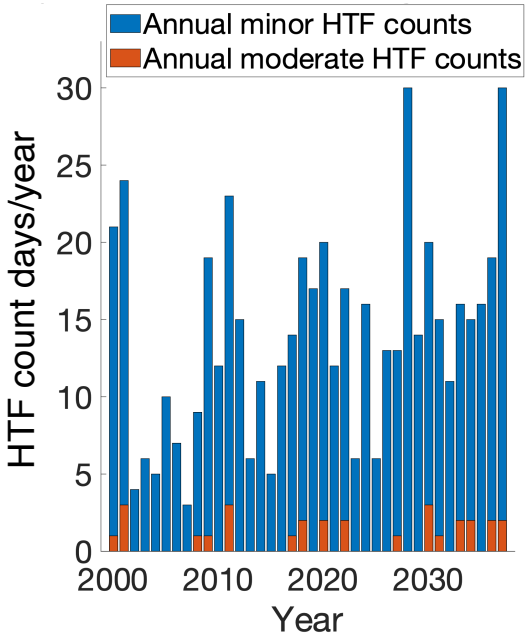

Figure 61: Historic and projected annual counts of HTF in Hong Kong, SAR China. Annual projections in HTF days were based on the linear trend model for MMSL and did not take into account historic residuals in MMSLs.

Increases in HTF were projected to cluster in fall and winter, nearly doubling in frequency during October and in December, while HTF events in summer were projected to decline (Figure 62).

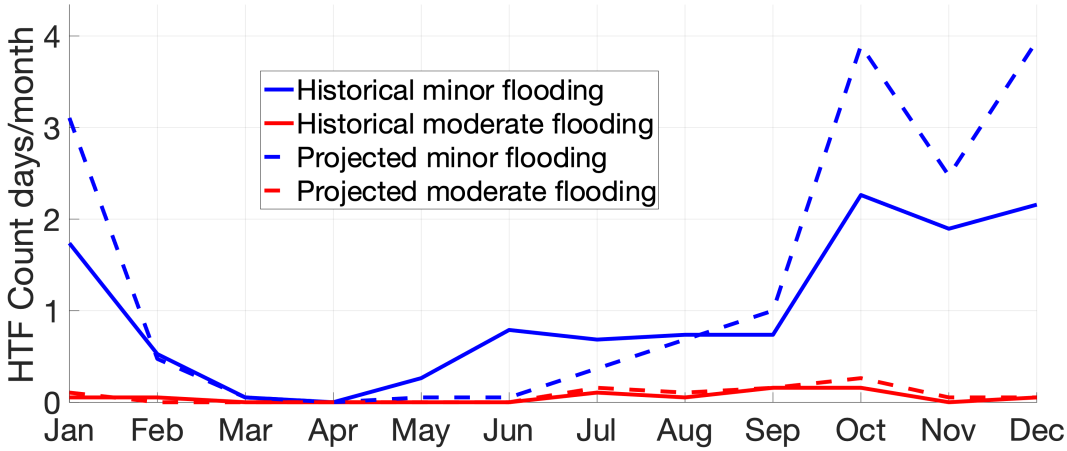

Figure 62: Average historical and average projected seasonal cycles in the frequency of HTF events in Hong Kong, SAR China. Average historical seasonal HTF frequency was calculated over the latest nodal cycle available from tide gauge data, and the average future projected seasonal HTF was calculated over the next full nodal cycle.

Months with at least five HTF days were projected to remain similar in frequency during the 2020's as between 2000 and 2018, before becoming more common during the 2030's (Figure 63). When

high positive residuals in historical MMSLs were accounted for, minor HTF frequencies between October and January were projected to reach and even exceed ten HTF days (Figure 63B).

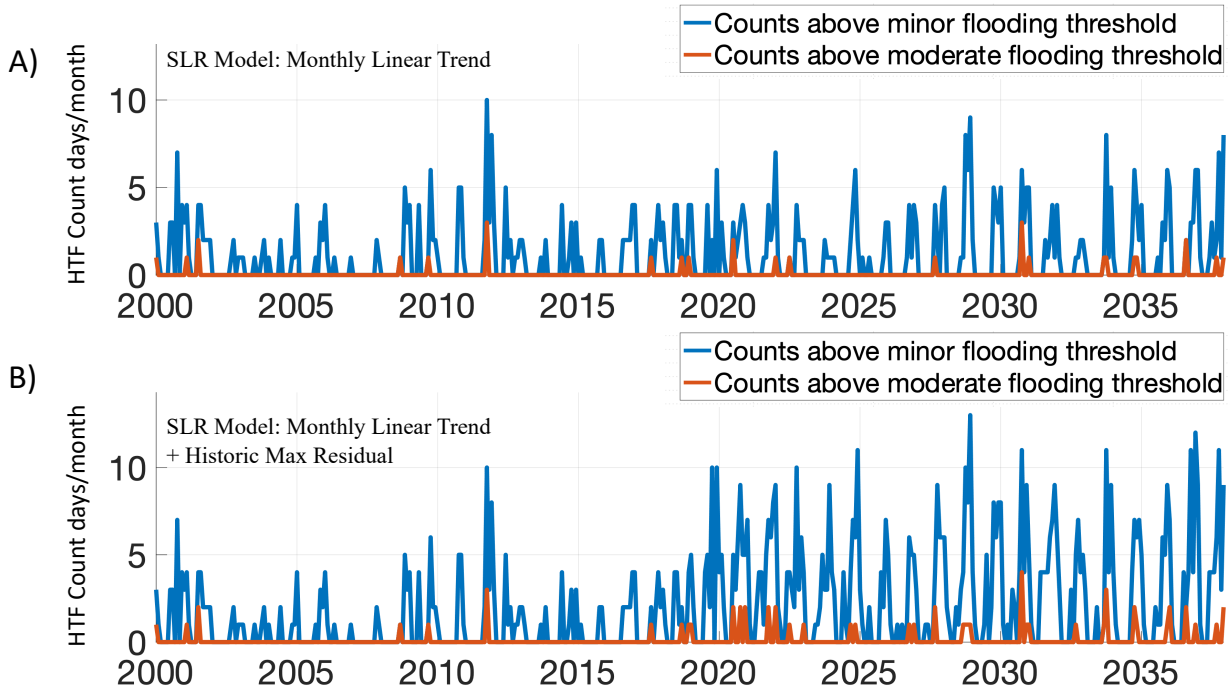

Figure 63: Time series of the historical and projected HTF event frequency in Hong Kong, SAR China. Figure A assumes a linear form in the trends of monthly sea level, while Figure B accounts for maximum residuals in MMSLs.

The nodal cycle was found to be the dominating lunar precession modulating high tide levels locally, with high tides projected to be amplified until 2028, before being dampened for several years (Figure 64). The greatest amplification of high tides by lunar precession over the projected nodal cycle was projected to be between 2022 and 2027. Astronomical high tides were found to be amplified to a maximum of 4.1 cm by the nodal cycle, and only 0.6 cm by the perigean cycle, as shown in Figure 64.

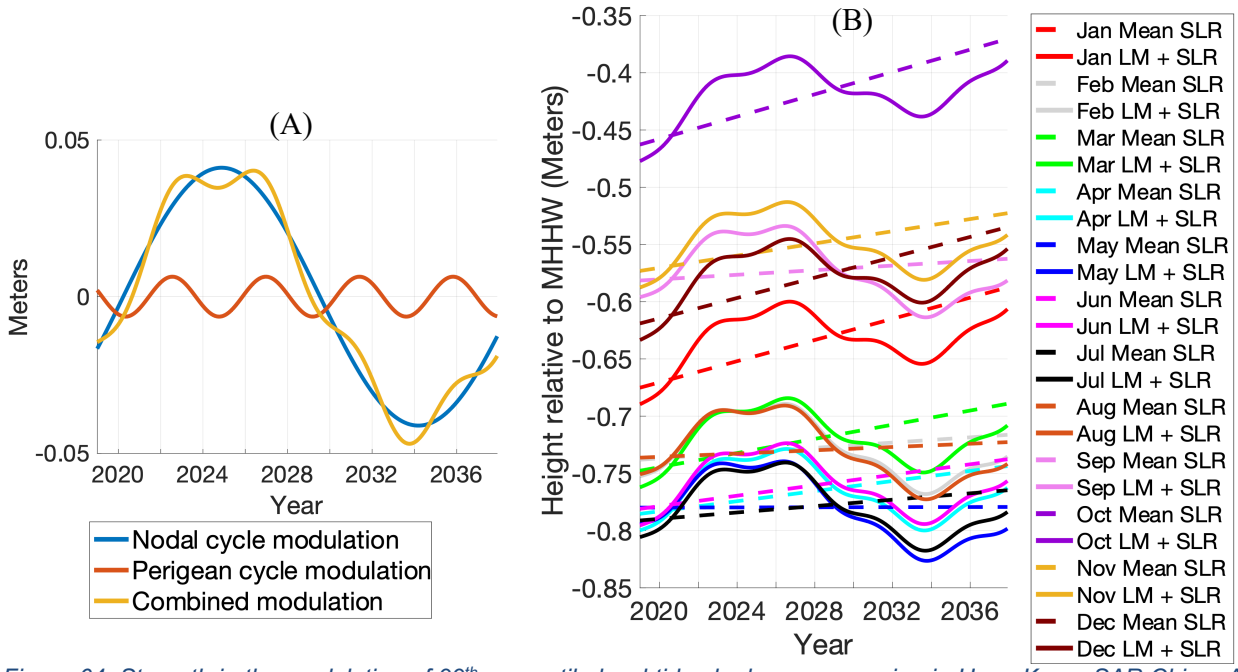

Figure 64: Strength in the modulation of 99th percentile level tides by lunar precession in Hong Kong, SAR China. A) Separate and combined modulation in strength and signal for the nodal and perigean cycles. B) Combined effect of lunar precession on the highest tides and seasonal SLR. SLR projections represent the linear extrapolation from historical data.

Most months were found to have followed slight positive trends in SLR on the order of only a handful of cm over a nodal cycle, with sea levels found to be the highest between September and December, and the lowest in April, May, June, and July (Figure 65). Average residuals in MMSL were found to be between 4 and 6 cm.

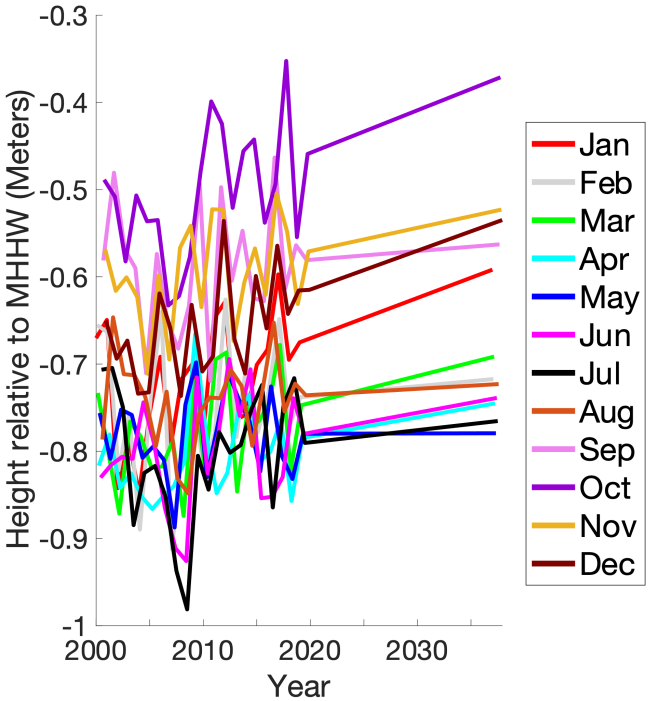

Figure 65: Historical MMSL in Hong Kong, SAR China and extrapolated linear trends.

Discussion

Overview of Results

In this thesis, near-future projections in HTF frequencies were made and presented in a novel way for the top ten popular travel destinations globally at the greatest risk from potential SLR based on the 2050 Climate Change City Index, including years and seasons with the greatest projected HTF numbers. Novel methods included taking into account the correlation of astronomical tides with sea level variability, the modeling of changing seasonality in intra-annual MMSL, and the characterization of differences in intra-annual SLC trends to be included in projections of sea level as the underlying basis for the projections of HTF events. The projection in high tide levels was conducted through a combination of projected tidal constituents, deterministic, seasonal predictions of surge, wave setup, and wave swash, and an array of underlying, extrapolated, seasonal, linear SLR projections (also taking into account large positive residuals in MMSL observed over the latest nodal cycle), over the next full nodal (~19 year) cycle relative to the end of the available data at each location. Cities included in the analysis were in Europe, North America, and Asia. It was found that certain locations will suffer very large increases in HTF frequency in the near future, although the majority of these events were projected to bring minor flooding, as opposed to moderate flooding or beyond. The results showed that Bangkok, Manila, New York City, and Jacksonville are projected to be the sites of large increases in the frequency of HTF events during the 2020's, and/or the 2030's. London, Cardiff, Hamburg, Philadelphia and Hong Kong were projected to see less obvious increases in HTF, while HTF frequency in Amsterdam, interestingly, was projected to remain similar, and even decline. The projected increases in HTF in New York City and Jacksonville were especially pronounced over the 2030's, which corroborates the findings of Thompson et al. (2021), who predict an inflection point in United States HTF events in the mid 2030's.

Thus, regarding investigation into how HTF frequency will change in the near future outlined in research question one, several prominent coastal cities were projected to suffer increases in HTF frequency earlier than is typically expected, although several cities included in the analysis were projected to see more subtle increases in HTF incidences in the near future. Bangkok and Manila were the cities projected to suffer unprecedented increases in HTF throughout the 2020's. Both minor and moderate flooding was projected to become more common in Bangkok, while the vast majority of HTF in Manila was projected to be minor. HTF frequencies in Bangkok and Manila were projected to remain high throughout the 2030's as well, increasing even further in Bangkok at the end of the projection in 2037. The most recent tide gauge data from Manila available at the time of this study only allowed projections until 2033. Increases in HTF frequency in New York City and Jacksonville were projected to occur mainly in the 2030's, becoming more common across the decade. The first year surpassing ten HTF days in Jacksonville was projected to be 2025. While HTF in New York City has already occurred during the 2000's and 2010's, HTF frequency was projected to remain similar during the 2020's, before doubling during the 2030's. Marginal increases in HTF frequency were projected in other cities, while HTF frequency in Amsterdam was projected to remain similar and even decline marginally until 2036.

In addition, regarding research question two stipulating an investigation into which seasons/months will be most affected by HTF, this thesis illustrated that increases in HTF events

are most often projected to be concentrated during particular season(s) or month(s) as opposed to being evenly spread out. Thompson et al. (2021) also project clustering in HTF events during extreme seasons or months, which leads to critical frequencies in HTF events capable of causing major disruptions within a city a decade or two earlier than would otherwise be expected (Thompson et al. 2021). In this study, fall and winter months of the Northern Hemisphere were generally projected to bring the most frequent HTF over all regions, although there are exceptions. For example, in Bangkok and Hong Kong, HTF was projected to take place overwhelmingly in the fall and winter months, while in Manila the danger was found to be greatest during summer months. This showed that even within the Southeast Asian region, there will be differences in which seasons coastal cities will be the most vulnerable to HTF. Furthermore, within the seasons of greatest risk to HTF themselves, the seasonal cycles of HTF were found to differ widely in shape between locations. For example, HTF in Bangkok was projected to peak during December and January within the local fall-winter HTF season with almost no HTF projected during spring and summer (Figure 17). By contrast, HTF in Manila was projected to be high during the whole summer, with lower frequencies projected in the fall and winter (Figure 32). In Europe, HTF was projected to be the most prevalent in the fall and winter as well, although the seasonal cycle of HTF in Cardiff was projected to be more evenly spread throughout the year, with peaks between January and April, and again between August and October. On the North American East Coast, New York City and Jacksonville followed the typical fall and winter inflection of HTF, although HTF in Philadelphia was projected to be the most frequent from April to October. The projected seasonality of HTF at a location was related to both differences in local extrapolated monthly trends in SLC, as well as seasonality of local weather phenomena driving storm surge and waves.

Regarding the magnitude of differences in local monthly trends in SLC outlined in research question 3, surprising differences in intra-annual SLC trends were found at certain locations. MMSL affecting HTF in Hamburg during December, for example, was projected to rise 24 cm during the next nodal cycle, while MMSL was projected to rise much more slowly on the order of a few cm during most other months, or even decline, which was projected for Hamburg in November and February. Projected trends in MMSL affecting Amsterdam, Cardiff, and London showed some similarities: MSL during December was also projected to rise at the fastest rates in London (5 cm per decade) and Amsterdam (2.5 cm per decade), while the projected rate of SLR during December was also among the fastest in Cardiff (11 cm per decade). Interestingly, projected MSL in Amsterdam during February (-9 cm per decade), and March (-5 cm per decade) was projected to decline sharply in the near future, while declines during February were also projected in Hamburg (-3 cm per decade) and London (-1 cm per decade). In London, February was the only month with a negative trend in MMSL. A similar phenomenon was observed in Jacksonville, USA, where rates of SLR were highest in November and December (13 and 11 cm per decade, respectively), and lower in the spring (Between 3 and 8 cm per decade). This may be an indication of changing seasonality; i.e. changing seasonality in the ice sheet, sea and land ice, and shelves' interface with the oceans (changes in the seasonal patterns of sea ice melting (earlier start in the melting of sea ice in the year due to rising temperatures as global mean temperatures warm (at rates that are amplified in the arctic (Gutiérrez et al. 2021; Griffith and Kozick-Kingston 2022), less multi-year ice (ice that remains solid for at least one summer), delayed freeze-up in the winter (Zheng et al. 2021), as well as cascading effects on global ocean circulation (thermohaline circulation) (Thibodeau et al. 2018), which in turn causes feedback loops in complex interactions occurring between different parts of the hydrological cycle, ocean-atmosphere interactions, and

ocean properties causing different patterns and trends during the different seasons creating varying trends in the net effect on MSL during different seasons (Commonwealth Scientific and Industrial Research Organisation). The unprecedented upwards trend in MMSL observed during December in the European cities sampled may be a result of the later freeze-up in the winter as temperatures are warmer than usual, leading to less sea and land ice in the early winter, and consequently more water in the oceans resulting in higher sea levels, although declining trends in MMSL during the late winter across several European cities would indicate more freezing later in the winter. However, there was no consistent pattern of trends in MMSL indicating earlier starts in the melting of sea ice in the late spring or early summer.

Regarding the investigation of modulating strength by lunar precession on the highest astronomical tides outlined in research question 4, modulation of 99th percentile level tides by lunar precession was detected at every location, typically on the order of several centimeters of modulation by either cycle. The strongest modulation was detected in Cardiff and Bangkok, with total modulations by the nodal cycle of 21.6 and 21.4 cm, respectively. Modulation by the nodal cycle was clearly visible in annual projections of HTF counts in Bangkok, Cardiff, and Manila, showing the importance of understanding the local strength and timing of lunar modulation by the nodal and perigean cycles on HTF frequency. Furthermore, the nodal cycle was found to dominate over the perigean cycle in terms of high tide modulation. By contrast to the 20+ cm of modulation in Cardiff and Bangkok, the strongest modulation by the perigean cycle was found to be 6.8 cm, also in Cardiff, while much smaller modulating strengths were found at all other locations.

Below, results are discussed for each city with regard to existing and planned flooding adaptation and mitigation measures.

1. Bangkok, Thailand

HTF frequency was projected to increase and remain at such a level and consistency over the 2020's in Bangkok that local decision-makers are urgently recommended to prioritize long-term measures such as the flood barriers, which are designed to stop flooding events from occurring, while the pumping stations are designed to mitigate the effects of floods after they have occurred. Emphasis is placed on making sure existing water pumping stations are functioning at peak efficiency. In addition, still existing wetlands are recommended to be protected, and planning laws enforced to stop continued urbanization in flooding-prone areas. Risks should be communicated to inform residents and future residents of the projected increase in HTF frequency and severity.

Between sixty and one-hundred annual minor HTF events were projected consistently over the 2020's and 2030's with moderate HTF events on the order of ten annually also projected. HTF events were also projected to cluster between October and February, with the absolute highest frequencies in December and January, which should be communicated to prioritize construction of adaptation measures in the spring and summer, and to warn locals and incoming travelers of these elevated flood risk conditions. The majority of days in December were projected to be HTF days on average over the 2020's and 2030's. In the case of years with higher MMSL than projected linearly, the counts of minor and moderate HTF events were found to be further amplified, with the majority of days in December and January projected to be flooded. The tide-amplifying phase of the nodal cycle was found to amplify high tides and thus supplement rates of SLR until 2028,

after which high tides will be effectively dampened by lunar precession, counteracting SLR until the mid 2030's. Peak high tide amplification will occur in 2024/2025.

Storm events during the monsoon season are also expected to bring worse flooding as sea levels increase. When storm surges, astronomical high tides, and strong rain events coincide over rising sea levels, more severe events are expected.

2. Amsterdam, the Netherlands

Although the Netherlands would likely be prepared for increasing HTF frequencies due to the array of existing flood defenses, projections showed similar frequencies of minor and moderate HTF in the near future as seen between 1999 and 2017. Furthermore, only limited modulation of high tide levels by lunar precession was found, with a maximum amplification of 1.6 cm projected in 2034 and 2035. Despite this, months/years of extreme MMSL on the order of those observed over the last nodal cycle covered by tide-gauge data were found to have the potential to cause increased HTF counts, especially in November and December. HTF counts in January, February, and March were projected to decline, and were instead projected to occur more often in November and December, which may be linked to changing seasonality in snowfall and sea ice freezing and melt (Räisänen 2014).

3. Cardiff, UK

Projections of total annual HTF counts showed that the frequency of HTF will remain similar during the 2020's as experienced during the 2010's, before both the frequency of minor and moderate flooding will increase again in the 2030's. As the city has planned for a new coastal flood defense system scheduled to be completed in 2025, this timeframe is adequate to protecting residents, businesses and infrastructure from intensifying flooding. Seasonality in HTF was projected to remain similar over the next nodal cycle, with January through April, and August through October projected to be the most affected by HTF. However, trends in SLC were found to be the greatest in February through April, June and December with over ten centimeters of SLR projected per decade during these months; HTF will thus likely become more common during these months. It was found that months and years with large residuals in mean sea level above the projected linear trends would cause a further two to four days of minor and moderate HTF monthly.

With a very high tidal range and large positive trends in SLR, Cardiff and locations towards the interior of the Bristol Channel will see a difference in the ratio of the local tidal forcing frequency to the period of the channel. If this ratio becomes closer to one by the tidal forcing frequency becoming more similar to the period of the channel, then a resonance between the two will result in amplification of astronomical tides. This would result in an even greater tidal range, and stronger combinations with storm surges resulting in heightened HTF frequency and intensity. The opposite is also possible if SLR causes the tidal forcing frequency to move away from resonance with the channel (Guerreiro et al. 2015). Pelling and Green (2014) and Idier et al. (2017) conduct modeling to ascertain the effect SLR will have on this phenomenon in the Bristol Channel. Pelling and Green (2014) find that the amplitude of the dominating local tidal constituent would decline by up to 10 cm under 1 meter of SLR, with barely noticeable changes at 50 cm of SLR. On the other hand, Idier et al. 2017 find differing effects of SLR on maximum tidal water level in the Bristol Channel depending on the point in the channel. At the model grid cells closest to the location of Cardiff

within the Bristol Channel, 1 meter of SLR is found to increase maximum tidal water levels by only a few cm. As SLR over the next nodal cycle was projected to increase by a maximum of only ~20 cm, the effect on local tidal range would thus be negligeable based on results from this study.

Modulation of astronomical tides by lunar precession, however, was found to be strong, with the nodal cycle projected to first dampen high tide levels during the 2020's, before reaching its tide-amplifying phase during the 2030's (Figure 29A and 29B). 10+ cm of amplification was projected between 2032 and 2037 due to combined forcing by the nodal and perigean cycles.

There was also an indication of outside disturbances in the tide gauge record at Hinkley Point, with unrealistically high readings that suggested either malfunctions in the tide gauge reading, or outside disturbances such as seismic/strong vibrational activity from nearby nuclear power plants at the Hinkley Point tide gauge location, as well as construction of the new Hinkley Point C nuclear power station (Bolton et al. 1979; Tromans et al. 2019). The uncharacteristically high mean sea level values following the period of missing data (Figure 30) is likely due to such a disturbance of the gauge. In months affected by this spike, the linear extrapolation of SLC may have been somewhat affected.

4. Manila, the Philippines

Manila was found to have some of the greatest projected increases in HTF flooding; during the 2020's an unprecedented increase was projected, although the overwhelming majority of these events were projected to be minor, as opposed to moderate or beyond. These events were projected to cluster mainly in the summer months, with lesser frequencies in the fall and winter. Frequencies of over ten minor flooding events during the summer months beginning in the mid 2020's were projected, with extreme mean sea levels on the order of magnitude of those seen during the observational period projected to result in fifteen counts during summer months.

The modulation of HTF by lunar precession was heavily evident, with the tide-amplifying phase of the nodal cycle found to supplement projected rates of SLR to produce the sudden increase in HTF events in the 2020's, before the tide-dampening phase of the nodal cycle counteracts some of the SLR in the early 2030's, projected to cause a dip in HTF frequency during that period compared to during the 2020's, although this will be temporary.

The fact that local news reports state that HTF is already very evident in parts of the city, while monthly HTF frequencies during the observational period showed maximums of five monthly HTF days means that flooding thresholds in Manila may be lower than those utilized in this paper, which stem from flooding thresholds in American coastal cities, or that the tide-gauge providing data for this study is located in a part of the city that is less prone to HTF. Either way, the discrepancy between HTF frequencies reported by local news reports which state that certain parts of the city become inundated with every high tide, and those presented in this study during the observational and projection periods means that HTF may increase even more strongly in frequency and severity than projected here, especially in vulnerable parts of the city. Thus, the recent formation of the MBSDM and related partnering with Royal HaskoningDHV to produce and implement flood protection plans is not a moment too soon in improving Manila's flood defenses and resilience to HTF, while also communicating the risk to residents living in hazard-prone areas. Those involved

in this initiative are urgently encouraged to continue their progress in light of HTF projections made here.

5. London, UK

London was projected to experience a marginal increase in minor flooding events, first in the mid-to-late 2020's, and then again in the mid-to-late 2030's. Increases were projected to be clustered in the fall and early winter, with December especially affected. One moderate HTF event was projected to occur every December on average until 2039. Although modulation of high tide height by lunar precession was found to be relatively weak compared to other locations, it was visible on projected HTF counts, with the marginal increase in HTF events projected during the mid-to-late 2030's coinciding with the tide-amplifying phase of the nodal cycle. In the case of higher-than-normal mean sea levels on the order of magnitude of those observed between 2002 and 2020, HTF frequency was projected to marginally increase by one to two extra days per month in the fall and early winter.

The effectiveness of existing and planned improvements (between 2035 and 2050) of flood defense systems in London in dealing with the marginal increases in HTF projected here may be based on their recent performance; it is uncertain that existing flood defense infrastructure will need to be updated to effectively handle marginal increases in minor HTF frequency before the anticipated 2035 to 2050 timeframe.

6. Hamburg, Germany

The same projected increase in December HTF projected in London was also projected in Hamburg, with minor HTF frequency projected to more than double on average until 2038, and moderate HTF frequency also projected to increase slightly. HTF frequency during all other months was projected to remain very similar to those observed between 2001 and 2019. Despite this, extreme mean sea levels on the order of magnitude of those observed between 2001 and 2019 were found to still be able to cause a projected doubling in minor and moderate HTF frequencies if they occur.

Modulation of astronomical tide heights by lunar precession was found to be weak, however, meaning that future frequencies of HTF will be mainly governed by sea level change and atmospheric conditions creating storm surge and waves.

During times of higher-than-normal mean sea levels, areas protected solely by linear flooding defenses may be at risk, thus it is recommended to strengthen and raise existing dikes and flood defense walls, and to add more sand to coastal dunes protecting the Elbe waterway.

7. Philadelphia, USA

Subtle increases in minor HTF were projected during the 2030's, although only around one HTF day during any given month was projected on average until 2039. In the case of exceptional mean sea levels above projected trends on the order of magnitude observed between 2002 and 2020 however, minor HTF frequencies were projected to exceed ten days during the most affected months, with the HTF season projected to be mainly between April and October. Modulation of

the highest astronomical tides by lunar precession was found to be weak compared to other locations, with combined nodal and perigean cycles amplifying high tides to a maximum of around one centimeter.

Due to the possibility of increasing frequencies of minor HTF in the 2030's during months/years of exceptional mean sea levels above local trends in SLR, findings in this thesis support the American Society of Civil Engineers' initiatives to innovate in the areas of flood prevention and resilience, as well as the strengthening of existing flood defenses prior to 2030. Thus, in the case of mean sea levels exceeding monthly trends in SLR by similar orders of magnitudes as seen between 2002 and 2020, an increase in flood days was projected even prior to the 2050 mark set by the NOAA.

8. New York City, USA

HTF frequency was projected to increase throughout the 2030's, with over thirty annual HTF days projected in the middle of the decade, although most of these were found to bring minor flooding, with fewer moderate high tide-induced flooding events. Seasonally, HTF was projected to increase almost year-round on average, although the strongest increases were projected for October and December. In the case of exceptionally high mean sea levels exceeding monthly trends in SLR by the orders of magnitude observed between 2000 and 2018, minor HTF days were projected to occur ten days per month during the most flooding prone months by the mid-2030's. Modulation by the nodal cycle was found to be in its tide-amplifying phase during this time, although coinciding amplification with the perigean cycle was projected to only amplify high tide levels by around 2 cm.

While the expensive and ambitious "Big U" project to construct a protective sixteen-kilometer barrier disguised as museums and various public spaces around the southern part of Manhattan to preserve the cultural tie to the waterfront is expected to provide flood protection to the borough of Manhattan, existing or planned flood defense infrastructure and strategies for the remaining boroughs of New York City are not included in the literature, and so may be neglected in terms of flood protection infrastructure. Thus, if such adaptive measures are not present or planned at waterfronts throughout the city, local planners and decision-makers are encouraged to support endeavors to improve HTF resilience throughout all boroughs to projected increases in HTF by 2030.

9. Jacksonville, USA

HTF projections showed an increase in the frequency of minor HTF events, building slowly during the 2020's before increasing further during the 2030's. Increases in HTF days were projected to be clustered in the fall and early winter, with November projected to be the most affected with an average of five minor HTF events projected until 2039. In the 2030's, months with up to ten days of HTF were projected, which was projected to rise to over twenty during the late 2030's in the case of exceptional mean sea levels on the order of magnitude of those observed between 2002 and 2020. The highest astronomical tides were found to be modulated relatively weakly by lunar precession, with roughly 2 cm of amplification projected in 2033 and 2037.

As the overwhelming majority of projected HTF events were identified as minor as opposed to moderate or beyond, the current flood resilience strategy in Jacksonville of restoring wetlands and expanding mangrove forests to provide a buffer to urban areas may be sufficient to avoid inundation of residential and commercial areas, although projected clustering of events in October and November may require additional, less attractive hard flood prevention mechanisms such as barriers and/or flood gates, as well as alteration of rivers to increase their capacity, and ideally pumping stations to mitigate the disruptive effects of HTF events that do breach the wetlands and natural areas surrounding the city.

10. Hong Kong, SAR China

Subtle increases in minor HTF frequency were projected from the second half of the 2020's to the mid-2030's, with HTF days projected to cluster mainly between October and January. In the case of exceptional mean sea levels on the order of magnitude observed between 2000 and 2018, HTF days were projected to exceed ten per month, while moderate HTF days were projected to become more frequent.

The nodal cycle was found to be the dominating local lunar precession modulating high tide levels, with high tides projected to be amplified until 2028, before being dampened for several years (Figure 64). The greatest amplification of high tides by lunar precession over the projected nodal cycle was projected to be between 2022 and 2027.

Hong Kong's well developed Flood Risk Management practices are expected to be able to effectively protect the city from projected HTF frequencies until the mid-2030's, although it is recommended for local leaders to expand the authority of the Hong Kong Planning Department in restricting building projects in flooding-vulnerable zones to avoid exposure of workers and new buildings to unnecessary flood-risk.

Underlying Projections in MMSL

The array of trends in MMSL over the latest full nodal cycle covered in existing sea level data used in this thesis to project SLR into the future taking into account seasonal cycles in weather were fitted over a shorter timeframe (19 years) than is typically customary (Tebaldi et al. 2012)). However, nineteen years resolved major cyclical climatic phenomena such as the El Niño Southern Oscillation (which tends to occur every three to five years) multiple times (NOAA(a)). Other circulation patterns such as the North Atlantic Oscillation, occur at much higher frequencies, and as such were resolved more often. Moreover, the shorter timeframe was designed to capture more recent trends in mean sea level fluctuation, as there is evidence that GMSL rise is accelerating (Oppenheimer et al. 2019).

Rates of projected SLC found at site-specific tide gauges in this thesis were unique from regional SLR projections by the Coupled Model Intercomparison Project Phase 6 (CMIP6) forced by Shared Socioeconomic Pathways SSP1 & 5 as they are presented by the advanced regional information IPCC WG1 Interactive Atlas (Eyring et al. 2016; Gutiérrez et al. 2021). The SSP1, sustainable socioeconomic development scenario is similar to the Representative Concentration Pathway RCP2.6, while the SSP5 fossil-fueled development scenario is similar to RCP 8.5,

representing the socioeconomic development scenario generating the most emissions, environmental damage, and highest rates of SLR globally (Abram et al. 2019). Although the most aggressive scenarios continue to be the best match over near to mid-term time frames when taking into account current and planned climate policies (Schwalm et al. 2020), projections made here showed that several cities were projected to have lower rates of SLR over the near term than is expected by even the most optimistic scenario forcing respective regional models. For example, in the European cities analyzed, Amsterdam, London and Hamburg were all projected to have lower rates of SLR than is suggested by the range of model outputs within CMIP6 following SSP1 (figure A.1), although rates of SLR in Cardiff were projected to be twice as high as projections within CMIP6. In Amsterdam especially, trends in MMSL between 1999-2017 used in the projection of near-term future sea levels were much lower than CMIP6 projections made with reference data only a few years older, and projected to a timeframe only a few years farther into the future. In North America, SLR was also projected to be less in Philadelphia and New York City than is projected by CMIP6 models for Eastern North America, although SLR projections for Philadelphia made here were very similar to the CMIP6 SSP1 projection (figure A.2). MMSL projections in Bangkok and Manila were higher than both CMIP6 SSP1 and SSP5 projections for the South East Asia Region (figure A.3), while the opposite was the case for MMSL projections made here for Bangkok, and the CMIP6 East Asia Region (figure A.4).

Modulation of HTF by Lunar Precession

Every city appeared to be affected to some degree by either the nodal cycle, perigean cycle, or both precessions in the Moon's orbital path. In cities that exhibited strong tidal modulations by cycles in the Moon's orbit, the influence of these cycles was visible in time-series of historical and projected monthly HTF frequency. Haigh et al. (2011) examine the influences of these cycles globally and also find variability in the strength in modulation of high tides globally ranging between an influence of only a few centimeters for the majority of locations up to thirty to forty centimeters of modulation by the nodal cycle in the strongest affected regions, such as in the South China Sea. Peng et al. (2019) find similar modulating strengths by these cycles, with maximum nodal cycle modulations of up to thirty centimeters in the Gulf of Tonkin, the English Channel, and the Bristol Channel. The strength in these modulations largely correspond to the strengths found in this thesis, although the modulation of over 40 cm that is detected by Haigh et al. (2011) in Beihei, China, and up to 30 cm that is detected by Peng et al. (2019) in the same region are much larger than those detected here at similar geographic locations in Hong Kong (8.1 cm) and Manila (13.4 cm). This is likely due to Beihei being located in the Gulf of Tonkin, which is macrotidal (tidal range of above 4 meters), while Hong Kong is mesotidal (tidal range between 2 and 4 meters), and Manila is microtidal (tidal range less than 2 meters), which is likely the reason for a greater lunar modulation of the highest tidal heights in Beihei (VanGraafeiland 2020). Furthermore, the high modulating strengths that Haigh et al. (2011) find in Beihei may also be related to local coastal geometry; nodal modulation of high tides affecting Bangkok in this study were found to be stronger (21.4 cm) than in Hong Kong (8.1 cm) and Manila (13.4 cm). Bangkok itself is also located in a gulf (the Gulf of Thailand), the resonance of which is known to be linked to the resonance of the South China Sea (Cui et al. 2019). As the highest tidal ranges typically occur in bays, channels, and narrow inlets due to resonance effects and the funneling of water into a narrow region (McLaughlin et al. 2022), coastal geometry and bathymetry are likely important factors linked to strong lunar modulations of high tide heights. The dominating lunar precession

in Bangkok, Manila and Hong Kong was found to be the nodal cycle as well; located within the hotspot of nodal (18.61-year) modulations that Haigh et al. (2011) also identify (Figures 7a and 8). The ranges in modulations by the nodal cycle detected at these locations also correspond well to those that Haigh et al. (2011) present for the South China Sea and the Gulf of Thailand. The strong modulation of the highest tides by mainly the nodal cycle found in Cardiff also matches the findings of Haigh et al. (2011) and Peng et al. (2019) in that nodal modulations in the Bristol Channel local to Cardiff are some of the strongest in the world. However, Haigh et al. (2011) also find a large perigean (4.425-year) modulation local to Cardiff and the Bristol Channel, while modulation of the highest tides by the perigean cycle in Cardiff was found to be around 7 cm in this study, with the nodal cycle found to be the dominant lunar precession modulating tidal heights.

Thompson et al. (2021) find modulation in the astronomical tides of American coastal cities, citing an influence of 4.7 cm in the modulation of the highest astronomical tides by the nodal cycle in St. Petersburg, Florida, USA. A HTF projection for Jacksonville, also a city in Florida, USA, was produced in this dissertation. The nodal cycle was found to be the dominant lunar precession modulating the highest tides, with an influence of 3.6 cm, a similar result. A lower modulating strength found here may again be due to factors related to differences in coastal geometry and bathymetry between St. Petersburg and Jacksonville.

Assumptions and Future Work

In the methods of this thesis, there was an assumption made in that predictions in elements of the tidal record attributable to surge, wave setup, and swash will not be altered by interactions with trends in MMSL, or changes in climate. As discussed in the background, changes in MSL can alter the ratio of the local tidal forcing frequency to the period of the respective ocean basin, which pushes the system either closer or farther away from achieving a resonance, which is when the highest tidal ranges occur (Guerreiro et al. 2015; Idier et al. 2017; Idier et al. 2019). This phenomenon was not explicitly included in the analysis and would require extensive modeling of ocean basins and coastal topography, and application of hydro-physics. In addition, while the deterministic prediction of surge, wave setup, and swash did implicitly account for forcings by differences in seasonal weather, and seasonal differences in MMSL's between months of the year, it did not explicitly account for forcings by phases in major tidal constituents, which Idier et al. 2019 investigate and find to be on the order of a meter for tidal modulation of surge, and on the order of ten centimeters for the tidal modulation of wave setup, depending on location. Furthermore, modeling of changes in elements of global thermohaline circulation such as the slow down of the Gulf Stream that Dong et al. (2019) find over past decades together with its effect on seasonal cycles in MMSL, other elements of sea level, and HTF as a whole remains of interest. Further investigation into these interactions for individual locations is recommended in future projections of HTF.

Thus, in a future study it would also be interesting to explicitly present the strength of seasonal modulations in MSL on the amplitudes of tidal constituents as well as on other sea level components such as wave-setup at each location. Theoretically, depending on coastal geometry, a rise in MSL would allow waves to break and astronomical tides to build with less frictional dampening by the sea floor (if seafloor topography is assumed to remain unchanged), creating

higher water levels (Idier et al, 2019). This would also give an indication of how potential SLR would affect the amplitudes of tidal constituents locally.

The next step would be to compare the deterministic, seasonal model of non-astronomical and non-MSL related tidal components to combined localized models of storm surge, wave setup and swash, and to include forcings by localized climate simulations in future projections of HTF frequency, specifically in the modeling of surge in response to projected atmospheric changes. The Global Tide and Surge Model Version 3.0 (GTSM3) is one such model; being a depth-averaged hydrodynamic model which estimates wind stress to model surge, which has a high coastal resolution of 2.5 km globally (1.25 km in Europe) and shows good performance when compared to observed sea levels (Muis et al. 2020). The Global Tide and Surge Reanalysis (GTSR) dataset (Muis et al. 2016) could also be applied to determine historical values of surge by month, as well as reanalysis wave model datasets such as ERA-interim (Dee et al. 2011), or GOW2 (Perez et al. 2017). However, Woodworth et al. (2021) have shown that sensitivity of coastal locations to rising sea levels tends to be overestimated by around thirty percent when modeling tide and surge derived from the GTSR dataset. Numerical models used in other studies have also produced overestimates of future coastal flooding risks (Hunter et al. 2017; Muis et al. 2017). The new and improved GTSM3 has not yet been evaluated in the same way, although Muis et al. (2020) cite a mean bias in the maximum annual sea levels half as large as in the earlier GTSR dataset.

Overlaying harmonic analysis of major tidal constituents with deterministic and reanalyzed datasets of surge and wave setup combined with local weather/climate could uncover valuable insights on interactions between major tidal constituents, surge, and wave setup to continue to develop projections in HTF.

The present analysis also assumed no existing or planned flood defenses to be in place. Thus, in cities with existing flood defenses, flooding thresholds are likely to be higher than those used here. Also, minor and moderate flooding thresholds of 0.5 and 0.8 meters above MHHW are values specifically for US coastal cities; these may be different in other parts of the world.

Lastly, there was another assumption made, which was that the detected phases and amplitudes of modeled tidal constituents were accurate, and that all relevant constituents at a respective location were accounted for. In regard to this assumption, tidal predictions from UTide are robust when compared to predictions by the NOAA (Thompson et al. 2021), and using lower signal to noise ratios (than the standard ratio of 2) in an attempt to detect smaller influences of other tidal constituents would run the risk of misidentifying influential tidal constituents and including them in the analysis.

Overall, to reiterate the discussion of HTF projections in the context of existing and planned flooding defenses discussed above, decision makers in most major coastal metropolises examined here are strongly encouraged to plan with increases in HTF events in the near future: the cities examined in this thesis are critical economic and cultural centers, and as such the impacts of HTF transcend far beyond the city itself. Movement of sewage and waste management systems to higher elevations where their integrity will not be compromised is a must to avoid the threat of disease and overall untidiness resulting from parts of a city being submerged. Sites of economic importance are encouraged to consider moving, and new housing and construction projects should

be wary of increases in incidences of HTF in the near future, and their development blocked by local government in flood-prone regions, near future meaning during the coming years as well as over the next decades. Mitigation and adaptation strategies to projected increases in consistent HTF are suggested to be updated in cities with large projected near-future increases in HTF, and policy makers are asked to act considering the years and seasons of greatest projected HTF frequencies presented for their respective locations.

Furthermore, the methods and results of this thesis are also relevant to insurance companies providing flood insurance to private and commercial properties in coastal areas, especially as the projection timeframe can be extended consistently as newer tide-gauge data becomes available.

Conclusion

The aim of this thesis was to create a novel HTF projection framework and early warning system specialized to model localized HTF frequency into the near future (over the next ~19-year nodal cycle) with the specific and unique ability to identify years and months/seasons of the greatest predicted HTF frequencies, the main motivation being to warn local residents, businesses and travelers, while galvanizing decision makers to implement appropriate mitigation and adaptation measures within appropriate time frames. Further motivations included addressing the lack of high granularity, near-future projections of coastal flooding, and the lack of attention to the projection of HTF frequencies. The novel features within the projection framework included the diversification of underlying SLC projections to characterize changing seasonality in the melting and freezing of sea ice and the effect on intra-annual SLC and climatic cycles modulating mean, non-tidal, sea level variability. Another novel method encompassed the consideration of the correlation of astronomical tides with sea level variability by conducting dedicated harmonic analysis on tide gauge data binned by month. Additionally, the methods implemented took into account the combined effects of SLC and modulations by precessions in the Moon's orbital path around the Earth on the heights of the highest astronomical tides, while a representation of seasonal extremes in MSL in a second projection of SLC was also included to quantify the upper bounds of projected HTF frequencies. The capabilities of the HTF projection framework presented in this thesis were shown by conducting monthly granularity predictions of minor and moderate HTF and presenting seasonal event patterns for the world's top ten popular travel destinations at the most risk from potential SLR according to the 2050 Climate Change City index.

Furthermore, this thesis was designed to answer the following research questions:

1. How will HTF frequency change in the near future for popular travel destinations at the greatest risk from potential SLR?
2. During which seasons/months will HTF be the most frequent?
3. How large are differences in intra-annual SLC trends?
4. How strong is the modulation of the highest tides by lunar precession?

(1) Bangkok, Thailand and Manila, the Philippines were projected to be the sites of large increases in the frequency of HTF events even during the 2020's, while Jacksonville and New York City, USA were projected to follow with increases in HTF frequency during the 2030's. London and Cardiff, UK, Hamburg, Germany, Philadelphia, USA and Hong Kong, SAR China were projected to see less obvious increases in HTF until 2040, while HTF frequency in Amsterdam, interestingly, was projected to remain similar, and even decline over the same time frame. These results showed that several popular coastal cities will experience flooding prior to time frames typically discussed in existing literature.

(2) Furthermore, increases in HTF events were most often projected to be concentrated during particular season(s) or month(s) as opposed to being projected to be evenly spread out. Especially in cities with the highest projected increases in HTF frequency, this phenomenon was found to be most pronounced, which may lead to the exceedance of critical frequencies in HTF able to cause major disruptions in coastal economic and cultural hubs decades earlier than expected.

(3) Surprising differences in intra-annual SLC trends were found in several locations, although mostly in Europe. In Hamburg, MMSLs in December showed an increasing trend much greater than during all other months. Interestingly, a pattern among discrepancies in MMSL trends became evident across several locations, with the highest rates of SLR in December, and lower rates of SLR and even declines in MSL found in the late winter and early spring. This may be an indication of changing seasonality in the ice sheet, sea ice, and shelves' interface with the oceans, specifically the delay in the freeze-up of sea and land ice. The recent slow down of the Gulf Stream is also known to be involved in rates of SLR regionally (Dong et al. 2019), and remains an area of potential research in regard to the regional effect on rates of SLR. Intra-annual differences in rates of SLC, especially considering months with declining rates in sea level coexisting with months of clear SLR at a given location is something that should be considered in future SLC predictions and projections of HTF.

(4) The heights of gravitational tides in every city appeared to be affected to some degree by either the nodal cycle, the perigean cycle, or by both precessions in the Moon's orbit. In cities that exhibited the strongest modulations by cycles in the Moon's orbit, the influence of lunar precession was visible in time-series of historical and projected annual and monthly HTF frequency. Typically on the order of several centimeters of modulation by either cycle, the strongest modulation was detected in Bangkok and Cardiff, with total modulations by the nodal cycle of 21.4 and 21.6 cm at the 99^{th} percentile level of astronomical tides, respectively.

The HTF projection framework presented here was set up to run with tide gauge data in TXT file format from version 3.0 of the GESLA Global Extreme Sea Level Analysis project, which features higher-frequency (hourly or more frequent) tide gauge data from over five-thousand records worldwide. HTF projections over updated timeframes are supported by the framework as new data becomes available.

References

Abram, N., Gattuso, J.P., Prakash, A., Cheng, L., Chidichimo, M.P., Crate, S., Enomoto, H., Garschagen, M., Gruber, N., Harper, S. and Holland, E., 2019. Framing and context of the report. *IPCC special report on the ocean and cryosphere in a changing climate*, pp.73-129.

Aerts, J.C. and Wouter Botzen, W.J., 2011. Flood-resilient waterfront development in New York City: Bridging flood insurance, building codes, and flood zoning. *Annals of the New York Academy of Sciences*, *1227*(1), pp.1-82.

Amadio, M., Essenfelder, A.H., Bagli, S., Marzi, S., Mazzoli, P., Mysiak, J. and Roberts, S., 2022. Cost–benefit analysis of coastal flood defence measures in the North Adriatic Sea. *Natural Hazards and Earth System Sciences*, *22*(1), pp.265-286.

Andreatta, R., Kirksey, T. Climate Signals. Coastal Flooding Increase : Coastal storms ride on top of rising seas. *Climate nexus Project*. Available at : https://www.climatesignals.org/climate-signals/coastal-flooding-increase#more (Accessed February 1st, 2022)

Andrews, M.B., Ridley, J.K., Wood, R.A., Andrews, T., Blockley, E.W., Booth, B., Burke, E., Dittus, A.J., Florek, P., Gray, L.J. and Haddad, S., 2020. Historical simulations with HadGEM3-GC3. 1 for CMIP6. *Journal of Advances in Modeling Earth Systems*, *12*(6), p.e2019MS001995.

Bailey, A.J., 2011. Population geographies and climate change. *Progress in Human Geography*, *35*(5), pp.686-695.

Barnard, P.L., Short, A.D., Harley, M.D., Splinter, K.D., Vitousek, S., Turner, I.L., Allan, J., Banno, M., Bryan, K.R., Doria, A. and Hansen, J.E., 2015. Coastal vulnerability across the Pacific dominated by El Nino/Southern oscillation. *Nature Geoscience*, *8*(10), pp.801-807.

Bolton, A.D., Furber, B.N., Parkin, M. and Walton, H., 1979. Evolution of the modifications designed to suppress the damaging vibration of the Hinkley Point'B'and Hunterston'B'gags. In *Vibration in nuclear plant. Proceedings of international conference held at Keswick, UK in May 1978*.

Bowen, A.J., Inman, D.L. and Simmons, V.P., 1968. Wave 'set-down'and set-up. *Journal of geophysical research*, *73*(8), pp.2569-2577.

Bundesanstalt für Wasserbau [German Federal Waterways Engineering and Research Institute]. Harmonic Analysis of Water Level. Competence for Waterways. Available at: https://wiki.baw.de/en/index.php/Harmonic_Analysis_of_Water_Level (Accessed October 17th, 2022)

Buchanan, M.K., Oppenheimer, M. and Kopp, R.E., 2017. Amplification of flood frequencies with local sea level rise and emerging flood regimes. *Environmental Research Letters*, *12*(6), p.064009.

Caldwell, P. C., M. A. Merrifield, P. R. Thompson (2015), Sea level measured by tide gauges from global oceans — the Joint Archive for Sea Level holdings (NCEI Accession 0019568), Version 5.5, *NOAA National Centers for Environmental Information*, Dataset, doi:10.7289/V5V40S7W.

Caldwell, P. C., Vitousek, S. & Aucan, J. P. Frequency and duration of coinciding high surf and tides along the North Shore of Oahu, Hawaii, 1981–2007. *Journal of Coastal Research*. 734–743 (2009).

Cardiff News Room. 2022. Council set to improve Cardiff flood defences. Accessed January 14, 2023 from: https://www.cardiffnewsroom.co.uk/releases/c25/29912.html

Chan, F.K.S., Chuah, C.J., Ziegler, A.D., Dąbrowski, M. and Varis, O., 2018. Towards resilient flood risk management for Asian coastal cities: Lessons learned from Hong Kong and Singapore. *Journal of Cleaner Production*, *187*, pp.576-589.

Cioffi, F., De Bonis Trapella, A., Giannini, M. and Lall, U., 2022. A Flood Risk Management Model to Identify Optimal Defence Policies in Coastal Areas Considering Uncertainties in Climate Projections. *Water*, *14*(9), p.1481.

Codiga, D.L., 2011. Unified Tidal Analysis and Prediction Using the UTide Matlab Functions. Technical Report 2011-01. Graduate School of Oceanography, University of Rhode Island, Narragansett, RI. 59pp.

Collini, Renee, 2021. High-tide flood risk is accelerating, putting coastal economies at risk. *Theconversation.com.* Mississippi State University.

Commonwealth Scientific and Industrial Research Organisation. Why does sea level change? Sea Level, Waves, and Coastal Extremes. Available at: https://research.csiro.au/slrwavescoast/sea-level/sea-level-change/ (Accessed November 27th, 2022)

Cui, X., Fang, G. and Wu, D., 2019. Tidal resonance in the Gulf of Thailand. *Ocean Science*, 15(2), pp.321-331.

Dee, D.P., Uppala, S.M., Simmons, A.J., Berrisford, P., Poli, P., Kobayashi, S., Andrae, U., Balmaseda, M.A., Balsamo, G., Bauer, D.P. and Bechtold, P., 2011. The ERA-Interim reanalysis: Configuration and performance of the data assimilation system. *Quarterly Journal of the royal meteorological society*, *137*(656), pp.553-597.

Delano, J.W. Sinking Land and Rising Seas Threaten Manila Bay's Coastal Communities. *Inside Climate News.* 2022. Accessed January 13, 2023: https://insideclimatenews.org/news/18112022/sinking-land-and-rising-seas-threaten-manila-bays-coastal-communities/

Devlin, A.T., Jay, D.A., Talke, S.A., Zaron, E.D., Pan, J. and Lin, H., 2017. Coupling of sea level and tidal range changes, with implications for future water levels. *Scientific Reports*, *7*(1), pp.1-12.

Dong, S., Baringer, M.O. and Goni, G.J., 2019. Slow down of the Gulf Stream during 1993–2016. *Scientific Reports*, *9*(1), pp.1-10.

Doodson, A.T., 1921. The harmonic development of the tide-generating potential. *Proceedings of the Royal Society of London. Series A, Containing Papers of a Mathematical and Physical Character*, *100*(704), pp.305-329.

Dupuits, E.J.C., Schweckendiek, T. and Kok, M., 2017. Economic optimization of coastal flood defense systems. *Reliability Engineering & System Safety*, *159*, pp.143-152.

Dusek, G., Sweet, W.V., Widlansky, M.J., Thompson, P.R. and Marra, J.J., 2022. A novel statistical approach to predict seasonal high tide flooding. *Frontiers in Marine Science*, *9*, p.1073792.

European Centre for Medium-Range Weather Forecasts. (2022, November 25). *CMIP6: Global Climate Projections.* ECMWF Confluence. Accessed December 30, 2022 from https://confluence.ecmwf.int/display/CKB/CMIP6%3A+Global+climate+projections

Environment Agency. November 2012. Thames Estuary 2100. Accessed January 14, 2023 from https://www.gov.uk/government/publications/thames-estuary-2100-te2100/thames-estuary-2100-te2100

Environmental Defense Fund Florida. *Let's Tackle Climate Change Florida*. 2023. Accessed January 17, 2023 from https://www.letstackleclimatechangeflorida.com/

EnvironmentAgencyTV. 2022. How does tidal flooding occur in London? *YouTube. December, 2022.*

Esri China (HK), 2022. Hong Kong 18 districts, 2022. [Shapefile]. Available at: https://opendata.esrichina.hk/datasets/eea8ff2f12b145f7b33c4eef4f045513_0/explore?location=22.356963,114.139117,10.98 (Accessed December 22nd, 2023).

Eyring, V. *et al.* (2016) 'Overview of the Coupled Model Intercomparison Project Phase 6 (CMIP6) experimental design and organization', *Geoscientific Model Development*, 9(5), pp. 1937–1958. doi: 10.5194/gmd-9-1937-2016.

Fairbridge, R.W. (1968). Swash, swash mark. In: Geomorphology. Encyclopedia of Earth Science. Springer, Berlin, Heidelberg. https://doi.org/10.1007/3-540-31060-6_364

Flood Risk Management Task Force, City of Philadelphia. *A Guide to Flooding in Philadelphia*. 2014. Accessed on January 14, 2023 from http://water.phila.org/

Friedrichs, C.T. and Aubrey, D.G., 1994. Tidal propagation in strongly convergent channels. *Journal of Geophysical Research: Oceans*, *99*(C2), pp.3321-3336.

Foreman, M.G.G. and Henry, R.F., 1989. The harmonic analysis of tidal model time series. *Advances in water resources*, *12*(3), pp.109-120.

Godin, G., 1986. The use of nodal corrections in the calculation of harmonic constants. *The International Hydrographic Review*.

Goldberg, L., Lagomasino, D., Thomas, N. and Fatoyinbo, T., 2020. Global declines in human-driven mangrove loss. *Global change biology*, *26*(10), pp.5844-5855.

Google Earth (a). Data SIO, NOAA, U.S. Navy, NGA, GEBCO Landsat / Copernicus IBCAO. 83°23'10"N, 177°41'25"W, Camera 39,556 km. Accessed on November 15, 2022 from http://www.earth.google.com

Google Earth (b). Data SIO, NOAA, U.S. Navy, NGA, GEBCO Landsat / Copernicus IBCAO. 00°00'00"N, 20°10'36"E, Camera 22,035 km. Accessed on November 15, 2022 from http://www.earth.google.com

Griffith, J. and Kozick-Kingston, M., 2022. Arctic Feedbacks: Not All Warming Is Equal. *The Science Teacher*, *89*(4), pp.38-45.

Guerreiro, M., Fortunato, A.B., Freire, P., Rilo, A., Taborda, R., Freitas, M.C., Andrade, C., Silva, T., Rodrigues, M., Bertin, X. and Azevedo, A., 2015. Evolution of the hydrodynamics of the Tagus estuary (Portugal) in the 21st century. *Revista de Gestão Costeira Integrada-Journal of Integrated Coastal Zone Management*, *15*(1), pp.65-80.

Gutiérrez, J.M., R.G. Jones, G.T. Narisma, L.M. Alves, M. Amjad, I.V. Gorodetskaya, M. Grose, N.A.B. Klutse, S. Krakovska, J. Li, D. Martínez-Castro, L.O. Mearns, S.H. Mernild, T.

Ngo-Duc, B. van den Hurk, and J.-H. Yoon, 2021: Atlas. In *Climate Change 2021: The Physical Science Basis. Contribution of Working Group I to the Sixth Assessment Report of the Intergovernmental Panel on Climate Change* [Masson-Delmotte, V., P. Zhai, A. Pirani, S.L. Connors, C. Péan, S. Berger, N. Caud, Y. Chen, L. Goldfarb, M.I. Gomis, M. Huang, K. Leitzell, E. Lonnoy, J.B.R. Matthews, T.K. Maycock, T. Waterfield, O. Yelekçi, R. Yu, and B. Zhou (eds.)]. Cambridge University Press, Cambridge, United Kingdom and New York, NY, USA, pp. 1927–2058, doi:10.1017/9781009157896.021.

Haigh, I.D., Eliot, M. and Pattiaratchi, C., 2011. Global influences of the 18.61 year nodal cycle and 8.85 year cycle of lunar perigee on high tidal levels. *Journal of Geophysical Research: Oceans*, *116*(C6).

Haigh, I.D., Marcos, M., Talke, S.A., Woodworth, P.L., Hunter, J.R., Hague, B.S., Arns, A., Bradshaw, E. and Thompson, P., 2021. GESLA Version 3: A major update to the global higher-frequency sea-level dataset. *Geoscience Data Journal*.

Hashemi, M.R., Neill, S.P., Robins, P.E., Davies, A.G. and Lewis, M.J., 2015. Effect of waves on the tidal energy resource at a planned tidal stream array. *Renewable Energy*, *75*, pp.626-639.

Held, I.M., Guo, H., Adcroft, A., Dunne, J.P., Horowitz, L.W., Krasting, J., Shevliakova, E., Winton, M., Zhao, M., Bushuk, M. and Wittenberg, A.T., 2019. Structure and performance of GFDL's CM4. 0 climate model. *Journal of Advances in Modeling Earth Systems*, *11*(11), pp.3691-3727.

Hijmans, Robert J, 2015 (a). University of California, Berkeley. Second-level Administrative Divisions, Germany, 2015. [Shapefile]. Available at: https://geodata.lib.utexas.edu/catalog/stanford-nz271ny2119(Accessed December 22nd, 2022).

Hijmans, Robert J, 2015 (b). University of California, Berkeley. Second-level Administrative Divisions, Netherlands, 2015. [Shapefile]. Available at: https://earthworks.stanford.edu/catalog/stanford-sq928md5963 (Accessed December 22nd, 2022).

Hijmans, Robert J, 2015 (c). University of California, Berkeley. Second-level Administrative Divisions, Philippines 2015. [Shapefile]. Available at: https://earthworks.stanford.edu/catalog/stanford-sq928md5963 (Accessed December 22nd, 2022).

Hijmans, Robert J, 2015 (d). University of California, Berkeley. Second-level Administrative Divisions, United Kingdom, 2015. [Shapefile]. Available at: https://earthworks.stanford.edu/catalog/stanford-mw379pp5559 (Accessed December 22nd, 2022).

Hijmans, Robert J, 2015 (e). University of California, Berkeley. Second-level Administrative Divisions, United States 2015. [Shapefile]. Available at: https://geodata.lib.utexas.edu/catalog/stanford-gv775hx4053(Accessed December 22nd, 2022).

Hino, M., Belanger, S.T., Field, C.B., Davies, A.R. and Mach, K.J., 2019. High-tide flooding disrupts local economic activity. *Science advances*, *5*(2), p.eaau2736.

Hobson, B., 2014. *Big U storm defences "will secretly protect Manhattan from flooding" says Bjarke Ingels*. Dezeen. Available at: https://www.dezeen.com/2014/07/11/movie-bjarke-ingels-big-u-storm-defences-protect-manhattan-flooding/ (Accessed January 15th, 2023).

Holgate, S.J. et al. 2011. New Data Systems and Products at the Permanent Service for Mean Sea Level. (In preparation).

Howarth, D., 2018. *BIG U flood defences for Manhattan move forward*. dezeen. Available at: https://www.dezeen.com/2018/07/20/big-u-storm-flood-defences-east-side-coastal-resiliency-manhattan-move-forward/ (Accessed January 15th, 2023).

Humanitarian Data Exchange, 2022. Thailand – Subnational Administrative Boundaries. *OCHA Regional Office for Asia and the Pacific (ROAP)*. Available from: https://data.humdata.org/dataset/cod-ab-tha (Accessed December 22nd, 2022).

Hunter, J.R., Woodworth, P.L., Wahl, T. and Nicholls, R.J., 2017. Using global tide gauge data to validate and improve the representation of extreme sea levels in flood impact studies. *Global and Planetary Change*, *156*, pp.34-45.

Idier, D., Paris, F., Le Cozannet, G., Boulahya, F. and Dumas, F., 2017. Sea-level rise impacts on the tides of the European Shelf. *Continental Shelf Research*, *137*, pp.56-71.

Idier, D., Bertin, X., Thompson, P. and Pickering, M.D., 2019. Interactions between mean sea level, tide, surge, waves and flooding: mechanisms and contributions to sea level variations at the coast. *Surveys in Geophysics*, *40*(6), pp.1603-1630.

IPCC, 2019: Summary for Policymakers. In: IPCC Special Report on the Ocean and Cryosphere in a Changing Climate [H.-O. Pörtner, D.C. Roberts, V. Masson-Delmotte, P. Zhai, M. Tignor, E. Poloczanska, K. Mintenbeck, A. Alegría, M. Nicolai, A. Okem, J. Petzold, B. Rama, N.M. Weyer (eds.)]. In press.

Jonkman, S.N., Hillen, M.M., Nicholls, R.J., Kanning, W. and van Ledden, M., 2013. Costs of adapting coastal defences to sea-level rise—new estimates and their implications. *Journal of Coastal Research*, *29*(5), pp.1212-1226.

Kirezci, E., Young, I.R., Ranasinghe, R., Muis, S., Nicholls, R.J., Lincke, D. and Hinkel, J., 2020. Projections of global-scale extreme sea levels and resulting episodic coastal flooding over the 21st Century. *Scientific reports*, *10*(1), pp.1-12.

Kopp, Robert E., Radley M. Horton, Christopher M. Little, Jerry X. Mitrovica, Michael Oppenheimer, D. J. Rasmussen, Benjamin H. Strauss, and Claudia Tebaldi. 'Probabilistic 21st and 22nd Century Sea-Level Projections at a Global Network of Tide-Gauge Sites'. Earth's Future 2, no. 8 (2014): 383–406. https://doi.org/10.1002/2014EF000239.

Lavery, S. and Donovan, B., 2005. Flood risk management in the Thames Estuary looking ahead 100 years. *Philosophical Transactions of the Royal Society A: Mathematical, Physical and Engineering Sciences*, *363*(1831), pp.1455-1474.

Lewis, M.J., Angeloudis, A., Robins, P.E., Evans, P.S. and Neill, S.P., 2017. Influence of storm surge on tidal range energy. *Energy*, *122*, pp.25-36.

Liu, Q.J., Wang, D.T., Wei, Z.P., Xu, H. and Sun, T.T., 2020. Study on the Set-up and Set-down Induced by Breaking Waves Over A Reef. *China Ocean Engineering*, *34*(6), pp.853-862.

Lui, W.H., 2018. On sea level rise and abnormal sea level in Hong Kong. Hong Kong Observatory.

McLaughlin, C., Law, B. and Mulligan, R., 2022. Modeling surface waves and tide–surge interactions leading to enhanced total water levels in a macrotidal bay. *Coastal Engineering Journal*, *64*(1), pp.24-41.

Meehl G A et al. 2007. Global climate projections Climate Change 2007: The Physical Science Basis. Contribution of Working Group I to the Fourth Assessment Report of the Intergovernmental Panel on Climate Change (Cambridge: Cambridge University Press)

Menéndez, P., Losada, I.J., Torres-Ortega, S., Narayan, S. and Beck, M.W., 2020. The global flood protection benefits of mangroves. *Scientific reports*, *10*(1), pp.1-11.

Miller, K.G., Kopp, R.E., Horton, B.P., Browning, J.V. and Kemp, A.C., 2013. A geological perspective on sea-level rise and its impacts along the US mid-Atlantic coast. *Earth's Future*, *1*(1), pp.3-18.

Muis, S., Verlaan, M., Winsemius, H. C., Aerts, J. C. & Ward, P. J. A global reanalysis of storm surges and extreme sea levels. *Nat. Commun.* **7**, 11969 (2016).

Muis, S., Verlaan, M., Nicholls, R.J., Brown, S., Hinkel, J., Lincke, D., Vafeidis, A.T., Scussolini, P., Winsemius, H.C. and Ward, P.J., 2017. A comparison of two global datasets of extreme sea levels and resulting flood exposure. *Earth's Future*, *5*(4), pp.379-392.

Muis, S., Apecechea, M.I., Dullaart, J., de Lima Rego, J., Madsen, K.S., Su, J., Yan, K. and Verlaan, M., 2020. A high-resolution global dataset of extreme sea levels, tides, and storm surges, including future projections. *Frontiers in Marine Science*, *7*, p.263.

National Oceanic and Atmospheric Administration (a). *El Niño and La Niña: The El Niño Southern Oscillation (ENSO) is one of the most important climatic phenomena on Earth*. Resources. Available at: https://www.noaa.gov/education/resource-collections/weather-atmosphere/el-nino/ (Accessed November 27th, 2022)

National Oceanic and Atmospheric Administration (b). *Storm Surge Overview*. National Hurricane Center and Central Pacific Hurricane Center. Available at: https://www.nhc.noaa.gov/surge/ (Accessed November 27th, 2022).

Naulin, M., Kortenhaus, A. and Oumeraci, H., 2015. Reliability-based flood defense analysis in an integrated risk assessment. *Coastal Engineering Journal*, *57*(01), p.1540005.

New York City Economic Development Corporation. March 2019. *Lower Manhattan Climate Resilience Study*. Available at: https://edc.nyc/sites/default/files/filemanager/Projects/LMCR/Final_Image/Lower_Manhattan_Climate_Resilience_March_2019.pdf (Accessed January 15th, 2023).

opendatasoft, 2019. World Adminstrative Boundaries – Countries and Territories. *World Food Programme (UN Agency)*. Available at: https://public.opendatasoft.com/explore/dataset/world-administrative-boundaries/information/ (Accessed December 22nd, 2022).

Oppenheimer, M., B.C. Glavovic , J. Hinkel, R. van de Wal, A.K. Magnan, A. Abd-Elgawad, R. Cai, M. Cifuentes-Jara, R.M. DeConto, T. Ghosh, J. Hay, F. Isla, B. Marzeion, B. Meyssignac, and Z. Sebesvari, 2019: Sea Level Rise and Implications for Low-Lying Islands, Coasts and Communities. In: IPCC Special Report on the Ocean and Cryosphere in a Changing Climate [H.-O. Pörtner, D.C. Roberts, V. Masson-Delmotte, P. Zhai, M. Tignor, E. Poloczanska, K. Mintenbeck, A. Alegría, M. Nicolai, A. Okem, J. Petzold, B.

Rama, N.M. Weyer (eds.)]. Cambridge University Press, Cambridge, UK and New York, NY, USA, pp. 321–445. https://doi.org/10.1017/9781009157964.006.

Pawlowicz, R., Beardsley, B. and Lentz, S., 2002. Classical tidal harmonic analysis including error estimates in MATLAB using T_TIDE. *Computers & Geosciences*, *28*(8), pp.929-937.

Pelling, H.E. and Green, J.M., 2014. Impact of flood defences and sea-level rise on the European Shelf tidal regime. *Continental Shelf Research*, *85*, pp.96-105.

Peng, D., Hill, E.M., Meltzner, A.J. and Switzer, A.D., 2019. Tide gauge records show that the 18.61-year nodal tidal cycle can change high water levels by up to 30 cm. *Journal of Geophysical Research: Oceans*, *124*(1), pp.736-749.

Perez, J., Menendez, M. and Losada, I.J., 2017. GOW2: A global wave hindcast for coastal applications. *Coastal Engineering*, *124*, pp.1-11.

Port of Hamburg, 2022. Tide. Available at: https://www.hafen-hamburg.de/en/tide/

Qiang, Y., Zhang, L., He, J., Xiao, T., Huang, H. and Wang, H., 2021. Urban flood analysis for Pearl River Delta cities using an equivalent drainage method upon combined rainfall-high tide-storm surge events. *Journal of Hydrology*, *597*, p.126293.

Rahman, M.M., Paul, G.C. and Hoque, A., 2017. A study on tidal potential and tide generating force. *GANIT: Journal of Bangladesh Mathematical Society*, *37*, pp.29-37.

Räisänen, J., 2014. 21st century changes in snowfall climate in Northern Europe in ENSEMBLES regional climate models. *Climate Dynamics, doi*, *10*.

Ray, R.D. and Merrifield, M.A., 2019. The semiannual and 4.4-year modulations of extreme high tides. *Journal of Geophysical Research: Oceans*, *124*(8), pp.5907-5922.

Resio, D.T. and Westerink, J.J., 2008. Modeling the physics of storm surges. *Physics Today*, *61*(9), p.33.

Royal HaskoningDHV. North Manila Bay Flood Protection Strategy. *Netherlands Enterprise Agency*. 2022. Available at: https://northmanilabayfps.ireport.royalhaskoningdhv.com/home

Schwalm, C.R., Glendon, S. and Duffy, P.B., 2020. RCP8. 5 tracks cumulative CO2 emissions. *Proceedings of the National Academy of Sciences*, *117*(33), pp.19656-19657.

Semmler, T., Danilov, S., Gierz, P., Goessling, H.F., Hegewald, J., Hinrichs, C., Koldunov, N., Khosravi, N., Mu, L., Rackow, T. and Sein, D.V., 2020. Simulations for CMIP6 with the AWI climate model AWI-CM-1-1. *Journal of Advances in Modeling Earth Systems*, *12*(9), p.e2019MS002009.

Seto, K.C., 2011. Exploring the dynamics of migration to mega-delta cities in Asia and Africa: Contemporary drivers and future scenarios. *Global Environmental Change*, *21*, pp.S94-S107.

Souchay, J., Mathis, S. and Tokieda, T. eds., 2012. *Tides in astronomy and astrophysics* (Vol. 861). Springer.

Strandberg, G. and Lind, P., 2021. The importance of horizontal model resolution on simulated precipitation in Europe-from global to regional models. *Weather and Climate Dynamics*, 2(1), pp.181-204.

Sweet, W., Dusek, G., Marcy, D.C., Carbin, G. and Marra, J., 2019. 2018 state of US high tide flooding with a 2019 outlook.

Sweet, W.V., Kopp, R.E., Weaver, C.P., Obeysekera, J., Horton, R.M., Thieler, E.R. and Zervas, C., 2017. Global and Regional Sea Level Rise Scenarios for the United States. NOAA Technical Report NOS CO-OPS 083. *Washington, DC: Center for Operational Oceanographic Products and Services National Ocean Service, National Oceanic and Atmospheric Administration*.

Sweet, W., Park, J., Marra, J., Zervas, C. & Gill, S. Sea level rise and nuisance flood frequency changes around the United States. *NOAA Technical Report NOS CO-OPS 073* (2014).

Szewczyk, W., Feyen. L., Matei, A., Ciscar, J.C., Mulholland, E., Soria, A., Economic analysis of selected climate impacts, EUR 30199 EN, Publications Office of the European Union, Luxembourg, 2020, ISBN 978-92-76-18459-1, doi:10.2760/845605, JRC120452

Tablazon, J., Caro, C.V., Lagmay, A.M.F., Briones, J.B.L., Dasallas, L., Lapidez, J.P., Santiago, J., Suarez, J.K., Ladiero, C., Gonzalo, L.A. and Mungcal, M.T.F., 2015. Probabilistic storm surge inundation maps for Metro Manila based on Philippine public storm warning signals. *Natural Hazards and Earth System Sciences*, *15*(3), pp.557-570.

Taherkhani, M., Vitousek, S., Barnard, P.L., Frazer, N., Anderson, T.R. and Fletcher, C.H., 2020. Sea-level rise exponentially increases coastal flood frequency. *Scientific reports*, *10*(1), pp.1-17.

Talke, S.A., Familkhalili, R. and Jay, D.A., 2021. The influence of channel deepening on tides, river discharge effects, and storm surge. *Journal of Geophysical Research: Oceans*, *126*(5), p.e2020JC016328.

Tebaldi, C., Strauss, B.H. and Zervas, C.E., 2012. Modelling sea level rise impacts on storm surges along US coasts. *Environmental Research Letters*, *7*(1), p.014032.

Thai PBS World (a). 2022. Bangkok's seasonal floods reveal the problem of short-term thinking. Available at: https://www.thaipbsworld.com/bangkoks-seasonal-floods-reveal-the-problem-of-short-term-thinking/ (Accessed January 13th, 2023).

Thai PBS World (b). Can flooding in Thailand get worse in the future? *YouTube. January 12, 2022.*

Thibodeau, B., Not, C., Zhu, J., Schmittner, A., Noone, D., Tabor, C., Zhang, J. and Liu, Z., 2018. Last century warming over the Canadian Atlantic shelves linked to weak Atlantic meridional overturning circulation. *Geophysical Research Letters*, *45*(22), pp.12-376.

Thompson, E.F. and Hadley, L.L., 1995. Numerical modeling of harbor response to waves. *Journal of coastal research*, pp.744-753.

Thompson, P.R., Widlansky, M.J., Hamlington, B.D., Merrifield, M.A., Marra, J.J., Mitchum, G.T. and Sweet, W., 2021. Rapid increases and extreme months in projections of United States high-tide flooding. *Nature Climate Change*, pp.1-7.

Tromans, I.J., Aldama-Bustos, G., Douglas, J., Lessi-Cheimariou, A., Hunt, S., Daví, M., Musson, R.M., Garrard, G., Strasser, F.O. and Robertson, C., 2019. Probabilistic seismic hazard assessment for a new-build nuclear power plant site in the UK. *Bulletin of earthquake engineering*, *17*(1), pp.1-36.

Union of Concerned Scientists. *Sea Level Rise and Tidal Flooding in Philadelphia, Pennsylvania*. Published March 31, 2016. Accessed January 14

US Census Bureau, Department of Commerce, 2021. TIGER/Line Shapefile, 2016, state, Florida, Current County Subdivision State-based. *Data.gov*. Available at:

https://catalog.data.gov/dataset/tiger-line-shapefile-2016-state-florida-current-county-subdivision-state-based (Accessed December 22nd, 2022).

VanGraafeiland, K. *Global Tidal Range Classification*. Esri feature service. 2020. "FES2014 was produced by Noveltis, Legos and CLS and distributed by Aviso+, with support from Cnes (https://www.aviso.altimetry.fr/)".

Van Loon-Steensma, J.M. and Vellinga, P., 2019. How "wide green dikes" were reintroduced in The Netherlands: a case study of the uptake of an innovative measure in long-term strategic delta planning. *Journal of Environmental Planning and Management*, *62*(9), pp.1525-1544.

Vitousek, S., Barnard, P.L., Fletcher, C.H., Frazer, N., Erikson, L. and Storlazzi, C.D., 2017. Doubling of coastal flooding frequency within decades due to sea-level rise. *Scientific reports*, *7*(1), pp.1-9.

Vousdoukas, M. I., Voukouvalas, E., Annunziato, A., Giardino, A. and Feyen, L., 2016, 'Projections of extreme storm surge levels along Europe', *Climate Dynamics* 47(9), pp. 3171–3190 (http://link.springer.com/article/10.1007/s00382-016-3019-5) accessed April 26, 2016.

Vousdoukas, M.I., Mentaschi, L., Mongelli, I., Ciscar Martinez, J.C., Hinkel, J., Ward, P., Gosling, S. and Feyen, L., 2020. Adapting to rising coastal flood risk in the EU under climate change. *Publications Office of the the European Union: Luxembourg*.

Voyles Pulver, D. 2019. *Rising seas mean higher tides*, *flooding 'new normal'*. Jacksonville.com. Available at: https://eu.jacksonville.com/story/news/2019/11/25/rising-seas-mean-higher-tides-flooding-new-normal/2199052007/ (Accessed January 15th, 2023).

Wahl, T., Haigh, I.D., Nicholls, R.J., Arns, A., Dangendorf, S., Hinkel, J. and Slangen, A.B., 2017. Understanding extreme sea levels for broad-scale coastal impact and adaptation analysis. *Nature communications*, *8*(1), pp.1-12.

Wang, Y., Heywood, K.J., Stevens, D.P. and Damerell, G.M., 2022. Seasonal extrema of sea surface temperature in CMIP6 models. *Ocean Science*, *18*(3), pp.839-855.

Ward, P.J., Jongman, B., Salamon, P., Simpson, A., Bates, P., De Groeve, T., Muis, S., De Perez, E.C., Rudari, R., Trigg, M.A. and Winsemius, H.C., 2015. Usefulness and limitations of global flood risk models. *Nature Climate Change*, *5*(8), pp.712-715.

Winterwerp, J.C. and Wang, Z.B., 2013. Man-induced regime shifts in small estuaries—I: theory. *Ocean Dynamics*, *63*(11), pp.1279-1292.

Woodworth, P.L. and Player, R. 2003. The Permanent Service for Mean Sea Level: an update to the 21st century. Journal of Coastal Research, 19, 287-295.

Woodworth, P.L. and Blackman, D.L., 2004. Evidence for systematic changes in extreme high waters since the mid-1970s. *Journal of Climate*, *17*(6), pp.1190-1197.

Woodworth, P.L., Hunter, J.R., Marcos, M., Caldwell, P., Menéndez, M. and Haigh, I., 2017. Towards a global higher-frequency sea level dataset. *Geoscience Data Journal*, *3*(2), pp.50-59.

Woodworth PL, Melet A, Marcos M, Ray R, Woppelmann G, Sasaki N, Cirano M, Hibbert A, Huthnance JM, Montserrat S (2019) Forcing factors causing sea level changes at the coast. Surv Geophys.

Woodworth, P.L., Hunter, J.R., Marcos, M. and Hughes, C.W., 2021. Towards reliable global allowances for sea level rise. *Global and Planetary Change*, *203*, p.103522.

Yeung, P. 2021. In Hamburg, Surviving Climate Change Means Living With Water. *Bloomberg*. Available from: https://www.bloomberg.com/news/features/2021-12-18/how-hamburg-learned-to-live-with-rising-water ((Accessed January 13th, 2023).

Zheng, L., Cheng, X., Chen, Z. and Liang, Q., 2021. Delay in Arctic sea ice freeze-up linked to early summer sea ice loss: Evidence from satellite observations. *Remote Sensing*, *13*(11), p.2162.

Appendix: SLC Projections vs CMIP6

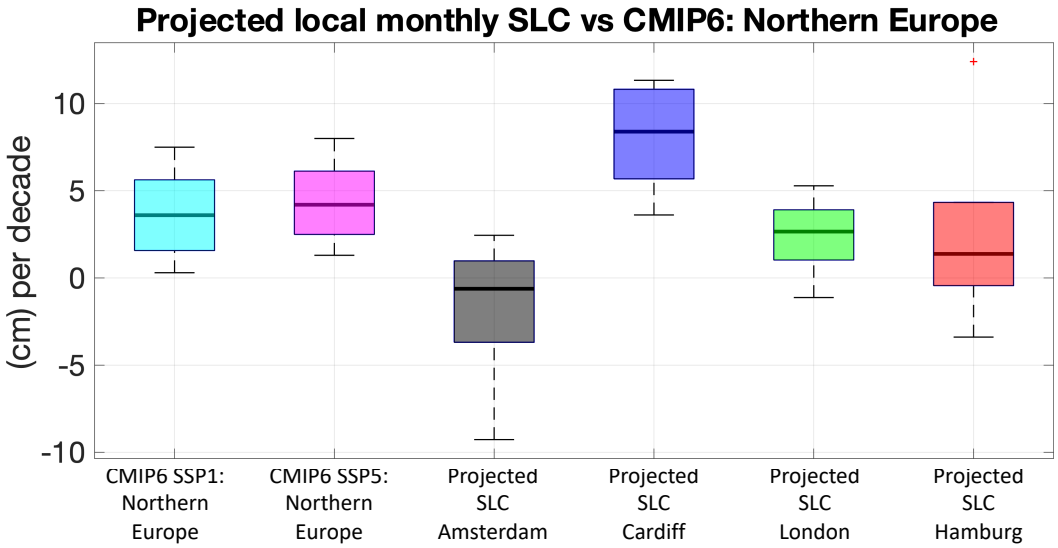

Figure A.1: Statistics of MMSL projections compared to ensemble CMIP6 projections for Northern Europe. CMIP6 projections are for the near term (2021 – 2040), based on baseline sea level data from 1995-2014.

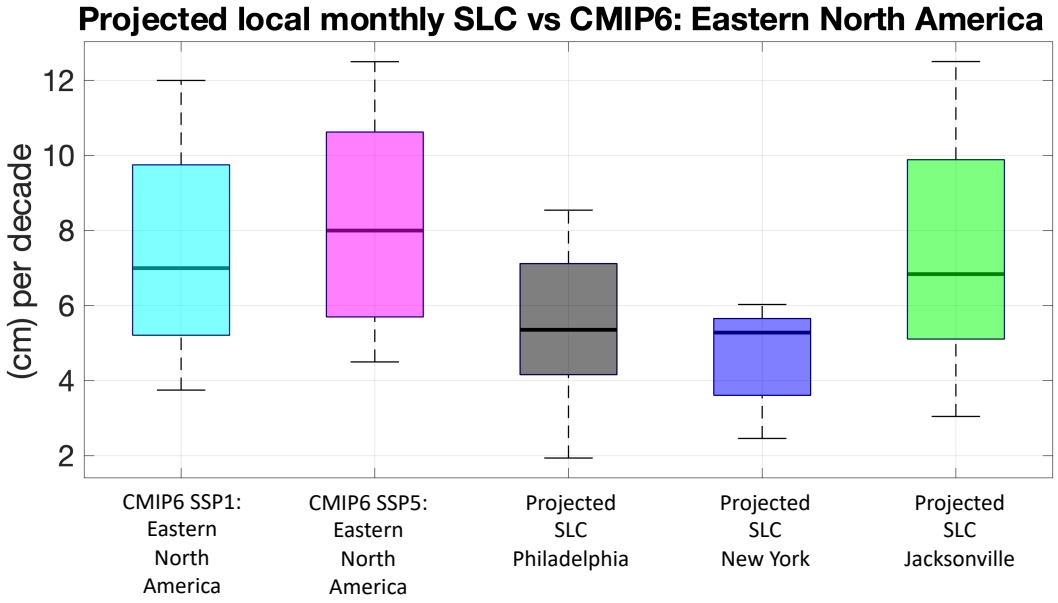

Figure A.2: Statistics of MMSL projections compared to ensemble CMIP6 projections for Eastern North America. CMIP6 projections are for the near term (2021 – 2040), based on baseline sea level data from 1995-2014.

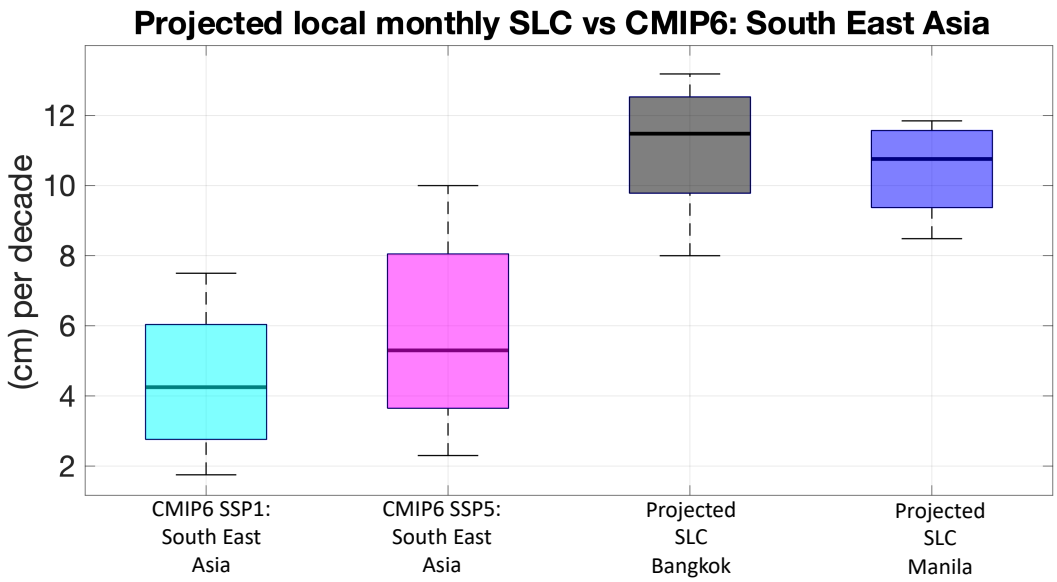

Figure A.3: Statistics of MMSL projections compared to ensemble CMIP6 projections for South East Asia. CMIP6 projections are for the near term (2021 – 2040), based on baseline sea level data from 1995-2014.

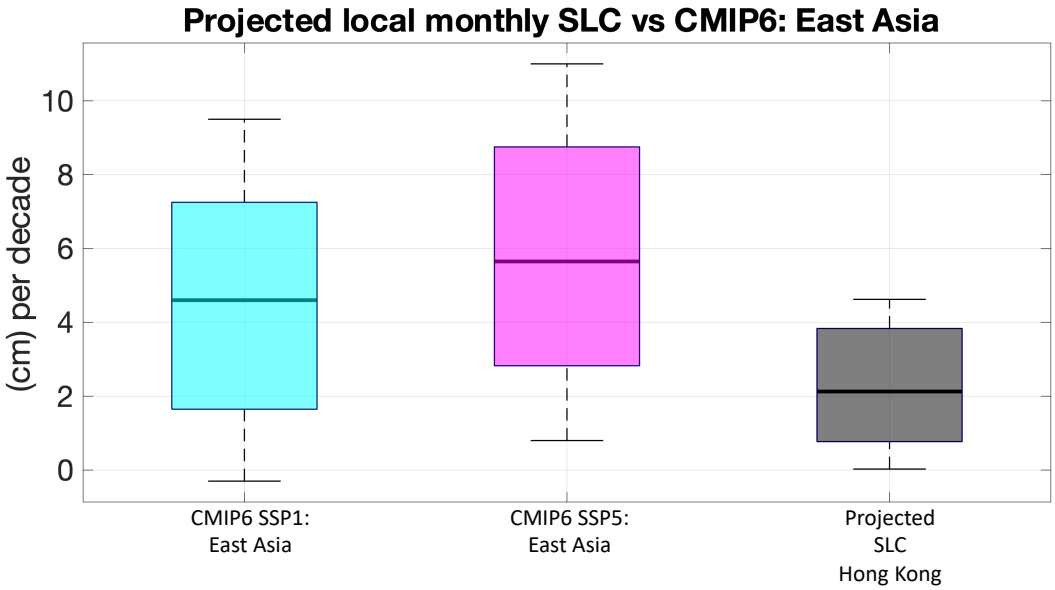

Figure A.4: Statistics of MMSL projections compared to ensemble CMIP6 projections for East Asia. CMIP6 projections are for the near term (2021 – 2040), based on baseline sea level data from 1995-2014.